CHARACTERIZATION OF MEMBRANE-ASSOCIATED PROTEINS INVOLVED IN *MYCOBACTERIUM TUBERCULOSIS* CELL ENVELOPE BIOGENESIS

by

Geoff Melly

A DISSERTATION

Presented to the Department of Molecular Microbiology & Immunology
and the Oregon Health & Science University
School of Medicine
in partial fulfillment of
the requirements for the degree of

Doctor of Philosophy

October 2019

School of Medicine

Oregon Health & Science University

CERTIFICATE OF APPROVAL

_____

This is to certify that the PhD dissertation of

Geoff Melly

has been approved

_____

Mentor / Georgiana Purdy

_____

Member / Scott Landfear

_____

Member / William Messer

_____

Member / Ujwal Shinde

_____

Member / Jonathan Pruneda

TABLE OF CONTENTS

FIGURES and TABLES

ACKNOWLEDGMENTS

An honest accounting of appreciation must begin with my mentor, **Dr. Georgiana Purdy**, to whom I am profoundly grateful. Her mentorship and support have been essential to my development as a researcher. I have strived to cultivate in myself the exemplary dedication and persistence with which she approaches her work. I count myself extremely privileged to have had her as a mentor.

I am also greatly indebted to the larger OHSU community. **Dr. Scott Landfear** has been an enduringly staunch supporter of MMI graduate education in general, and of myself in particular. I am deeply appreciative of the training support and career development activities that he has facilitated, and for his time and energy chairing my dissertation advisory committee. The members of my DAC have been instrumental in guiding my training in myriad ways. **Dr. William Messer** has been a fount of stimulating conversation and scientific nous. **Dr. Ujwal Shinde** has been exceedingly generous with his time and expertise. **Dr. Fikadu Tafesse** has been an enthusiastic advocate, and has provided a valuable perspective on my work. I am also grateful to **Dr. Jonathan Pruneda**, for agreeing to be the outside reader of this dissertation, and for making an immediate positive impact on the MMI department. I would also like to acknowledge **Dr. Kimberly Beatty** who has been an unfailingly beneficent influence throughout the course of my graduate training.

Science is truly a collaborative endeavor, and I am thankful to have worked with a talented group of researchers. In particular, **Catherine Wright** and **Patrick Davidson** were stalwart Purdy Lab compatriots for many years. Additionally, **José Santinni Roma**, **Jennifer Dunaj**, and **Haley Stokas** have all made critical contributions to the work described in this dissertation. It has been a pleasure and a privilege to work alongside such committed individuals. Additionally, much of the work described herein would have been impossible to accomplish without the assistance of our steadfast network of collaborators, principally the laboratories of **Dr. Edward Yu**, at Case Western Reserve University, and **Dr. Fong-Fu Hsu**, at Washington University.

Finally, I am immensely grateful for the support of my friends and family. My parents, **Christopher** and **Mary Lou Melly**, brother, **Jacob Melly**, and cognata, **Laura Calabria,** have been perpetual sources of encouragement. A **Lauren Magee**, **David Lara-Arregui**, y **Carmelo Arregui-Magee** les agradezco su gran amistad y apoyo. And I am lucky beyond all reason to have **Amanda Jensen** as my partner.

ABSTRACT

Mycobacterium tuberculosis (*Mtb*) is the etiologic pathogen of tuberculosis (TB), the leading infectious cause of death. *Mtb* is a diderm bacillus that is exquisitely well-adapted to its human host. The mycobacterial cell envelope, a complex structure comprising the inner membrane, the peptidoglycan core, the mycobacterial outer membrane (mycomembrane), and the capsule, plays a foundational role in *Mtb* virulence and pathogenicity. Of particular importance is the mycomembrane, which is composed of unique lipids that act as a protective barrier against antibiotics and directly modulate host immune responses. Thus, mycobacterial cell envelope lipids are virulence factors that potentiate bacterial survival in the host, and targeting their biosynthesis and transport is an effective means by which to treat TB. Mycobacterial membrane protein Large (MmpL) proteins are integral inner membrane transporters that are implicated in the export of cell envelope lipids. However, the precise mechanisms and regulation of MmpL-mediated envelope lipid transport are incompletely described. In this work, we identify the lipoprotein LpqN as a periplasmic interacting partner of the mycolate transporters MmpL3 and MmpL11, and of secreted mycolyltransferases. Furthermore, we report that LpqN is capable of binding lipids that resemble the substrates of these proteins, suggesting that LpqN is a transport adaptor protein that supports cell envelope biogenesis. Additionally, we dissect the structural basis of MmpL11-mediated lipid export by identifying specific residues and structural domains that are crucial for transporter function.

Finally, we present data suggesting that MmpL11 function is differentially regulated by phosphorylation, illuminating heretofore undescribed adaptive mechanisms that enable *Mtb* to modulate the contents of the cell envelope in response to external signals. Together, this work furthers our understanding of the bacterial physiology underlying the biogenesis of the mycobacterial cell envelope, perhaps the most critical interface between the host and pathogen.

CHAPTER 1

INTRODUCTION

A portion of this introduction was published as a review in *Microorganisms* in March 2019 (Melly and Purdy, 2019).

Scope

Mycobacterium tuberculosis (*Mtb*) is the causative bacterial pathogen of the human disease tuberculosis (TB). TB remains one of the most devastating diseases in the world. In 2017, there were approximately 10 million new cases and 1.3 million deaths attributable to TB disease, making TB the leading cause of death due to a single infectious agent (World Health Organization, 2018).

Mtb transmission primarily occurs through the respiratory system when bacilli contained in aerosolized particles are expelled from the lungs of an individual suffering from active TB disease. These infectious aerosols are subsequently inhaled by an uninfected individual and traverse the host airway to arrive at the alveoli, the distal sites of gas exchange in the lungs and the initial site of *Mtb* infection. Exposure to *Mtb* can have three potential outcomes: eradication, latent TB infection, or active TB disease. In approximately 70% of exposures, no *Mtb* infection is established, either due to the failure of *Mtb* to encounter an amenable replicative niche or to the successful eradication of *Mtb* by the host innate immune system (Manabe and Bishai, 2000). In approximately 30% of exposures, *Mtb* is able to establish an infection. Only 10% of primary *Mtb* infections result in active TB disease, characterized by actively replicating bacteria. In the remaining cases, *Mtb* bacteria persist in the human host and avoid eradication by the host immune system. Individuals that harbor *Mtb* bacteria but don't show the signs and symptoms of active TB disease are considered to have latent TB infection (LTBI). Without treatment, 10% of patients with LTBI will progress to active TB

disease at some point in their lives (Philips and Ernst, 2012). Estimates suggest that up to 23% of the global population are latently infected with *Mtb* bacteria and therefore at risk of developing active disease (World Health Organization, 2018). Risk factors for the development of TB disease include diabetes, malnutrition, air pollution, and conditions that alter the normal function of the immune system, such as HIV infection, immunosuppressive drug treatment, and immunosenescence (Lönnroth et al., 2009). There is also a disproportionate TB burden associated with low socio-economic status.

Currently available TB treatments are associated with harmful side effects, and require lengthy treatment regimens in order to achieve sterilizing eradication of *Mtb* from an infected individual (World Health Organization, 2010). Even drug susceptible TB requires sustained treatment for 3-9 months with a multiple antibiotic cocktail. Furthermore, many antibiotics are becoming increasingly ineffective at treating TB disease. Multi-drug resistant TB (MDR-TB) and extensively drug resistant TB (XDR-TB) can require treatment durations of 20-32 months (Marks et al., 2014). Novel therapeutic options are desperately needed to increase the efficacy of TB treatment and counteract the emergence of antimicrobial resistance. Therapies that target latent TB would be particularly beneficial, given that the majority of TB disease occurs as LTBI.

Initial Infection and the Granuloma

Mtb is a consummate human pathogen due to its ability to counteract host immunity. This begins early on in infection, when alveolar macrophages (AMs) in the lungs encounter *Mtb* bacilli upon inhalation of aerosolized bacteria (Cohen et al., 2018). Normally, tissue resident AMs internalize bacteria via phagocytosis, forming an intracellular bacteria-containing vesicle known as a phagosome. Vesicular trafficking events that are directed by a network of host signaling enzymes and molecules result in fusion of the phagosome with the lysosome. The lysosomal environment is harsh and bactericidal, containing hydrolases and antimicrobial peptides that kill susceptible bacteria (Rosales and Uribe-Querol, 2017). However, internalized *Mtb* manipulates host intracellular trafficking to prevent fusion of the lysosome with the *Mtb*-containing phagosome (Kang et al., 2005b; Patin et al., 2017; Vergne et al., 2005). Inhibition of phagolysosomal fusion is critical to *Mtb*'s initial exploitation of the intracellular niche afforded by alveolar macrophages. *Mtb* also maintains its niche by actively inhibiting apoptosis of AMs (Balcewicz-Sablinska et al., 1998; Velmurugan et al., 2007). Instead, intracellular bacterial replication induces necrosis of AMs and releases *Mtb* bacteria into the extracellular milieu (Chen et al., 2006; Pajuelo et al., 2018).

In immunocompetent patients, the failure of innate immunity is counterbalanced by the eventual mounting of an adaptive immune response in an attempt to limit the spread of infection. This process is dependent on dendritic cells (DCs) taking up *Mtb* bacilli and trafficking to the lymph nodes, where they initiate the adaptive

immune response (Chackerian et al., 2002; Wolf et al., 2008; 2007). The outcome is the classic immunologic response to TB infection known as the granuloma. Long considered the histopathological hallmark of TB, the granuloma is an ordered assemblage of leukocytes, circularly arrayed about a central focus of *Mtb* infection, that functions to wall off and limit the spread of the *Mtb* infection in the lungs (Russell, 2007; Saunders and Britton, 2007).

Granuloma formation and structure is remarkably complex and exhibits substantial heterogeneity. Nevertheless, observations from experimental animal infections, primarily mouse, guinea pig, non-human primate (NHP), and zebrafish models, have granted a degree of insight into the immunologic processes that generate this hallmark of TB disease. Perhaps most commonly used is the mouse model, which is amenable to intranasal infection and genetic manipulation. However, mice do not develop the typical chronic infection as observed in human cases. A better model that recapitulates the chronic/progressive character of human TB disease is the guinea pig. Guinea pigs develop necrotic lung lesions that closely resemble human granulomas, however this model is less genetically tractable than the mouse. It is therefore more difficult to investigate the contributions of host immunity to TB disease/control in this model (Flynn, 2006). Zebrafish embryos form granulomas in response to infection with the natural pathogen *Mycobacterium marinum*, and are optically transparent, enabling real-time observations of the immune cell migration that is a prerequisite of granuloma formation (Cronan and Tobin, 2014).

NHP models, specifically the cynomolgus macaque, most closely recapitulate human TB disease in terms of immunopathology and disease latency. However, these models are less amenable to genetic manipulation and are substantially more difficult to maintain (Flynn et al., 2015). While none of these experimental systems completely recapitulate the human granulomatous response, together they have greatly contributed to our understanding of how granulomas form and progress.

Tuberculous granulomas initially arise as a response to sustained pro-inflammatory signaling induced by mycobacterial activators of innate immunity. Host pattern recognition receptors (PRRs) sense pathogen-associated molecular patterns (PAMPs) on *Mtb* and signal to upregulate pro-inflammatory genetic programs. Toll-like receptors (TLRs), especially TLR1/ 2/ 4, are important PRRs for sensing of *Mtb* (Bulut et al., 2005; Means et al., 1999; Tapping and Tobias, 2003). The TLR signaling cascade results in the nuclear translocation of the critical host inflammatory transcriptional regulator nuclear factor κB (NF-κB) and the subsequent induction of pro-inflammatory cytokines, principal among them tumor necrosis factor-α (TNF) (Fallahi-Sichani et al., 2012; Kempe et al., 2005).

TNF is of critical importance during the initial phages of granuloma formation (Algood et al., 2005; Roach et al., 2002). TNF acts in a feed-forward loop to induce macrophage cytokine and chemokine production, thereby increasing the secretion of immune-attractant chemokines such as CCL5, CXCL9, and CXCL10

(Algood et al., 2004). Neutrophils also play a key role in the early recruitment stages of granuloma formation, primarily via production of CXCL9 and CXCL11 (Seiler et al., 2003). Together, the AMs and neutrophils can be thought of as "first-responder" cells that activate a chemokine alarm system that recruits additional immune cells and initiates the granulomatous response to *Mtb* infection.

The characteristic circular structure of the granuloma is derived in large part from the differentiation of epithelioid macrophages circumferentially arranged about the central focus of infection (Cronan et al., 2016). A multitude of additional immune cells traffic to the site of the nascent granuloma in response to chemokine signaling. These cells include monocytes, macrophages, neutrophils, and T and B lymphocytes (Gonzalez-Juarrero et al., 2001; Saunders et al., 2002). Of particular importance are interferon-γ (IFN-γ) producing CD4+ T-cells (Cowley and Elkins, 2003; Flynn et al., 1993). CD4+ T-cells also play a role in driving the differentiation of a type of multinucleated giant cells, known as Langhans cells, which form by fusion of macrophage-monocyte precursors (Sakai et al., 2012). The mature granuloma is frequently surrounded by a fibrotic capsule that further segregates the infectious focus (Dheda et al., 2005).

There is significant heterogeneity in granuloma formation, pathology, and outcome. In terms of bacterial eradication, granulomas exhibit a wide spectrum of efficacy, with some granulomas resulting in complete sterilization, some reaching

a détente with their enclosed bacteria, and others rupturing and disseminating infectious *Mtb* (Lin et al., 2014; Martin et al., 2017). Granuloma outcomes exhibit extraordinary variation even within single individuals, implying that granulomas are sensitive to the local immune microenvironment and the localized context of the infection. In the event of the failure of the host adaptive immune response, persistent bacteria contained in latent granulomas are able to resume active replication and serve as a source for development of active TB disease.

While granulomas are typically considered to be host-protective, there is a growing appreciation of the fact that *Mtb* benefits from granuloma formation as well. One of the ways that *Mtb* is able to persist in the granuloma is due to its specialization in using host lipids as carbon sources during chronic infection. Chronic mycobacteria-induced inflammation causes granuloma macrophages to accumulate lipids such as cholesterol, phospholipids, and triacylglycerides (D'Avila et al., 2006). These lipids aggregate in lipid droplets, converting these macrophages into “foamy macrophages (FMs),” or foam cells. FM formation is induced by certain *Mtb* cell envelope components and may be advantageous to *Mtb* survival (Daniel et al., 2011; Lee et al., 2013; Peyron et al., 2008; VanderVen et al., 2015). *Mtb* bacilli contained in FMs enter dormancy and acquire phenotypic drug tolerance, further contributing to bacterial persistence (Daniel et al., 2011; Peyron et al., 2008).

The functional outcome of many granulomas is an equilibrium between *Mtb* and the human host that enables the persistence of the pathogen without the acute pathology of active TB disease. This asymptomatic equilibrium may be maintained for decades, until the immune response of the host falters and active bacterial replication resumes along with concomitant disease symptoms and potential transmission. In a nutshell, this is why *Mtb* is such a pernicious pathogen. Humans are both the reservoir and the medium in which *Mtb* replicates, and the host to which *Mtb* is so exquisitely adapted. The initial and primary means by which *Mtb* potentiates its survival in humans is through the *Mtb* cell envelope. This complex and multifaceted bacterial structure is the most crucial interface between bacteria and host and is absolutely essential to the success of *Mtb* as a human pathogen.

The *Mtb* Cell Envelope

The cell envelope of *Mtb* and other mycobacteria is a unique and robust structure that is generally considered to comprise four regions that define the border between the bacterial cytoplasm and the extracellular environment. These are the: (1) plasma membrane (PM), (2) arabinogalactan/peptidoglycan (AGP) core, mycobacterial outer membrane (MOM, or mycomembrane), and (4) “outer layer” (OL, or capsule) (Chiaradia et al., 2017). The organization of these layers resembles that of classical Gram-negative bacteria, with the mycomembrane analogous to an outer membrane (**Figure 1.1**). Together, they form a robust physical barrier that contributes to the intrinsic resistance of *Mtb* against host

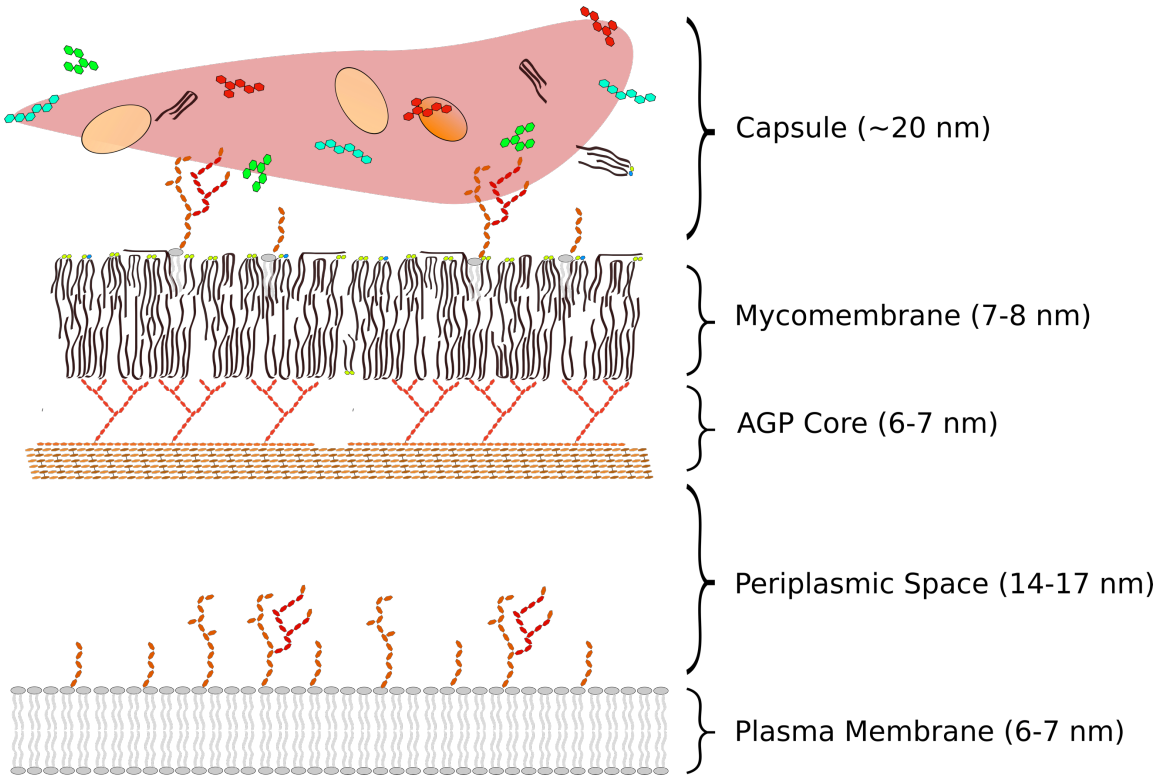

Figure 1.1. Cartoon representation of the mycobacterial cell envelope, illustrating the plasma membrane, the arabinogalactan-peptidoglycan (AGP) core, the mycobacterial outer membrane (mycomembrane), and the capsule. *Figure and legend adapted from (Melly and Purdy, 2019)*.

antimicrobial defenses and limits the access of chemotherapeutics into the bacterial cytoplasm (Brennan and Nikaido, 1995). Additionally, certain cell envelope components directly interfere with aspects of host immunity and contribute to bacterial survival (Blanc et al., 2017; Indrigo, 2003; Patin et al., 2017; Vergne et al., 2005). Thus, the cell envelope is a critical aspect of *Mtb* physiology and virulence. Investigating the biological processes that generate the cell envelope has the potential to greatly improve the treatment of TB disease.

The mycobacterial PM is primarily composed of phospholipids, including phosphatidylethanolamine (PE), phosphatidylserine (PS), cardiolipin (CL), and phosphatidylinositol, and is approximately 6-7 nm thick (Hoffmann et al., 2008; Jackson, 2014; Zuber et al., 2008). Mannosylated phosphatidylinositols, or PIMs, are also prevalent in the inner membrane, and can serve as an attachment for more elaborate lipoglycans which are thought to be anchored into the periplasmic leaflet and project out from the PM. These include molecules such as lipomannan (LM), which consists of branched mannose residues linked to a mannosyl phosphate inositol (MPI) anchor, and lipoarabinomannan (LAM), which has complex branched arabinose chains appended to the MPI-anchored mannose backbone of LM (Jankute et al., 2015). In pathogenic mycobacteria such as *Mtb*, the terminal arabinose residues of LAM are “capped” with mannose, resulting in man-LAM. Man-LAM is an important virulence-associated glycolipid and plays a multitude of roles in *Mtb* pathogenesis (Turner and Torrelles, 2018).

The next major structure of the mycobacterial cell envelope is the AGP core, which is separated from the PM by an approximately 14-17 nm wide periplasmic space (Zuber et al., 2008). Mycobacterial peptidoglycan (PG) consists of polymers of alternating N-acetylglucosamine (GlcNAc) and muramic acid sugars connected via β(1-4) linkages (**Figure 1.2**) (Alderwick et al., 2015). Interestingly, mycobacterial PG contains a mixture of N-acetylmuramic (MurNAc) and N-glycolylmuramic (MurNGlyc) residues in an approximately 1:2 ratio (Mahapatra et al., 2005; Petit et al., 1969; Raymond et al., 2005). The presence of MurNGlyc in mycobacterial PG is noteworthy and relatively rare in bacteria. Strands of GlcNAc-MurN(Ac/Glyc) are crosslinked to each other via covalent 3-4 linkages between diaminopimelic acid (DAP) and alanine residues in the tetrapeptide sidechains of MurN(Ac/Glyc). Interestingly, the character of these peptide crosslinks changes to 3-3 linkages between DAP-DAP upon entry into stationary phase (Lavollay et al., 2008). These linked chains form a mesh-like sacculus that provides rigidity and structure to the bacterium.

The branched arabinogalactan complex is covalently attached to a portion of the muramic acid residues of PG. This attachment occurs by way of a disaccharide "linker unit," consisting of a unique rhamnose sugar in L-conformation appended to a D-GlcNAc reside, itself substituted at the 6-position of PG muramic acid by phosphodiester bond (McNeil et al., 1990). A linear polymer of ~ 30 D-galactofuranosyl (Gal*f*) residues, connected via alternating β(1-5) and β(1-6) linkages, is built off of the rhamnosyl residue of the linker unit

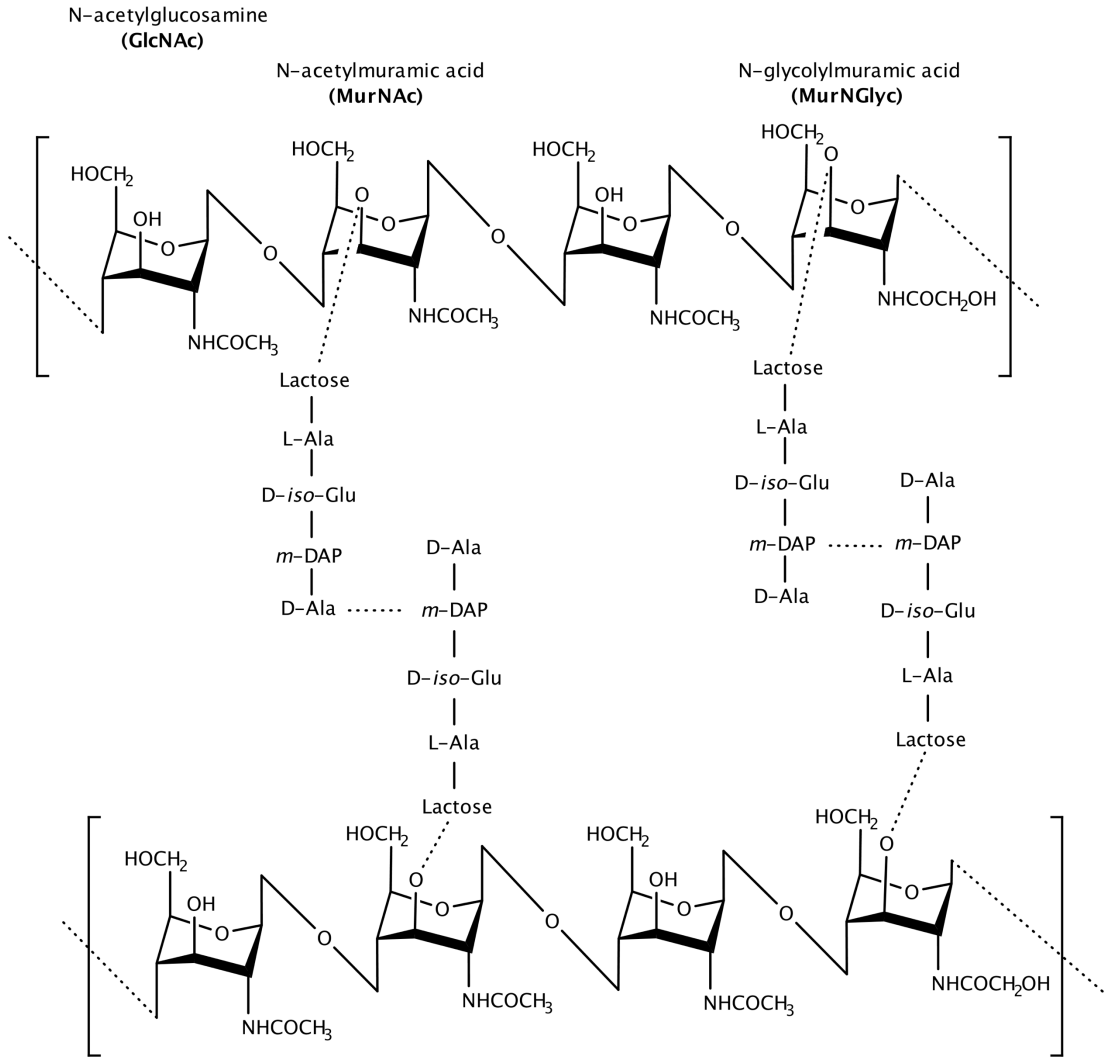

Figure 1.2. Structure of mycobacterial peptidoglycan. N-acetylglucosamine and N-(acetyl/glycolyl)muramic acid (MurNAc/Glyc) sugars are linked via β(1-4) glycosidic bonds. Tetrapeptide side chains appended to the lactosyl moiety of MurNAc/Glyc can be crosslinked to each other by 3-4 [meso-diaminopimelic acid (m-DAP) – D-alanine] or 3-3 (m-DAP – m-DAP) linkages.

(McNeil et al., 1987). Branched polymers of ~10-30 D-arabinofuranosyl (Ara*f*) sugar residues are attached to the linear galactan backbone (**Figure 1.3**). Based on evidence obtained from the related *Corynebacterium glutamicum* species, it is believed that each linear galactan chain possesses up to three arabinan complexes attached at the C-5 position of the 8^{th}, 10^{th}, and 12^{th} Gal*f* residues (Alderwick et al., 2005).

The portion of each arabinan chain closest to the galactan is linearly connected via α(1-5) bonds between residues; more distally, the chain bifurcates twice via successive α(3-5) connections, resulting in four terminal Ara*f* residues. Thus, a single arabinan complex is analogous to a tree, with a linear "trunk" serving as the foundation at the Gal*f* base and the distal Ara*f* residues projecting in a branch-like fashion. The four distal-most residues are attached via β(1-2) linkages. These β(1-2) Ara*f* "caps," and their immediately preceding residues, can be decorated with mycolic acids appended at the C-5 positions (McNeil et al., 1991). Thus, there are 8 potential mycolate attachment sites for a single Ara*f* "tree," and 24 per Gal*f* backbone. Approximately two-thirds of these potential sites are actually mycolylated (McNeil et al., 1991). Non-mycolylated Ara*f* complexes can have either succinate or galactosamine attached to the C-2 position of the distal α(3-5) Ara*f* branch point. The width of the entire AGP core has been measured to be between 6-7 nm (Zuber et al., 2008). Together, the AGP complex serves as an anchoring foundation for the mycomembrane.

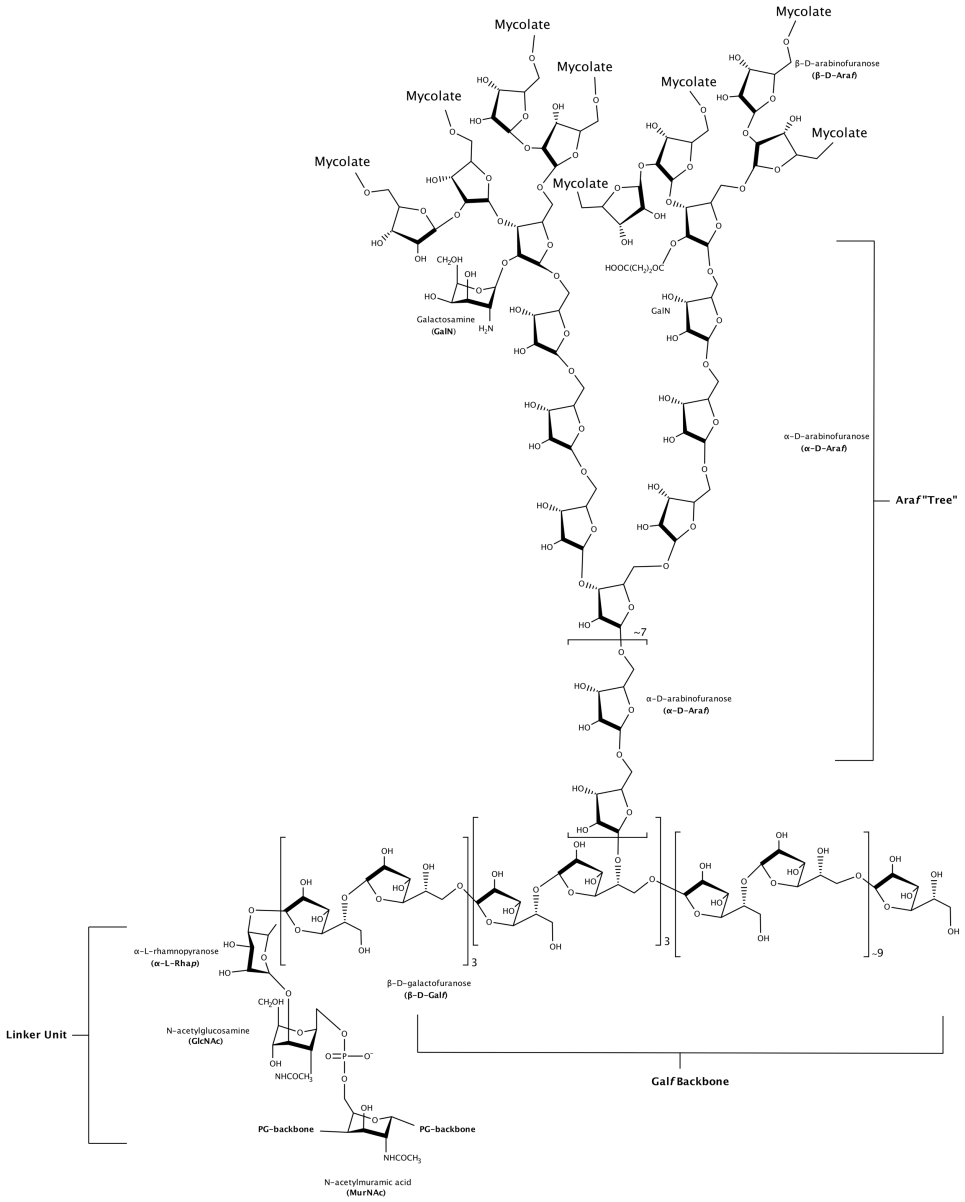

Figure 1.3. Structure of mycobacterial arabinogalactan (AG). AG is anchored to C-6 of PG MurNAc via the rhamnose-GlcNAc-P disaccharide linker unit. The galactan backbone consists of galactofuranose (Gal*f*) sugars connected via alternating β(1-5) and β(1-6) glycosidic bonds. Arabinofuranose (Ara*f*) "tree-like" projections are attached to C-5 of the 8/10/12th Gal*f* residues. Ara*f* residues are connected via linear α(1-5) glycosidic bonds, except for the branch points, which have α(3-5) linkages, and terminal Ara*f* caps, which have β(1-2) connections. Approximately two thirds of terminal and penultimate Ara*f* residues are mycolylated at C-5, forming the inner leaflet of the mycomembrane. Distal Ara*f* branch points can be decorated with succinate or galactosamine at C-2.

The mycomembrane is analogous to the outer membrane of Gram-negative bacteria. It is a lipid bilayer, and has been experimentally measured to be approximately 7-8 nm wide (Hoffmann et al., 2008; Zuber et al., 2008). While membrane phospho- and glycolipids (such as PIMs, CL, PE, and LAM) are present in the mycomembrane, the most crucial components of the mycomembrane are mycolic acids and their derivatives (Chiaradia et al., 2017). Mycolic acids are dual-chain ($C_{60\text{-}90}$) α-alkyl β-hydroxy fatty acids that consist of a shorter ~C_{26} α-chain and a much longer ~C_{56} "meromycolate" chain (**Figure 1.4**; (Barry et al., 1998; Marrakchi et al., 2014; Quémard, 2016)). These unique lipids are characteristic of mycobacteria and related bacterial genera (e.g *Corynebacteria*) and are fundamental to the structure of the mycomembrane and to *Mtb* virulence.

In *Mtb*, there are three major types of mycolic acids: α, keto, and methoxy. These are differentiated by the character of the chemical modifications found at the proximal and distal substitution sites of the meromycolate chain (**Figure 1.4**). All three types have a cyclopropane functional group at the proximal site, which is invariably in the *cis*-conformation for α-mycolic acids, but can be either *cis*- or *trans*- in the case of the oxygenated (keto- and methoxy-) mycolic acids (Glickman et al., 2001; 2000). The distal site of α-mycolic acid also has a *cis*-cyclopropane group, while the distal sites of keto- and methoxy-mycolic acids are substituted with their eponymous functional groups (Dubnau et al., 2000; Glickman, 2003). These chemical modifications contribute to the virulence of

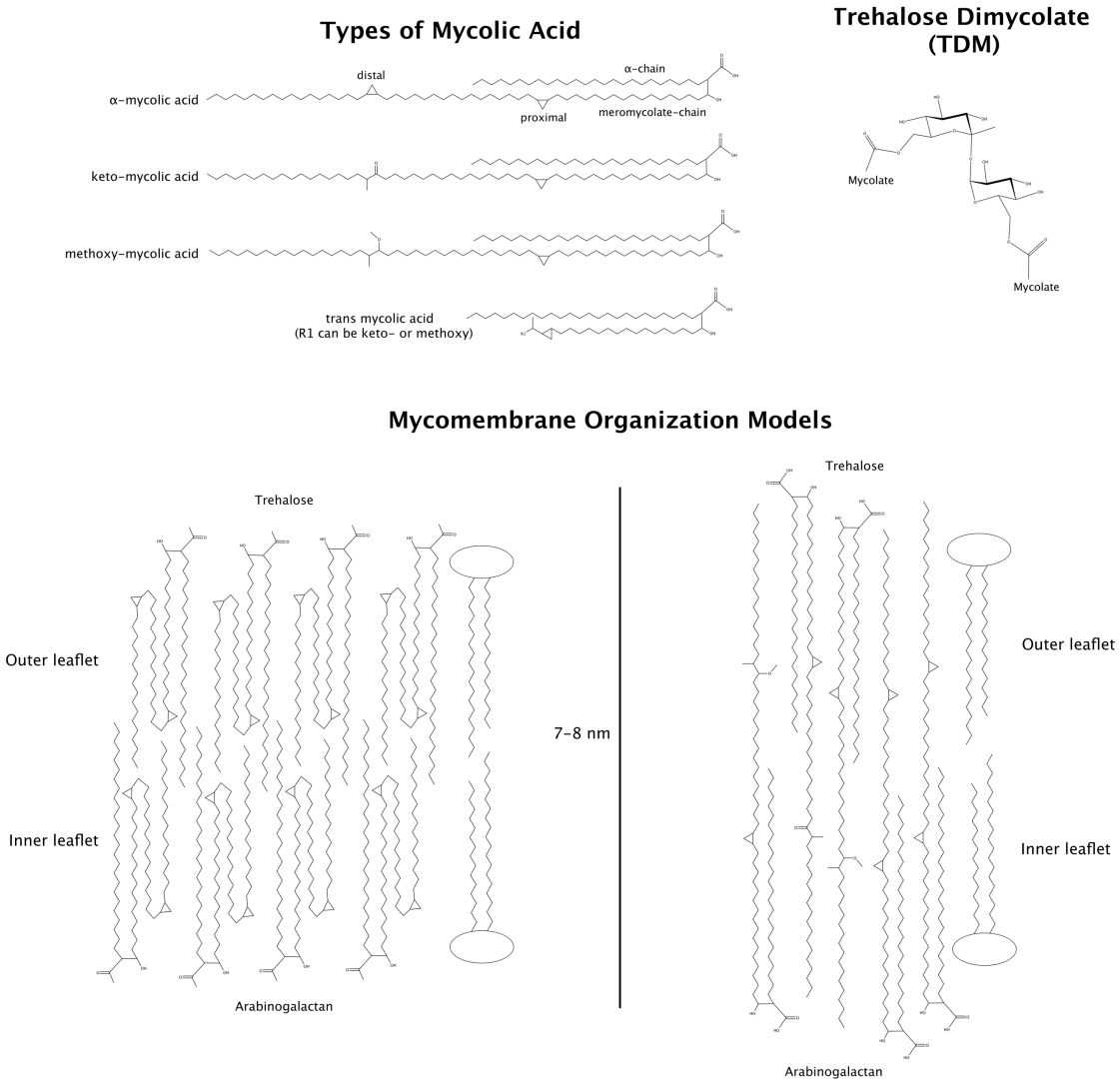

Figure 1.4. Structural features of mycolic acids and the mycomembrane. Mycolic acids are extremely long α-alkyl β-hydroxy fatty acids. The shorter α-chain is unmodified, while the longer meromycolate chain is chemically functionalized with methyl, keto, methoxy, and/or cyclopropane groups. Mycolic acids are the major component of the mycomembrane, where they are primarily esterified to trehalose or the cell wall arabinogalactan. A number of theoretical models have been proposed regarding the organization of mycolic acids within the mycomembrane. These primarily differ in the degree of extension predicted for the meromycolate chain.

Mtb, given that bacteria lacking derivatized mycolic acids are attenuated in *in vivo* infection models (Dubnau et al., 2000; Glickman et al., 2000).

The width of the mycomembrane is only ~7-8 nm wide, a noteworthy observation as this is not significantly larger than the width of the PM. It is nearly universally accepted that mycolic acids are the primary component of the mycomembrane (Jackson, 2014; Minnikin, 1991). Since mycolic acids are so much longer than the carbon chains of typical PM phospholipids, it is surprising that the experimentally-visualized mycomembrane is approximately the same thickness as the PM. This observation has led to a number of models that attempt to reconcile the microscopic observations with the genetic and biochemical data that implicate mycolic acids as being the main component of the mycomembrane. These models primarily differ in the degree to which the long meromycolate chain is predicted to either be in an extended or a bent "W" conformation, and to what extent they are entirely contained within the hydrophobic phase of the mycomembrane (**Figure 1.4**; (Daffe et al., 2017; Hoffmann et al., 2008; Villeneuve et al., 2005)). Regardless of the exact manner in which they are able to pack together to form the mycomembrane, it is clear that mycolic acids are an essential component of the cell envelope.

Mycolic acids play a central structural role in contributing to the impermeability and the hydrophobicity of the mycomembrane (Gebhardt et al., 2007; Jarlier and Nikaido, 1990). When esterified to the terminal Ara*f* residues of the AGP

complex, they constitute the inner leaflet of the mycomembrane (Foley et al., 2016; Minnikin, 1991). They are also found in the outer leaflet, as non-covalently associated glycolipids. The most prevalent and important mycolate-containing glycolipids are trehalose mono- and di-mycolates (TMM/TDM), which consist of the disaccharide trehalose esterified with mycolic acids at the C-6 and/or C-6' positions (**Figure 1.4**; (NOLL et al., 1956). TDM is perhaps the quintessential *Mtb* virulence-associated glycolipid and plays a number of important roles in TB pathogenesis, including granuloma formation (Hunter et al., 2006a; Welsh et al., 2013).

The mycomembrane is also composed of a diverse array of other free lipids, many of which play an important role in survival and persistence in the host. These lipids are predicted to be non-covalently associated in the outer leaflet of the mycomembrane. Pthiocerol dimycocerosate (PDIM) is a virulence-associated cell envelope lipid that has been demonstrated to mask mycobacterial PAMPs, thereby limiting activation of host PRRs (Cambier et al., 2014). Sulfolipids are another class of mycomembrane free lipid that contributes to *Mtb* virulence. Sulfolipids actively antagonize host innate immune receptors, downregulating the host response in favor of Mtb survival (Blanc et al., 2017). Other cell envelope associated lipids, such as long-chain triacylglycerols and mycolate wax esters, contribute to persistence in the host (Wright et al., 2017). Additionally, lipoglycans such as PIM, LM, and LAM have also been observed in the mycomembrane, suggesting that this membrane is highly heterogeneous

(Chiaradia et al., 2017). The preponderance of virulence-associated and immunomodulatory lipids in the mycomembrane highlight this structure as one of the most critical interfaces between the pathogen and host.

The outermost layer of the mycobacterial cell envelope is the capsule, or outer layer (OL). Historically, this layer has been understudied and underappreciated due to the difficulties inherent in examining it. Liquid culture of mycobacteria is routinely performed in the presence of detergents such as Tween-80 to reduce bacterial clumping. Since the OL is only loosely associated with the cell envelope, it is easily dissociated in such conditions (Daffe and Etienne, 1999). Nevertheless, cryo-electron microscopy (cryo-EM) of *M. smegmatis* and *M. marinum* following culture in media lacking detergent has allowed the mycobacterial capsule to be visualized. For these mycobacterial species, the OL appears to be a diffuse layer of approximately 20 nm (Sani et al., 2010). Some capsular contents have been identified via immuno-gold EM. Polysaccharides, such as α-glucans and non-acylated arabinomannan, and glycolipids such as PIMs are prevalent in the OL, consistent with reports that these sugar-containing molecules are the primary constituents of the capsule (Daffe and Etienne, 1999; Ortalo-Magne et al., 1995; Sani et al., 2010). Proteins, notably Type-VII secretion system-associated proteins such as EsxA, are also present in the capsule, although to a lesser extent than polysaccharides. This has functional consequences for the pathogenicity and immunomodulatory capacity of the bacteria (Raffetseder et al., 2019; Sani et al., 2010).

Together, the four regions of the mycobacterial cell envelope comprise a formidable barrier that enables *Mtb* to resist host immune responses and persist in the face of drug treatment. In addition to acting as a passive physical barrier, many cell envelope components directly alter the host immune response. These two roles are foundational to the success of *Mtb* as a pathogen and demonstrate the degree to which *Mtb* has evolved to infect and survive in human hosts. The complex bioactive lipids found in the mycomembrane are perhaps the most distinctive feature of *Mtb* and influence the host-pathogen interaction at multiple levels. These lipids are unique to mycobacteria and require specialized biosynthetic and transport machineries to ensure that they are properly exported out of the cell and integrate into the mycomembrane. These biosynthetic and transport pathways remain incompletely understood, but represent attractive druggable targets. Interfering with these critical physiological processes has the potential to cure TB disease by selectively and specifically killing *Mtb*.

Envelope Lipid Transporters in *Mtb*

The best-characterized family of cell envelope lipid transporters is the **M**ycobacterial **m**embrane **p**rotein **L**arge (MmpL) family of integral membrane transporters. The primary role of the MmpL family is to translocate complex, virulence-associated envelope lipids, and siderophores, across the plasma membrane into the periplasmic space where they are subsequently incorporated into the mycomembrane. The genome of the H37Rv strain of *Mtb* has open reading frames (ORFs) corresponding to 13 MmpL proteins (MmpL1-13) (Cole et

al., 1998; Domenech et al., 2005). The majority of MmpL family members are predicted to be >100-kDa, and to consist of 11-12 transmembrane domains (TMD) and two periplasmic loop domains (D1/2) (Domenech et al., 2005; Krogh et al., 2001; Sandhu and Akhter, 2015). Exceptions include MmpL6, which is truncated to 42-kDa (five TMD), and MmpL13, which comprises two adjacent ORFs, *mmpL13a* and *mmpL13b*, that are predicted to encode proteins of 32-kDa (four TMD) and 50-kDa (seven TMD), respectively (Domenech et al., 2005; Sandhu and Akhter, 2015).

The MmpL family is largely conserved amongst mycobacteria. However, other species of mycobacteria harbor different numbers of MmpL proteins. *M. leprae*, often considered to possess a “minimal” mycobacterial genome as a result of reductive evolution, only has five intact *mmpL* genes (*mmpL3/ 4/ 7/ 10/ 11*), as well as a similarly-split *mmpL13a-b* locus (Eiglmeier et al., 2001; Kapopoulou et al., 2011). These six MmpL proteins likely represent the core set of MmpL transporters, given that they exhibit a high degree of syntenic conservation in both slow growing (e.g. *Mtb*, *M. leprae*, *M. avium*, and *M. marinum*) and rapidly growing mycobacteria (e. g. *M. smegmatis* and *M. abscessus*) (Viljoen et al., 2017). On the other hand, *M. abscessus* possesses up to 31 putative MmpL transporters (Kapopoulou et al., 2011). This illustrates the increased prevalence of genes coding for MmpL transporters in the genomes of rapidly growing, as compared to slow growing, mycobacteria species (Viljoen et al., 2017).

Given *Mtb*'s specialization as a human pathogen, the set of 13 H37Rv *Mtb* MmpL proteins is uniquely interesting from a biomedical perspective. Since H37Rv is the most widely used *Mtb* laboratory reference strain, this context is the most useful in which to investigate MmpL physiology. These transporters, and their substrates, make immense contributions to *Mtb* virulence and pathogenesis in the host. Therefore, gaining insight into how they function is an opportunity to develop new techniques to combat TB disease.

Interestingly, a subset of H37Rv *mmpL* genes (*mmpL1*/ *2*/ *4*/ *5*) are accompanied by accessory *mmpS* (**M**ycobacterial **m**embrane **p**rotein **S**mall; *mmpS1*/ *2*/ *4*/ *5*) open reading frames, which are each predicted to contain one to two TMD (Cole et al., 1998; Krogh et al., 2001). MmpS4 and –S5 proteins have been shown to interact with their cognate MmpL transporters to permit substrate extrusion (Wells et al., 2013). Little is known about the other MmpS proteins and their potential roles in the transport of MmpL substrates. *rv2198c* was initially annotated as *mmpS3* due to partial homology with other *mmpS* genes, though it was not located in an operon with a cognate *mmpL* gene. Recently, MmpS3 was shown to be a component of the mycobacterial division machinery and renamed LamA (Rego et al., 2017).

MmpL Transporters Belong to the RND Protein Superfamily

The MmpL family members have traditionally been categorized as belonging to the **R**esistance, **N**odulation, and cell **D**ivision (RND) superfamily of integral

membrane permeases, based on their topological organization (Domenech et al., 2005; Tekaia et al., 1999). Phylogenetic comparison has further classified the 10 “full-length” MmpLs into two hydrophobe/ amphiphile efflux (HAE) subfamilies of the RND superfamily. MmpL1/ 2/ 4/ 5/ 8/ 10/ 12 belong to the HAE2 family of Gram-positive efflux pumps, while MmpL3/ 7/ 11 belong to the HAE3 archaeal family (Sandhu and Akhter, 2015; Tseng et al., 1999). A similar two-cluster MmpL classification scheme based on predicted topological/ structural motifs was proposed by Chim et al. (Chim et al., 2015). MmpL cluster I comprises MmpL1/ 2/ 4/ 5/ 6/ 7/ 8/ 9/ 10/ 12, and is distinguished by the presence of a predicted docking domain in the periplasmic D2 loop region. MmpL cluster II comprises MmpL3/ 11, and the predicted MmpL13a-b fusion protein. Cluster II possesses a substantial C-terminal cytoplasmic tail domain, but lacks the D2 periplasmic docking domain (**Figure 1.5**). Both proposed classification schemes concur in their classification of MmpL3 and MmpL11 as distinct from the other MmpL transporters.

Many RND family proteins contribute to antibiotic resistance and stress-response in Gram-negative bacteria (reviewed in (Delmar et al., 2014)). The best characterized RND protein is AcrB of *E. coli*. AcrB, along with a membrane fusion protein (MFP) and an outer membrane factor (OMF), functions as a multidrug efflux pump to extrude substrates through the periplasm to the extracellular environment (Dinh et al., 1994; Ma et al., 1993; Okusu et al., 1996; Paulsen et al., 1997; Zgurskaya and Nikaido, 1999).

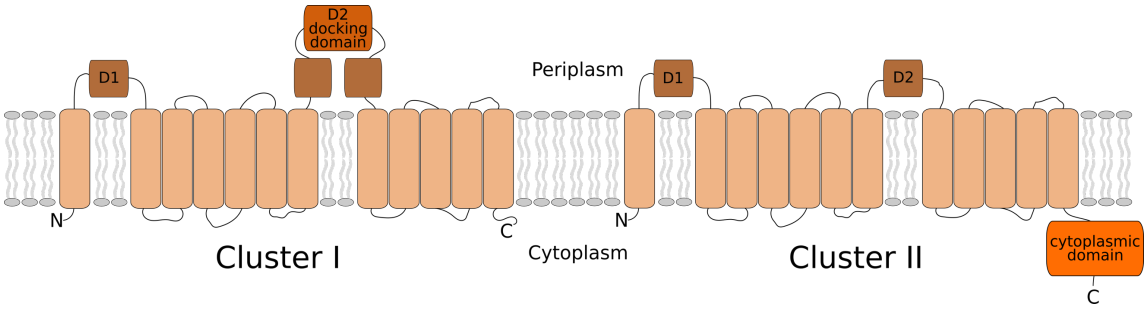

Figure 1.5. *M. tuberculosis* MmpL proteins can be categorized into two clusters based on the complexity of the D2 periplasmic domain and the presence of a cytoplasmic C-terminal domain. Cluster I = MmpL1/ 2/ 4/ 5/ 6/ 7/ 8/ 9/ 10; cluster II = MmpL3/ 11/ 13a/b. *Figure and legend adapted from (Melly and Purdy, 2019).*

The association of RND-MFP-OMF proteins to form an extrusion channel through the periplasm is paradigmatic in Gram-negative bacteria, with notable examples found in *P. aeruginosa* (MexAB/OprM) and *C. metalluridans* (ZneABC) (De Angelis et al., 2010; Pak et al., 2013; Poole et al., 1993; Sennhauser et al., 2009). While *Mtb* exhibits pseudo-Gram-negative membrane organization, it remains to be determined if MmpL proteins interact with periplasmic/ outer membrane proteins to form a similar tripartite export apparatus that would enable efficient translocation and proper localization of their substrates.

Lipoproteins as Potential Transport Adaptor Proteins

Mycobacterial lipoproteins are secreted periplasmic proteins of diverse function. Thus, they may be candidate MFP/ OMF-like proteins and might facilitate MmpL-mediated substrate export through the periplasm. There are 99 putative lipoprotein ORFs in the genome of H37Rv Mtb, representing 2.5% of *Mtb* predicted coding capacity (Sutcliffe and Harrington, 2004).

In general, lipoproteins are characterized by an N-terminal hydrophobic signal sequence of ~20-30 amino acid residues that targets them for secretion and lipidation (Babu et al., 2006; Sutcliffe and Harrington, 2004). Lipoprotein secretion and processing occurs sequentially, and has been thoroughly investigated in both Gram-negative and Gram-positive bacteria (reviewed in (Schneewind and Missiakas, 2014; Tsirigotaki et al., 2017)). Upon translation, the signal sequence directs the nascent unfolded polypeptide to be secreted via the

general secretory pathway (Hayashi and Wu, 1985). Subsequent maturation of the lipoprotein occurs on the periplasmic leaflet of the PM (Wu et al., 1983). Cleavage of the signal peptide, along with lipidation of the new N-terminus at the characteristic “lipobox” motif, results in a mature membrane-anchored lipoprotein that projects into the periplasmic space (Babu et al., 2006; Rezwan et al., 2007).

In mycobacteria, there are two forms of general, signal-peptide mediated secretion pathways, differing in their respective requirement for either the SecA1 or SecA2 secretory ATPase (Braunstein et al., 2001; DiGiuseppe Champion and Cox, 2007). SecA1-dependent secretion is conserved and essential, whereas SecA2 secretion is dispensable (reviewed in (Zulauf et al., 2017)). The SecA2 pathway is known to export substrates that are important for virulence, at least some of which lack a canonical signal sequence (Braunstein et al., 2003; Kurtz et al., 2006; Sullivan et al., 2012). Although some *M. smegmatis* lipoproteins were demonstrated to be secreted via SecA2, most lipoproteins are presumed to be secreted via SecA1-dependent secretion (Gibbons et al., 2007; Zulauf et al., 2017).

Processing of lipoproteins in *Mtb* closely resembles canonical pathways (**Figure 1.6**). The first post-secretory step occurs when the diacylglyceryl transferase Lgt acylates the invariant lipobox cysteine residue. This enzyme covalently attaches diacylglycerol to the cysteine sulfhydryl group via thioether bond, converting the pre-prolipoprotein into a prolipoprotein (Tschumi et al., 2009). The next

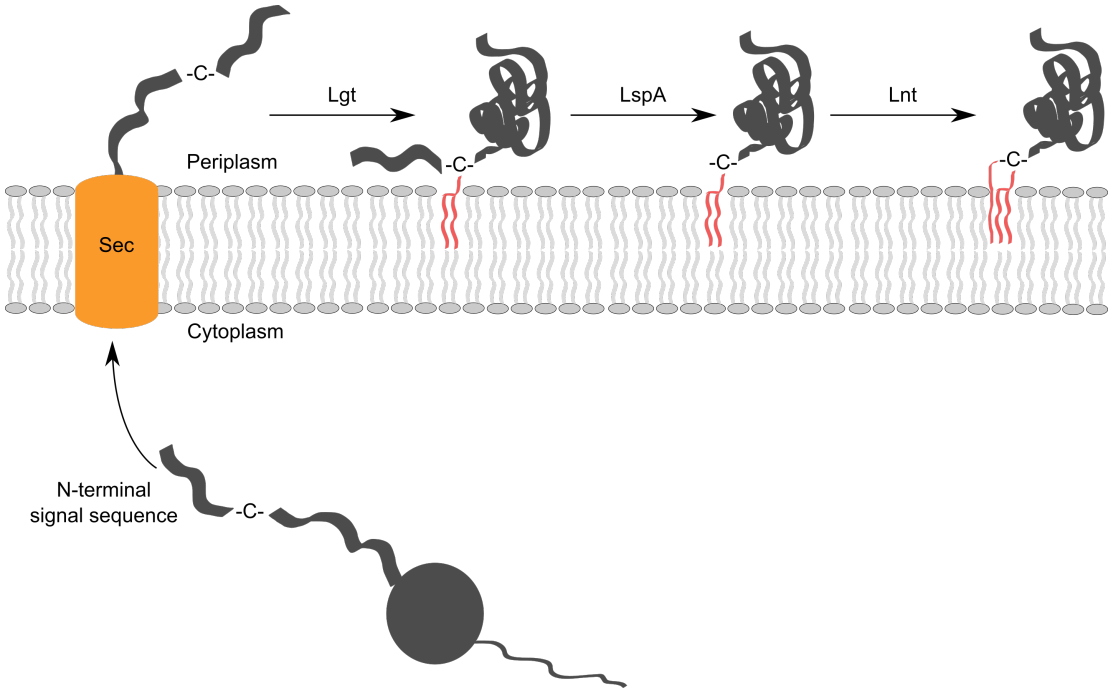

Figure 1.6. Lipoprotein processing in mycobacteria. The N-terminal secretion signal is recognized and the nascent polypeptide is secreted by the general secretory pathway. In the periplasm diacylglyceryl transferase (Lgt) installs a diacylglycerol anchor at the lipobox cysteine residue. Signal peptidase (LspA) cleaves the signal sequence and the new N-terminus is further acylated by the N-acyltransferase domain (Lnt) of Ppm1, generating the mature tri-acylated lipoprotein.

processing step is cleavage of the signal peptide by the signal peptidase LspA, which generates an apolipoprotein (Sander et al., 2004). The final biosynthetic step is accomplished by acylation of the N-terminal amino group by the N-acyltransferase domain (Lnt) of Ppm1, a bifunctional *Mtb* mannosyl/acyltransferase (Tschumi et al., 2012). It is likely that membrane phospholipids are the acyl donors for lipoprotein processing. Accordingly, a C_{16} fatty acid was identified as the N-terminal acylation, while C_{16} and C_{19} (possibly tuberculostearic) fatty acids were identified as the acyl constituents of the thioether-linked diacylglycerol (Tschumi et al., 2009). Therefore, mature mycobacterial lipoproteins are anchored in the PM by their tri-acylated N-termini, and likely project into the periplasm.

Certain lipoproteins are associated with transport of cell envelope components, suggesting that they may be acting as MFPs or OMFs. Notable examples include LprG, which is required for proper surface expression of LAM, and LppX, which is implicated in transport of PDIM (Gaur et al., 2014; Sulzenbacher et al., 2006). However, these lipoproteins have not been shown to interact with any MmpL transporter, as is expected for canonical RND-MFP interactions. MmpS proteins may also be candidate MFPs. Both MmpS4 and MmpS5 interact with their corresponding MmpL4 and MmpL5 transporters, and are required for export of their siderophore substrates (Wells et al., 2013). However, only some MmpL transporters have cognate MmpS proteins, and MmpL-MmpS protein-protein interactions have not been demonstrated for MmpS1 or MmpS2.

Both lipoproteins and MmpS proteins are predicted to be tethered to the PM, by N-terminal lipidation and integral TMDs, respectively. Due to their subcellular localization, they are likely involved with proximal substrate transport, presumably assisting in substrate release and transport through the periplasm. Therefore, these proteins are more likely to function as MFPs rather than OMFs.

Whether MmpL-mediated substrate transport requires the presence of an OMF is unknown. The majority of known MmpL substrates are hydrophobic components of the mycomembrane and are expected to be membrane-permeable. Since OMFs normally provide a pathway for substrate export through the outer membrane, it is unclear whether the presence of an OMF is a requirement for MmpL-mediated transport. Nevertheless, a number of mycobacterial outer membrane proteins have been identified. In *Mtb*, CpnT has been described as an outer membrane porin, and thus may be a putative OMF (Danilchanka et al., 2015; 2014). However, whether CpnT plays a role in substrate export is unknown. In *M. smegmatis*, MspA is an outer membrane porin that is primarily involved with transport of hydrophilic substrates; thus, it is unlikely to be required for transport of bulky, hydrophobic outer membrane lipids (Niederweis et al., 1999; Stahl et al., 2001). Furthermore, since *Mtb* does not have an MspA homologue it is unlikely that this outer membrane porin participates in the conserved pathways of MmpL-mediated substrate transport.

Insights into MmpL Structure and Function

For many years, structural insight into the MmpL family proved elusive. This was due to the inherent difficulty of working with these large, topologically-complex, membrane-bound proteins. However, a number of recent advancements have illuminated how MmpL proteins function as membrane transporters.

Importantly, the crystal structures of the *apo*- and inhibitor bound *M. smegmatis* MmpL3 orthologue were recently reported, representing a critical advancement in the field (Zhang et al., 2019). A concurrent study also obtained a crystal structure of MmpL3 in complex with the membrane phospholipid PE (Su et al., 2019). Both groups found that MmpL3 was monomeric, which was corroborated by native protein electrophoresis. This differs from most known bacterial RND permeases, which typically associate as either homodimers or homotrimers (Kumar et al., 2017; Murakami et al., 2002; Sennhauser et al., 2009). Indeed, a previous structural study of the purified Corynebacterial MmpL3 orthologue CmpL1 via size exclusion chromatography and negative staining electron microscopy (EM) indicated homotrimeric association (Belardinelli et al., 2016). A subsequent MmpL3 structure, modeled on the EM-refined CmpL1 homology model, suggested that *Mtb* MmpL3 also associates as a homotrimer. Additional structures and analyses are needed to reconcile these apparently conflicting observations and determine whether the functional MmpL transporter units differ by species and if all MmpL proteins are monomeric.

The transmembrane region of *apo*-MmpL3 exhibited pseudo-two-fold symmetry, with the central TM4 and TM10 domains hydrogen-bonded to each other via a pair of Asp-Tyr dyads (Zhang et al., 2019). The periplasmic region was observed to contain three openings leading to a central cavity. The opening between TM7 and TM10 is exposed to the outer leaflet of the PM, while the bound PE ligand was observed in the central cavity (Su et al., 2019). This strongly suggests a transport mechanism wherein which MmpL3 takes up lipids from the outer PM leaflet and extrudes them through the central cavity into the periplasm. Interestingly, MmpL3 also demonstrated preferential binding for its physiological substrate TMM, although the precise structural details of this interaction were not ascertained (Su et al., 2019).

Individually, the structure of each periplasmic MmpL3 D1 and D2 subdomain broadly resembled that of the isolated Mtb MmpL11 D2 domain, obtained by Chim et al. (Chim et al., 2015). This work demonstrated homology between the MmpL11 D2 domain and the periplasmic transporter/porter subdomains of the RND permeases MexB and ZneA. Furthermore, the MmpL11 D1 and D2 periplasmic domains were shown to interact with each other. This interaction was also observed for the MmpL3 D1 and D2 periplasmic domains, suggesting that intra- or inter-MmpL interactions occur in the periplasmic space (Chim et al., 2015).

The proton motive force (PMF) is understood to be the underlying energetic basis for most RND-mediated substrate transport (Su et al., 2006; Thanassi et al., 1997; Zgurskaya and Nikaido, 1999). RND proteins generally function as antiporters, coupling proton translocation across the inner membrane to conformational changes that result in substrate extrusion (Murakami et al., 2006; Seeger et al., 2006). A suite of conserved residues found in TM4 and TM10 are critical for proton transfer down the membrane electrochemical gradient (Guan and Nakae, 2001; Murakami and Yamaguchi, 2003; Su et al., 2006). Multiple sequence alignments of the Mtb H37Rv MmpL proteins identified similarly conserved regions in MmpL TM4/10 (Bernut et al., 2016). These include the central Asp/Tyr-containing TM4/10 segments observed in the *M. smegmatis* MmpL3 crystal structure, strongly suggesting that the core of each MmpL monomer is responsible for proton translocation (Zhang et al., 2019). Indeed, mutation of either the TM10 D640 or Y641 residues completely abrogated MmpL3 function (Bernut et al., 2016), while mutation of the homologous Y610 residue likewise resulted in cessation of MmpL11-mediated lipid transport (see Chapter 3). Furthermore, several ostensible chemical inhibitors of MmpL3 appear to function by non-specifically disrupting the PMF (Foss et al., 2016; Li et al., 2014; Williams et al., 2019). Others, including the developmental therapeutic drug SQ109, directly bind MmpL3 in the putative proton translocation channel defined by TM4/10 (Zhang et al., 2019). However, the observation that SQ109 failed to inhibit MmpL3-mediated substrate transport in a spherophast-based assay raises questions about whether this interaction is sufficient to abrogate

MmpL3 transporter activity (Xu et al., 2017). Regardless of the exact mechanism of action of SQ109, the data strongly suggest that MmpL substrate transport is energetically dependent on the PMF, like that of most other RND permeases.

MmpL Proteins Export Substrates that Contribute to Virulence

The mycomembrane is the most critical point of interaction between *Mtb* and the human host. MmpL proteins are essential for generating this unique outer membrane. MmpL-transported lipids are incorporated into both leaflets of the mycomembrane, from which *Mtb* derives much of its intrinsic resistance and immunomodulatory capacity. Thus, MmpL proteins indirectly contribute to *Mtb* virulence and pathogenesis via transport and proper localization of their substrates. Most, but not all, identified MmpL substrates are virulence-associated envelope lipids. Other MmpL substrates are important for responding to environmental and nutrient stress. How MmpL substrates influence *Mtb* virulence is therefore essential for understanding the importance of the MmpL protein family to the pathogenic lifestyle of *Mtb*. The following sections constitute a brief survey of H37Rv *Mtb* MmpL substrates and the manner in which they contribute to *Mtb* virulence and pathogenesis (**Figure 1.7**).

MmpL3 (Rv0206c) transports TMM

MmpL3 is responsible for transporting trehalose monomycolate (TMM), and is the only MmpL for whom transporter activity has been directly demonstrated via biochemical assay (Xu et al., 2017). TMM transport by MmpL3 has also been

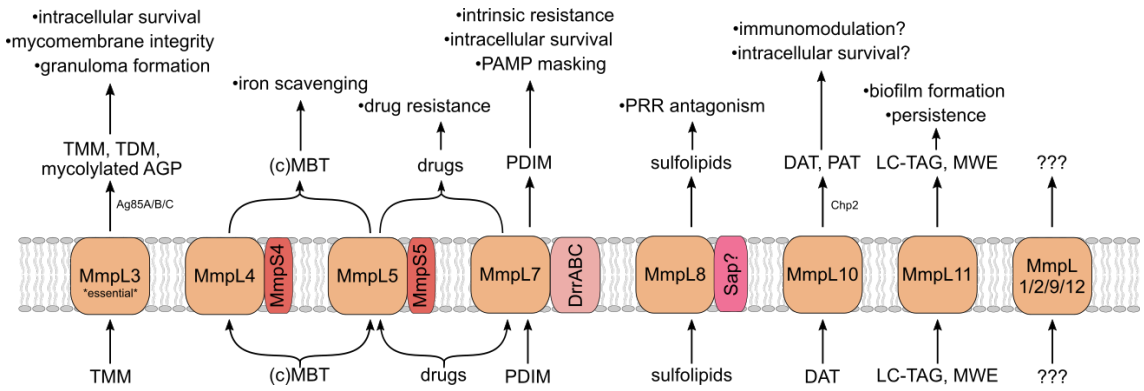

Figure 1.7. MmpL transporters export substrates that are important for virulence and pathogenicity. MmpL proteins and membrane-associated transport partners, exported substrates, and contributions to virulence/pathogenicity of the mature exported substrates. TMM/TDM = trehalose mono/di-mycolate. AGP = arabinogalactan/peptidoglycan complex. (c)MBT = (carboxy)mycobactin. PDIM = phthiocerol dimycocerosate. PAMP = pathogen-associated molecular pattern. PRR = pattern recognition receptor. DAT/PAT = di/poly-acyl trehalose. LC-TAG = long-chain triacylglycerol. MWE = mycolate wax ester. *Figure and legend adapted from (Melly and Purdy, 2019)*.

demonstrated indirectly, based on the observation that genetic or chemical ablation of MmpL3 activity reduces cell envelope mycolylation (Grzegorzewicz et al., 2012; Tahlan et al., 2012).

TMM transport is the primary manner in which mycolic acids are exported to the mycomembrane. Biosynthesis of mycolic acids is initiated in the cytoplasm. The α-chain is generated by **F**atty **A**cid **S**ynthase-I (FAS-I), which primarily produces C_{18}, C_{24} and C_{26} fatty acids (Zimhony et al., 2004). The β–hydroxy-containing carbon chain is referred to as the meromycolate chain and is extremely long (C_{54-56}). It is elongated from FAS-I-generated precursor fatty acids by the so-called FAS-II complex (Slayden and Barry, 2002). The meromycolate chain can contain a variety of chemical modifications, including cyclopropane, methyl/methoxy, and keto functional groups, which contribute to the intrinsic resistance and immunomodulatory capacity of *Mtb* (Dubnau et al., 2000; Yuan et al., 1995; 1998). Condensation of the α- and the meromycolate chains generates a mature α-alkyl β–hydroxy mycolic acid molecule, which can then be appended to the trehalose disaccharide, forming TMM.

Once exported, mycolic acid transfer in the cell envelope is catalyzed by the members of the secreted antigen 85 mycolyltransferase complex (Ag85A/ B/ C) (Backus et al., 2014; Belisle et al., 1997; Kremer et al., 2002). When esterified to the non-reducing ends of the cell wall AGP core, mycolic acids constitute the inner leaflet of the mycomembrane (Foley et al., 2016; Hoffmann et al., 2008;

Minnikin, 1991). Additionally, mycolic acid transfer between molecules of TMM generates trehalose dimycolate (TDM), the abundant and important virulence-associated free lipid (Backus et al., 2014; Belisle et al., 1997; Kremer et al., 2002).

Genetic approaches to knock out *mmpL3* have been uniformly unsuccessful; however, conditional knockdown and chemical inhibition strategies revealed that reduction or inhibition of MmpL3 caused accumulation of TMM in the cytoplasm and a reduction of cell envelope mycolylation (Degiacomi et al., 2017; Domenech et al., 2005; Grzegorzewicz et al., 2012; Li et al., 2016; Varela et al., 2012). MmpL3 is therefore the only essential MmpL protein, underscoring the importance of mycolic acid export to *Mtb* physiology. These observations also highlight MmpL3 as an attractive drug target (Li et al., 2016; 2018).

Apart from their importance to the covalently-anchored inner leaflet of the mycomembrane, mycolic acids are also an essential component of TDM (Hunter et al., 2006a; Welsh et al., 2013). TDM was originally described as a “cord factor,” referring to the tendency of mycobacteria harboring TDM to aggregate about their long axes to form “cords” of bacteria (BLOCH, 1950; NOLL et al., 1956). It plays an extremely important role in the infectious context by promoting *Mtb* survival in the macrophage by inhibiting phagosomal maturation via recruitment of the host PRR Mincle during Fcγ-R mediated phagocytosis (Patin et al., 2017). Furthermore, purified TDM induces granuloma formation, also in a

Mincle-dependent manner (Baba et al., 1997; Bowdish et al., 2009; Hamasaki et al., 2000; Hunter et al., 2006b; Ishikawa et al., 2009).

MmpL7 (Rv2942) transports PDIM

MmpL7 is associated with transport of phthiocerol dimycocerosates (PDIM), a family of long-chain β-diols esterified with polymethyl-branched fatty acids (Cox et al., 1999). Interestingly, PDIM translocation is also dependent on the DrrABC (Rv2936-8) transporter in addition to MmpL7, a unique requirement for the transport of MmpL substrates (Camacho et al., 2001). Once exported into the periplasm, the proper surface localization of PDIM is mediated by the lipoprotein LppX (Rv2945c), potentially via a direct protein-lipid interaction (Sulzenbacher et al., 2006).

The genes responsible for PDIM biosynthesis and transport are clustered together in the *Mtb* genome (Camacho et al., 1999). PDIM production occurs in the cytoplasm, and is likely spatially and temporally coordinated with MmpL7-mediated transport (Jain and Cox, 2005; Trivedi et al., 2005). This model was suggested by an observed protein-protein interaction between the D2 domain of MmpL7 and the PDIM biosynthetic polyketide synthase PpsE (Rv2935) in a two-hybrid system (Jain and Cox, 2005). This was initially surprising, given that the D2 domain was expected to be periplasmic, while PpsE is cytoplasmic. However, subsequent homology modelling based on the observed MmpL3 crystal structure

indicates that MmpL7 D2 is potentially cytoplasmic, thus reconciling the observed interaction with PpsE (Purdy Lab, unpublished data).

MmpL7 is required for virulence in mouse models of infection due to its role in PDIM transport (Domenech et al., 2005; Lamichhane et al., 2005). PDIM plays multiple roles in the virulence of *Mtb*. The highly hydrophobic nature of PDIM limits the permeability of the *Mtb* cell envelope and contributes to intrinsic resistance against antimicrobial compounds (Camacho et al., 2001; Rousseau et al., 2004). PDIM also promotes the uptake of Mtb by permissive macrophages and appears to enable phagosomal escape upon internalization (Astarie Dequeker et al., 2009; Augenstreich et al., 2017; Cambier et al., 2014; Lerner et al., 2018; Quigley et al., 2017). Additionally, PDIM contributes to *Mtb* virulence by masking the recognition of pathogen-associated molecular patterns by host innate immune receptors (Cambier et al., 2014).

MmpL8 (Rv3823c) transports sulfolipids

MmpL8 transports a unique class of sulfated glycolipids collectively referred to as sulfolipids (Converse et al., 2003; Domenech et al., 2004). Sulfolipids consist of a sulfated trehalose tetra-acylated with both straight chain and multiple polymethyl-branched fatty acids (Goren et al., 1976; Kumar et al., 2007). The diacylated SL_{1278} precursor is synthesized in the cytoplasm through the sequential esterification of sulfated trehalose with palmitate and (hydroxy)phthioceranoate by the polyketide synthase-associated proteins PapA2 (Rv3820c) and PapA1

(Rv3824c), respectively (Kumar et al., 2007). Two subsequent (hydroxy)phthioceranoate additions are performed by the cytoplasmic membrane-associated acyltransferase Chp1 (Rv3822) to generate mature tetra-acylated sulfolipid-1 (SL-1), which is then transported by MmpL8 (Seeliger et al., 2012). The integral membrane protein Sap (Rv3821), while not absolutely required for SL-1 transport, appears to enhance surface expression of SL-1. It is suggested that Sap interacts with MmpL8 and the sulfolipid biosynthetic enzymes to coordinate biosynthesis and transport (Seeliger et al., 2012).

Sulfolipids contribute to *Mtb* virulence by inhibiting activation of the host pattern recognition receptor TLR2, thereby limiting the innate immune response to *Mtb* infection (Blanc et al., 2017). This immunomodulation is contingent upon proper localization of sulfolipids in the mycobacterial cell envelope. MmpL8-deficient *Mtb* exhibits attenuated growth and reduced virulence in mouse infection models (Converse et al., 2003; Domenech et al., 2004; 2005; Lamichhane et al., 2005).

MmpL10 (Rv1183) transports acylated trehaloses

MmpL10 translocates diacyltrehaloses (DAT) across the plasma membrane, where they are further acylated to generate penta-acyltrehaloses (PAT) (Belardinelli et al., 2014). DAT biosynthesis is initiated in the cytoplasm by the esterification of a straight chain fatty acid to the 2-position of trehalose by the acyltransferase PapA3 (Rv1182), which is likely also responsible for incorporation of a polymethyl-branched fatty acid at the 3-position (Hatzios et al.,

2009). MmpL10-mediated transport of DAT to the periplasm allows the transfer of additional polymethyl-branched fatty acid moieties between DATs by the periplasmic acyltransferase Chp2 (Rv1184c) to generate PAT (Belardinelli et al., 2014). The topological discontinuity of PAT biosynthesis is reminiscent of TDM biosynthesis, with transport of a cytoplasmic precursor to the periplasm where extracellular enzymes generate the mature cell envelope lipid.

The contribution of DAT/PAT to *Mtb* virulence is not completely understood. Purified DAT inhibits T-cell proliferation and production of proinflammatory cytokines by macrophages *in vitro* (Lee et al., 2007), however MmpL10 did not appear to contribute to *Mtb* virulence in a mouse aerosol infection model, implying that its substrates are dispensable for a typical *Mtb* infection (Domenech et al., 2005). Another study found that an *mmpL10* mutant was attenuated in an intravenous mouse infection (Lamichhane et al., 2005). Perplexingly, a different study showed that a DAT/PAT-deficient strain of *Mtb* more readily infected macrophages and was hypervirulent in an intravenous, but not a respiratory, mouse infection model (Rousseau et al., 2003). Finally, a recent study found that an *Mtb* DAT/PAT mutant was attenuated only in the absence of PDIM, leading the researchers to conclude that these methyl-branched cell envelope lipids may be functionally redundant (Passemar et al., 2014).

MmpL11 (Rv0202c) transports LC-TAG and MWE

MmpL11 transports long-chain triacylglycerols (LC-TAG) and mycolate wax esters (MWE) in *Mtb* (Wright et al., 2017). These lipids are of particular importance during biofilm formation. Since *Mtb* in biofilms is phenotypically drug tolerant, LC-TAG and MWE may contribute to the extensive drug treatment regimens necessary to cure TB disease (Ojha et al., 2008). Furthermore, these lipids may play a role in persistence in the host. *Mtb mmpL11* mutants are attenuated for survival in an *in vitro* granuloma model and during long-term infections in mice, suggesting that MmpL11 lipid substrates are required for the maintenance of long-term *Mtb* infection (Domenech et al., 2005; Lamichhane et al., 2005; Wright et al., 2017).

MmpL4 and MmpL5 transport siderophores

MmpL4 and MmpL5 are unique in that they do not transport a cell envelope lipid, but instead export mycobacterial siderophores. Iron is critical for many cellular processes and iron restriction is a common host strategy to combat infection. *Mtb* produces two siderophores to scavenge iron from the environment: lipophilic mycobactin (MBT) and hydrophilic carboxymycobactin (cMBT). The MmpL4/ 5 transporters (Rv0450c/ 0676c) and their cognate MmpS4/5 accessory proteins (Rv0451c/ 0677c) coordinate biosynthesis and transport of these siderophore substrates (Wells et al., 2013). MmpL4 and MmpL5 are at least partially redundant, given that single mutants of either *mmpS4* or *mmpS5* are not affected in iron-limited culture conditions. However, an *mmpS4/ 5* double mutant exhibited

a significant growth defect in low-iron culture, failed to produce and export siderophores, and was markedly less virulent in a mouse infection model compared to wild-type *Mtb* (Wells et al., 2013). Interestingly, a genetic method in the same study showed that MmpL5 was capable of interacting with either MmpS4 or MmpS5, whereas MmpL4 was only capable of interacting with MmpS4.

Siderophore export likely depends on MmpL/ MmpS interactions in the periplasm. For MmpL4, this was suggested by the fact that the MmpL4 D1 periplasmic region co-precipitates with the periplasmic region of MmpS4 (Wells et al., 2013). Another group demonstrated, via molecular dynamics simulations, that MBT is taken up from the cytoplasm by MmpL5, and that the periplasmic interaction between MmpL5 and MmpS5 was likely required for MBT release into the periplasm (Sandhu and Akhter, 2017). While *in vitro* models of iron sensitivity have suggested that the MmpL/ S4 and S5 systems are functionally redundant, an *mmpl4* single mutant was attenuated in a mouse model of infection (Domenech et al., 2005). However, another group observed growth attenuation of *mmpL5* mutants in the lungs of infected mice after intravenous inoculation (Lamichhane et al., 2005). Interestingly, the same study reported a reduction in *mmpL4* mutant growth in the spleen compared to wild-type *Mtb*. Combined, these observations imply that the two different siderophore export systems have differing levels of importance depending on the infection context.

Other MmpL transporter substrates are unidentified

The substrates and function of the *Mtb* MmpL1/ 2/ 6/ 9/ 12/ 13ab transporters have not yet been conclusively identified. However, these transporters are not as critical as the aforementioned MmpL for virulence of *Mtb* as assessed by the mouse model of infection (Domenech et al., 2005). Nevertheless, some clues as to the functions of these transporters can be derived from the genomic contexts of their loci, and through comparison with orthologous proteins in other mycobacterial species.

The genes encoding MmpL1 (Rv0402c) and MmpL12 (Rv1522c) are both located near *pks* and *fad* genes, implying that they transport complex glyco- or polyketide lipids similar to TMM or PDIM (Kapopoulou et al., 2011). Indeed, the exported substrate of MAB_0855, a putative *M. abscessus* orthologue of MmpL12, was recently identified as a glycosyl diacylated nonadecyl diol, suggesting that the substrate of MmpL12 in *Mtb* is a heretofore undescribed complex cell envelope glycolipid (Dubois et al., 2018).

Very little is known about MmpL2 (Rv0507). The genomic context of the *mmpL2* gene does not give any clues as to the nature of its putative substrate. MmpL2 is dispensable during pulmonary models of infection, and there are conflicting reports regarding its relevance during intravenous infection (Camacho et al., 1999; Domenech et al., 2005; Lamichhane et al., 2005). MmpL9 (Rv2339) is similarly mysterious. It appears to be involved in the inhibition of phagosomal

maturation; however, loss of this capability did not impact the survival of a Δ*mmpL9* mutant strain of *Mtb* in *ex vivo* infections (MacGurn and Cox, 2007). Another study observed increased susceptibility of an *mmpL9* mutant to *in vitro* oxidative stress (Mestre et al., 2013). Despite these observations, *mmpL9*-deficient Mtb is still able to replicate effectively in mouse infection models (Domenech et al., 2005; Lamichhane et al., 2005).

MmpL13a/ b (Rv1145/ 1146) is a unique case. An intact full-length MmpL13 orthologue is found in both *M. bovis* and *M. canettii*, suggesting that a gene split occurred during the evolution of modern *Mtb* (Sandhu and Akhter, 2015). Interestingly, these genes appear to be separate, functional ORFs in H37Rv *Mtb*, whereas they are pseudogenes in *M. leprae*, implying that the *mmpL13* gene is currently undergoing a pseudogenization process in modern *Mtb*.

MmpL6 is truncated relative to the other MmpLs in H37Rv *Mtb*. This likely occurred during the evolution of modern circulating *Mtb* strains, during which its cognate *mmpS6* gene was completely lost (Brosch et al., 2002). A recent paper demonstrated that an un-truncated “ancestral” version of the *mmpL/ S6* operon conferred oxidative stress resistance to “modern” *Mtb* lineages (Arumugam et al., 2018). However, it is not known whether this increased resistance is linked to substrate export or to some other mechanism. Production of reactive oxygen species is a well-described defense mechanism of innate immunity (Ehrt and

Schnappinger, 2009). Thus, it is somewhat perplexing how this ostensibly beneficial mediator of intrinsic resistance was lost during *Mtb*-host co-evolution.

Some MmpLs can function as drug exporters

In addition to transporting their endogenous cell envelope or siderophore substrates, certain MmpL transporters may also act as drug efflux pumps. This has been most convincingly shown for the MmpL/ S5 transporter system in both *Mtb* and nontuberculous mycobacteria (NTM). Increased resistance to azole drugs, as well as to clofazimine and bedaquiline, can arise through mutations in *rv0678*, a transcriptional repressor that inhibits expression of *mmpL5/ S5* (Hartkoorn et al., 2014; Milano et al., 2009). Altering the repressive ability of Rv0678 results in overexpression of *mmpL5/ S5* and resistance to the aforementioned drugs via drug efflux. Similarly, mutations in the transcriptional repressor of an MmpL5/ S5 orthologue also augmented resistance to clofazimine and bedaquiline in the clinically important NTM species *M. abscessus* (Richard et al., 2019). De-repression of a different MmpL5/ S5 orthologue in *M. abscessus* likewise conferred increased resistance to thioacetazone-based chemotherapeutics (Halloum et al., 2017). In addition to MmpL5/ S5, MmpL7 has also been implicated in drug efflux. The upregulated expression of *mmpL7* in response to isoniazid treatment increases mycobacterial resistance to this important frontline TB antibiotic through direct export (Pasca et al., 2005; Rodrigues et al., 2012).

Transcriptional Regulation of MmpL Transporters

A number of transcriptional regulators that bind to *mmpL* genomic regions have been identified via ChIP-seq (Galagan et al., 2013). These include Rv0302, Rv1816, and Rv3249c. Further studies revealed that these transcriptional regulators modulate their activity by binding fatty acid ligands, implying that *Mtb* alters its cell wall in response to metabolic cues (Chou et al., 2015; Delmar et al., 2015; Jain et al., 2007; Lee et al., 2013; Radhakrishnan et al., 2014). This is particularly relevant during infection because *Mtb* metabolizes fatty acids in the host (Lee et al., 2013; McKinney et al., 2000). Rv0302 is a TetR-family transcriptional regulator that binds in the intragenic regions of *mmpL1/ 2/ 7/ 9*, upstream of *mmpL3* and in the promoters of *mmpL6* and *mmpL11* (Chou et al., 2015; Galagan et al., 2013). Upon binding palmitic acid, the Rv0302 dimer dissociates from its target DNA (Chou et al., 2015). Rv3249c is also a TetR-like transcription factor that binds the promoters of *mmpS1* and *mmpL3*, and inside *mmpL11*. It also releases from its target DNA sequences upon binding palmitic acid (Delmar et al., 2015). Rv1816 binds to promoter and intergenic regions of *mmpL3*, *mmpL7* and *mmpL11* (Delmar et al., 2015). Additionally, it binds *kasA*, which is involved in mycolic acid biosynthesis (Slayden and Barry, 2002). Thus, Rv1816 represents a single point of control at which production of cell envelope components may be transcriptionally regulated. Rv1816 binds two fatty acid ligands, lauric acid and palmitic acid; however, palmitic acid was the only ligand that reduced DNA binding activity (Delmar et al., 2015). Rv0678 is a member of the MarR family of transcriptional regulators that binds the promoter regions of

mmpL2, *mmpL4/ S4*, and *mmpS5* as a dimer (Radhakrishnan et al., 2014). The binding of 2-stearoylglycerol by Rv0678 reduced its ability to interact with target sequences (Radhakrishnan et al., 2014).

Combined, these observations suggest that *Mtb* monitors its metabolic state and adjusts its cell envelope composition in response to metabolic cues. This would presumably enable *Mtb* to better persist in the face of the host immune response during the course of establishing an infection.

Post-translational Regulation of MmpL Transporters

MmpL transporter function may also be regulated through post-translational modification. A likely means of MmpL regulation is via phosphorylation by serine/threonine protein kinases (STPKs). Mtb has 11 STPKs, nine of which contain a cytoplasmic kinase domain, a transmembrane domain, and an extracellular sensor domain (reviewed in (Prisic and Husson, 2014)). STPK-mediated phospho-regulation of protein function is therefore an immediate way to alter cellular processes in response to external stimuli.

MmpL7 is a potential substrate of the PknD kinase (Pérez et al., 2006). The identified phospho-residues were initially predicted to be periplasmic, however subsequent structural insight has suggested that the domain containing the target residues may be cytoplasmic and thus capable of acting as a substrate for

the intracellular kinase domain of PknD. Whether phosphorylation affects MmpL7 transporter function has not yet been determined.

MmpL3 and MmpL11 may also be regulated via phosphorylation. Both have substantial C-terminal cytoplasmic domains that are likely sites of phospho-regulation by mycobacterial STPKs. Indeed, both MmpL3 and MmpL11 were found to be phosphorylated in a comprehensive survey of *Mtb* phospho-proteins (Prisic et al., 2010). MmpL3 has extensive C-terminal phosphorylation, with multiple phospho-residues identified in a variety of culture and *in vitro* stress conditions. Intriguingly, the MmpL11 C-terminus was only phosphorylated at a single residue when grown with acetate as the sole carbon source, suggesting that phosphorylation of MmpL proteins occurs in response to metabolic cues (Prisic et al., 2010). Investigating the effects of phosphorylation on MmpL transporter activity will likely prove to be a fecund area for future research. Characterization of MmpL11 phosphorylation and attendant impacts on lipid transport is discussed in Chapter 3.

CHAPTER 2

STRUCTURAL AND FUNCTIONAL EVIDENCE THAT LIPOPROTEIN LPQN SUPPORTS CELL ENVELOPE BIOGENESIS IN *M. TUBERCULOSIS*

Geoff C. Melly[1], Haley Stokas[1], Jennifer L. Dunaj[1], Fong Fu Hsu[2], Malligarjunan Rajavel[3], Chih-Chia Su[3], Edward W. Yu[3] and Georgiana E. Purdy[1]

[1]Oregon Health & Science University, Department of Molecular Microbiology & Immunology, Portland, OR, 97239, United States

[2]Department of Internal Medicine, Mass Spectrometry Resource, Division of Endocrinology, Diabetes, Metabolism, and Lipid Research, Washington University School of Medicine, St. Louis, MO 63110

[3]Case Western Reserve University, Department of Pharmacology, Cleveland, OH, 44106, United States

Contributions: **Figures 2.5** and **2.6** were generated by F.-F. Hsu; **Table 2.4**, and **Figures 2.7** and **2.8** were generated by M. Rajavel, C.-C. Su, and E. Yu.

This manuscript was accepted for publication by the *Journal of Biological Chemistry* in August 2019 (Melly et al., 2019).

ABSTRACT - The mycobacterial cell envelope is crucial to host-pathogen interactions as a barrier against antibiotics and the host immune response. In addition, cell envelope lipids are mycobacterial virulence factors. Cell envelope lipid biosynthesis is the target of a number of frontline TB treatments, and has been the focus of much research. However, the transport mechanisms by which these lipids reach the mycomembrane remain poorly understood. Many envelope lipids are exported from the cytoplasm to the periplasmic space via the Mycobacterial membrane protein Large (MmpL) family of proteins. In other bacteria, lipoproteins can contribute to outer membrane biogenesis through direct binding of substrates and/or protein-protein associations with extracytoplasmic biosynthetic enzymes. In this report, we investigate whether the lipoprotein LpqN plays a similar role in mycobacteria. Using a genetic two-hybrid approach, we demonstrate that LpqN interacts with periplasmic loop domains of the MmpL3 and MmpL11 transporters that export mycolic acid-containing cell envelope lipids. We observe that LpqN also interacts with secreted cell envelope biosynthetic enzymes such as Ag85A via pull-down assays. The x-ray crystal structures of LpqN and LpqN bound to dodecyl-trehalose suggest that LpqN directly binds trehalose monomycolate, the MmpL3 and Ag85A substrate. Finally, we observe altered lipid profiles of the Δ*lpqN* mutant during biofilm maturation, pointing toward a possible physiological role for the protein. The results of this study suggest that LpqN may act as a membrane fusion protein, connecting MmpL transporters with periplasmic proteins, and provide general insight into the role of lipoproteins in *Mycobacterium tuberculosis* cell envelope biogenesis.

INTRODUCTION

Mycobacterium tuberculosis (*Mtb*) is the causative agent of the human disease tuberculosis (TB). TB is one of the most devastating human diseases, and it remains a major public health concern. In 2017, there were approximately 10 million new cases and 1.3 million deaths due to TB (World Health Organization, 2018). The cell envelope of *Mtb* is a waxy, lipid-rich structure that acts as a robust physical barrier to host antimicrobial defenses and antibiotics. This intrinsic resistance is largely conferred by mycolic acids, extremely long chain ($C_{60\text{-}90}$) α-alkyl-β-hydroxy fatty acids that are major constituents of the mycobacterial cell envelope (Barry et al., 1998). Mycolic acids and their derivatives form an outer layer analogous to the outer membrane of Gram-negative bacteria, termed the mycomembrane. The mycomembrane consists of an inner leaflet of mycolylated arabinogalactan (AG) anchored to peptidoglycan (the mAGP complex) and an outer leaflet of predominantly mycolylated free lipids (Chiaradia et al., 2017; Marrakchi et al., 2014). In addition to acting as a passive physical barrier, certain cell envelope components can directly interfere with host immune responses (Blanc et al., 2017; Cambier et al., 2014). Therefore, the *Mtb* cell envelope plays a crucial role at the host-pathogen interface to promote bacterial survival.

The biogenesis of the mycobacterial cell envelope is complex and incompletely described. One class of proteins involved in transport of cell envelope

components is the Mycobacterial membrane protein Large (MmpL) family. The MmpLs are polytopic membrane proteins that mediate transport of large hydrophobic substrates from the cytoplasm of the bacterium to the periplasmic space, where they are subsequently incorporated into the cell envelope (Chalut, 2016; Melly and Purdy, 2019; Viljoen et al., 2017). The MmpLs are considered members of the resistance-nodulation-cell division (RND) superfamily of membrane transporters that typically couple the proton motive force (PMF) to export of their substrates (Domenech et al., 2005; Owens et al., 2013; Ruggerone et al., 2013). A subset of MmpLs (MmpL1/2/4/5) are accompanied in the genome by genes encoding mycobacterial membrane protein small (MmpS) proteins (Cole et al., 1998) that are predicted to contain 1-2 transmembrane segments and are likely involved in substrate transport by their cognate MmpL protein.

The substrates of a number of MmpL transporters have been identified. Of particular interest are those MmpL proteins that transport mycolic acid-containing lipids. Most importantly, MmpL3 (Rv0206c) transports trehalose monomycolate (TMM) into the periplasmic space (Grzegorzewicz et al., 2012). There, mycolic acid transfer catalyzed by members of the antigen 85 (Ag85) enzyme complex generates the free lipid trehalose dimycolate (TDM) and AG-anchored mycolic acids, which together form the mycomembrane (Backus et al., 2014; Belisle et al., 1997; Grzegorzewicz et al., 2012). MmpL3 is therefore an essential *Mtb* protein, due to the central role of mycolic acids in mycobacterial physiology

(Degiacomi et al., 2017; Li et al., 2016). Another important MmpL transporter is MmpL11 (Rv0202c), which we showed exports species-specific mycolic-acid containing storage lipids such as the mycolate wax ester (MWE) and long-chain triacylglycerols (LC-TAGs) in *Mtb* and meromycolyl diacylglycerol in M. smegmatis (Pacheco et al., 2013; Wright et al., 2017). These lipids are important for *Mtb* persistence, since MmpL11-deficient *Mtb* exhibit attenuated survival during *in vitro* and *in vivo* models of infection and in an *in vitro* model of dormancy (Domenech et al., 2005; Wright et al., 2017).

Many of the insights into MmpL transporter function have been gleaned from comparison to other protein members of the larger RND transporter superfamily. RND superfamily proteins are primarily associated with antibiotic resistance and stress-response in Gram-negative bacteria (reviewed in (Delmar et al., 2014)). They typically function in concert with a membrane fusion protein (MFP) and an outer membrane factor (OMF) to form a tripartite export apparatus that extrudes substrates through the periplasm directly to the extracellular environment (Dinh et al., 1994; Ma et al., 1993; Okusu et al., 1996; Paulsen et al., 1997; Zgurskaya and Nikaido, 1999). While *Mtb* exhibits pseudo-Gram-negative membrane organization, it remains to be determined if the MmpLs interact with periplasmic and outer membrane proteins to form a similar tripartite pump that would enable efficient translocation and proper localization of their substrates. Some secreted lipoproteins direct the proper localization of virulence-associated lipids within the cell envelope, suggesting that these proteins may be functioning as MFPs in *Mtb*.

Notably, translocation of phthiocerol dimycocerosate (PDIM) to the mycomembrane depends on the lipoprotein LppX, presumably through direct binding of PDIM by LppX (Sulzenbacher et al., 2006). Similarly, the lipoprotein LprG binds both the virulence-associated glycolipid lipoarabinomannan and triacylglycerides, and is required for translocation of these substrates to the cell envelope (Martinot et al., 2016). Furthermore, LprG interacts with the Ag85A mycolyltransferase, implicating this lipoprotein in the transmycolylation processes that generate the mycomembrane (Touchette et al., 2017). The MmpS proteins are also candidate MFPs, given that MmpS4/5 interact with their cognate MmpL4/5 partners and are required for transport of their siderophore substrates (Sandhu and Akhter, 2017; Wells et al., 2013). However, only a minority of MmpL transporters have cognate MmpS proteins (MmpS1/2/4/5), and MmpL-MmpS protein-protein interactions have not been demonstrated for MmpS1/2. This raises the possibility that there are unidentified *Mtb* proteins that function as quasi-MFPs to assist in delivering MmpL-transported lipids through the periplasm to their cell envelope destinations.

We sought to identify proteins that might function as MFPs with MmpL3 and MmpL11. Using genetic methods, we identified the secreted lipoprotein LpqN (Rv0583c) as a periplasmic interacting partner of both MmpL3 and MmpL11. Biochemical and genetic studies suggested that LpqN may also associate with members of the Ag85 enzyme complex, and plays a role in cell envelope lipid changes during biofilm maturation. These results suggest that LpqN may function

as an MFP of MmpL3/11. This model is supported by the crystal structures of *apo*- and lipid-bound LpqN reported herein.

RESULTS

LpqN interacts with D2 loops of mycolate lipid transporters MmpL3 and MmpL11 - MmpL3 and MmpL11 are structurally similar and categorized into the Hydrophobe/Amphiphile Efflux-3 (HAE3) subfamily of the larger RND transporter superfamily (Tseng et al., 1999). They possess two periplasmic loop domains, termed D1 and D2, as well as a cytosolic C-terminal domain (Chim et al., 2015). The D1, D2, and C-terminal domains are therefore the most likely regions of interaction between MmpL11 and biosynthetic enzymes or other transport machinery. To identify periplasmic proteins that interact with $MmpL11_{TB}$, we used the mycobacterial protein fragment complementation (M-PFC) system (Singh et al., 2006). In this two-hybrid system, the “bait” and “prey” are expressed independently as fusion proteins with two fragments of the murine dihydrofolate reductase (DHFR [F1,2] and DHFR [F3]). Functional reconstitution by two interacting mycobacterial proteins when expressed in *M. smegmatis* results in trimethoprim resistance. Integrative plasmids were constructed containing D1 and D2 domains in-frame with the DHFR [F3] fragment and then transformed into *M. smegmatis* to generate a “bait” strain. An H37Rv *Mtb* “prey” library of over 10^6 independent clones was generated in pUAB300. Clones encoding putative proteins that interact with $MmpL11_{TB}$ were obtained by transforming the library

constructs into the *M. smegmatis* “bait” strain and selecting for trimethoprim resistance. Ultimately, no positive clones were identified using the D1 domain. Using the D2 construct, we isolated 2 independent clones that contained a DHFR [F1,2]-LpqN fusion. LpqN was the only positive clone identified using the MmpL11 D2 domain as bait. This suggests that LpqN (Rv0583c) interacts with the periplasmic D2 domain of $MmpL11_{TB}$.

MmpL11 and MmpL3 are topologically similar conserved transporters of mycolic acid-containing lipids. Therefore, we theorized that LpqN might interact with the periplasmic domains of MmpL3 as well. To address this and validate our initial M-PFC screen, we assessed the interactions between the MmpL3 and MmpL11 periplasmic D1 and D2 loops with LpqN using a directly-cloned (non-library) LpqN “prey” construct, which contained the soluble domain of LpqN fused to DHFR [F1,2]. We found that the D2, but not the D1, loops of both MmpL3 and MmpL11 conferred trimethoprim resistance when co-expressed with LpqN (**Table 2.1**). These results suggest that LpqN interacts with the D2 periplasmic regions of both MmpL3 and MmpL11.

To verify the interaction between LpqN and MmpL11 *in vivo*, we heterologously expressed affinity-tagged *Mtb* protein in *M. smegmatis*. While both proteins were successfully expressed, we were unfortunately unable to co-purify LpqN with MmpL11 in the absence or presence of crosslinking (**Figure 2.1**).

Table 2.1. M-PFC assessed via trimethoprim minimal inhibitory concentrations (MICs) of MmpL3/11$_{TB}$ D1 and D2 domain – LpqN interactions. *This screen was performed by Jennifer Dunaj (Purdy Lab).*

Insert in pUAB200	**Insert in pUAB300**	**Trim MIC (µg/mL)**
-	Rv2763 (dfr) positive control	>200
-	LpqN	<6.25
MmpL3 D1	-	<6.25
MmpL3 D1	LpqN	<6.25
MmpL11 D1	-	<6.25
MmpL11 D1	LpqN	<6.25
MmpL3 D2	-	<6.25
MmpL3 D2	LpqN	100
MmpL11 D2	-	<6.25
MmpL11 D2	LpqN	50

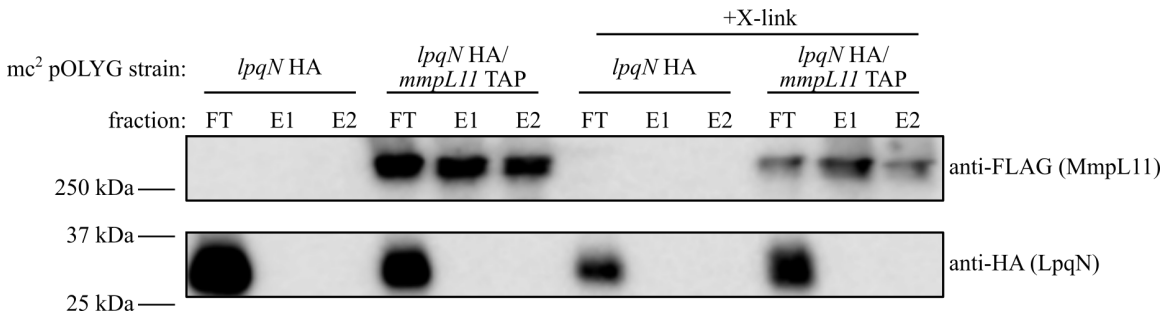

Figure 2.1. $LpqN_{TB}$ does not co-purify with $MmpL11_{TB}$ when co-expressed in *M. smegmatis*. HA-tagged LpqN and tandem (FLAG + HIS) affinity purification (TAP)-tagged MmpL11 were co-expressed in *M. smegmatis* mc^2155 in the presence/absence of protein cross-linking agent (1% formaldehyde, +X-link). MmpL11-TAP was purified via HisPur affinity resin. Resin flow through (FT) and elutions 1 and 2 (E1/E2) were analyzed for the presence of MmpL11/LpqN protein via Western blot with anti-FLAG/anti-HA antibodies. *M. smegmatis* solely expressing HA-tagged LpqN serves as a negative control for non-specific binding.

LpqN Interacts with Cell Envelope Lipid Biosynthetic Enzymes - We hypothesized that LpqN might act as an adaptor protein in the periplasm to facilitate interactions between MmpL proteins and periplasmic proteins. To identify secreted interacting partners of LpqN, we performed a pull-down purification of affinity-tagged LpqN incubated with *Mtb* culture filtrate proteins (CFP) in the presence/absence of formaldehyde as a protein cross-linking reagent. Interacting proteins were subsequently identified via mass spectrometry and categorized as weak or strong LpqN interacting partners based on whether or not protein cross-linking was required for co-purification (**Table 2.2**). As a control, we analyzed the background binding of CFP to the metal affinity resin. Intriguingly, secreted cell envelope biosynthetic enzymes, such as the mycolyltransferase Ag85A and the mycocerosic acid synthase Mas, were enriched in the LpqN co-purified samples relative to background. Ag85B also co-purified with LpqN, although to a lesser degree. Ag85 and Mas enzymes are responsible for the biosynthesis of the cell envelope lipids TDM and PDIM, respectively. These data suggest that LpqN interacts with periplasmic cell envelope biosynthetic enzymes.

The possible interaction between Ag85A and LpqN was interesting, given the key role that the Ag85 complex plays in the biogenesis of the mycobacterial cell envelope. Furthermore, the primary substrate of the Ag85 enzymes is TMM, which is exported by MmpL3. Attempts to demonstrate a direct interaction between LpqN and Ag85A using a heterologous dual-expression *M. smegmatis*

Table 2.2. Interacting partners of LpqN in the culture filtrate. *Technical assistance was provided by the OHSU Proteomics Shared Resource.*

[a]Cell values are the summed spectral counts of identified peptides corresponding to the indicated protein, from 3 biological replicate experiments.

Protein	CFP (background)[a]	CFP + LpqN (strong interactions)	Cross-linked (weak interactions)
Rv0583c | lipoprotein lpqN	54	1862	1774
Rv2220 | glutamine synthetase glnA1	15	54	121
Rv3804c | fibronectin-binding protein antigen fbpA, Ag85A	18	35	100
Rv1908c | catalase-peroxidase-peroxynitritase T katG	22	46	83
Rv2780 | secreted L-alanine dehydrogenase ald	11	32	76
Rv1475c |aconitate hydratase A acn	3	25	60
Rv1980c | Immunogenic protein mpt64	16	21	20
Rv0350 |Chaperone protein dnaK	50	60	51
Rv0896 | citrate synthase I gltA2	3	2	57
Rv006c |isocitrate dehydrogenase icd2	0	0	33
Rv3248c | adenosylhomocysteinase sahH	4	4	49
Rv0440 | 60 kDa chaperonin groEL2	9.818	15.6	18.947
Rv1098c | fumarate hydratase fumC	8	8	20
Rv0211 | phosphoenolpyruvate carboxykinase pckA	4	6	26
Rv2940c | mycocerosic acid synthase mas	0	3	27
Rv0363c | fructose-bisphosphate aldolase fba	2	11	23
Rv2467 | aminopeptidase N pepN	2	5	23
Rv3418 |10 kDa chaperonin groS	7	4	22
Rv2030c | uncharacterized protein	1	8	21
Rv0462 | dihydrolipoamide dehydrogenase lpd	0	2	20
Rv1017c | Ribose-phosphate pyrophosphokinase prsA	7	13	20
Rv1074c |acetyl-CoA acetyltransferase fadA3	0	3	20

Rv1886c | secreted fibronectin-binding protein fbpB, Ag85B	0	3	19
Rv1093 | serine hydroxymethyltransferase 1 glyA1	3	6	19
Rv2244 | meromycolate extension acyl carrier protein acpM	14	13	18
Rv2031c | Alpha-crystallin hspX	1	4	17
Rv0315 | probable beta-1,3-glucanase precursor	0	0	12
Rv2146c | N-acetyltransferase eis	0	4	11
Rv1837c | malate synthase G glcB	0	0	7
Rv0934 | periplasmic phosphate-binding lipoprotein pstS1	0	1	6
Rv0379 | protein transport protein secE2	2	0	5
Rv1860 | alanine and proline rich secreted protein apa	2	0	5
Rv1392 | S-adenosylmethionine synthetase metK	0	0	5
Rv0164 | conserved hypothetical protein TB18.5	0	0	4
Rv1448c | transaldolase tal	0	0	4
Rv1449c | transketolase tkt	0	0	4
Rv3628 | inorganic pyrophosphatase ppa	0	0	4

co-immunopurification strategy were unsuccessful (**Figure 2.2**). However, there is precedent for interactions between lipoproteins and members of the Ag85 complex, as evidenced by the recently reported LprG-Ag85A interaction (Touchette et al., 2017). LprG (Rv1411c) binds phosphatidylinositol-containing glycolipids, rather than mycolic acids (Drage et al., 2010). Nevertheless, LprG appears to contribute to mycolylation of cell wall analogues (Touchette et al., 2017). We performed head-to-head M-PFC assays to determine whether the MmpL3 or MmpL11 D2 domains are capable of interacting with other LpqN family members (LpqT, Mtc28), or LprG. LpqT and Mtc28 also interact with the MmpL11 D2 domain, but not the MmpL3 D2 domain, via M-PFC (**Table 2.3**). The structurally distinct LprG protein also interacted with the MmpL11, but not MmpL3, D2 domain via M-PFC. These results suggest the possibility that multiple lipoproteins act as adaptors for the MmpL transporters.

LpqN Contributes to Mtb Biofilm Lipid Composition – MmpL3 transports TMM, which is essential for replication, whereas MmpL11 transports cell envelope lipids that are important for biofilm formation. To investigate a possible role for LpqN in mycobacterial cell envelope biogenesis, we generated an *lpqN*-deletion mutant in H37Rv *Mtb* (Δ*lpqN*) via allelic exchange (**Figure 2.3A-B**). There was not a growth defect in either 7H9 or Sauton's media (**Figure 2.3C-D**). We then characterized *Mtb* wild-type, Δ*lpqN*, and complemented strain cell envelope lipids from bacteria grown planktonically and in biofilms by thin-layer

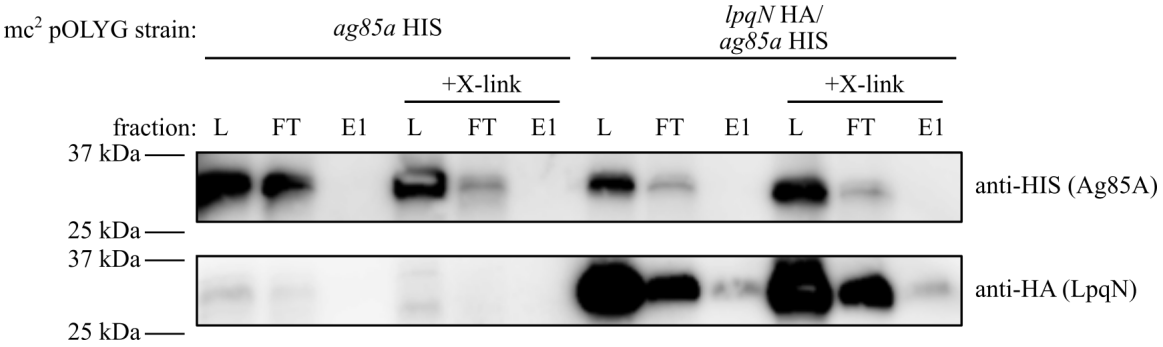

Figure 2.2. $LpqN_{TB}$ does not co-purify with $Ag85A_{TB}$ when co-expressed in *M. smegmatis*. HA-tagged LpqN and HIS-tagged Ag85A were co-expressed in *M. smegmatis* mc^2155 in the presence/absence of protein cross-linking agent (1% formaldehyde, +X-link). LpqN HA was purified via anti-HA affinity resin. Crude lysate (L), resin flow through (FT), and elution 1 (E1) were analyzed for the presence of Ag85A/LpqN protein via Western blot with anti-HIS/anti-HA antibodies. *M. smegmatis* solely expressing HIS-tagged Ag85A serves as a negative control for non-specific binding.

Table 2.3. Trimethoprim minimal inhibitory concentrations (MICs), determined via M-PFC, to assess interactions between MmpL3/11$_{TB}$ D2 domains and LpqN-family proteins.

Insert in pUAB200	Insert in pUAB300	Trim MIC (µg/mL)
-	Rv2763 (dfr) positive control	>200
-	LpqT	25
-	LprG	25
-	Mtc28	12.5
MmpL3 D2	-	<6.25
MmpL3 D2	LpqT	<6.25
MmpL3 D2	LprG	<6.25
MmpL3 D2	Mtc28	<6.25
MmpL11 D2	-	<6.25
MmpL11 D2	LpqT	50
MmpL11 D2	LprG	50
MmpL11 D2	Mtc28	25

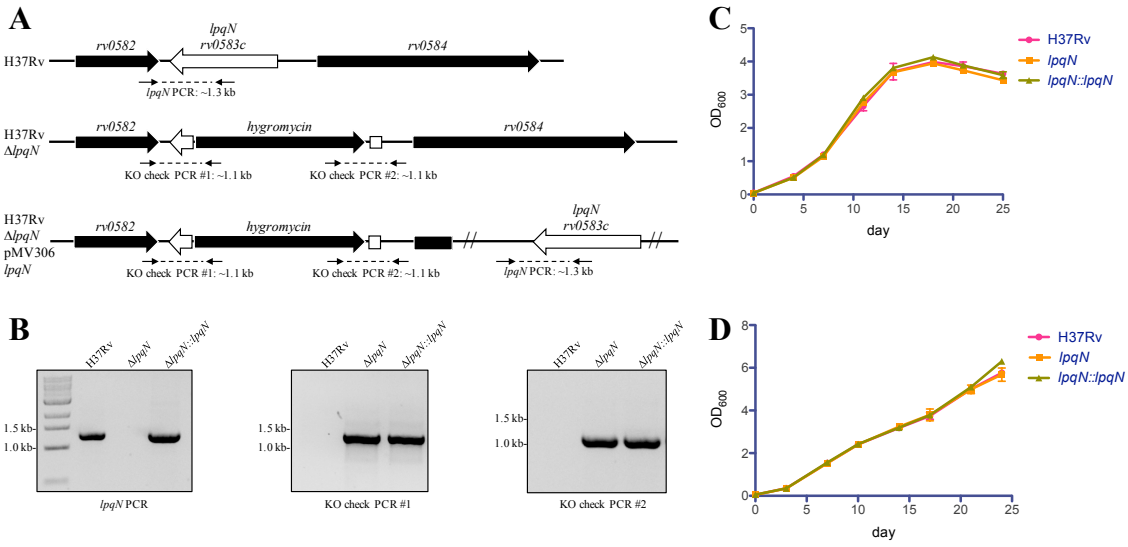

Figure 2.3. Generation of H37Rv Δ*lpqN*. **(A)** Genomic organization of *rv0583c*/*lpqN* in *Mtb* H37Rv, *hyg* resistance cassette allelic exchange strategy (Δ*lpqN*), and chromosomal complementation of *lpqN* using plasmid pMV306 (Δ*lpqN*::*lpqN*). Diagnostic PCR products are indicated with dashed lines. **(B)** Diagnostic PCRs performed with genomic template DNA isolated from H37Rv, Δ*lpqN*, and Δ*lpqN*::*lpqN* Mtb. Primers used = *lpqN* PCR: lpqN +367/lpqN +1637; KO check PCR #1: hyg primer 3500/lpqN +1637; KO check PCR #2: hyg primer 22/lpqN -865. (C) Growth of *Mtb* strains in 7H9 medium. (D) Growth of *Mtb* strains in Sauton's medium.

chromatography (TLC). We did not observe any differences in TMM and TDM levels between the wild-type, mutant, or complemented mutant (*Mtb* Δ*lpqN*::*lpqN*) lipid profiles using the chloroform:methanol:ammonium hydroxide (80:20:2) solvent system (**Figure 2.4A-B**). We also analyzed the mycolic acid methyl esters of mAGP, which did not differ significantly between strains (**Figure 2.4C**). Consistent with these results, we also did not see significant differences in the LC/MS profiles among the lipid extracts, in particular, of TMM and TDM (**Figures 2.5-2.6**). This was not surprising since the Δ*lpqN* mutant did not possess a growth defect.

Our analyses of *Mtb* biofilms over time indicates that the lipid profiles shift as the biofilm matures. While there were no differences between wild type and Δ*lpqN* mutant lipids at 3 weeks (**Figure 2.4D**), we noted the relative accumulation of an apolar lipid in the *lpqN* mutant samples that ran with a similar Rf to the wax ester standard in 4-week lipids (* asterisk, **Figure 2.4E**). We speculated that the apolar lipid (* in **Figure 2.4E**) in the mutant was a wax ester. However, mass spectrometric analysis of the extract of this apolar TLC spot did not yield mass spectra that directly identified any known mycobacterial lipids. These results countered our assumption that the spot is wax ester and are consistent with HPLC/MS results that showed no difference in wax ester between WT and Δ*lpqN* (**Figure 2.5E**). The Δ*lpqN* mutant biofilm also appeared to accumulate a less-apolar band that was similarly recalcitrant to identification (** asterisks, **Figure 2.4E**). Together, these biofilm lipid profiles suggest that LpqN may contribute to

Figure 2.4. LpqN contributes to biofilm lipid composition in late biofilm cultures. *Mtb* was grown in either complete 7H9 medium or Sauton's medium lacking tween for planktonic and biofilm cultures, respectively. *Mtb* cell envelope surface lipids were harvested by hexanes extraction from planktonic culture (**A**) or from biofilms harvested at 3 (**B** and **D**) or 4 (**E**) weeks and analyzed via thin-layer chromatography (TLC). mAGP was isolated from planktonic *Mtb* cell walls and mycolic acid methyl esters (MAMEs) generated and visualized by TLC (**C**). The solvent systems used for TLC were: 80:20:2, v:v:v, $CHCl_3$:MeOH:NH_4OH; (**A** and **B),** 99:5, v:v, hexanes:ethyl acetate **(C),** and 99:1, v:v, toluene:acetone **(D** and **E)**. TDM, TMM, TAG, and WE standards are indicated (Sigma). All TLCs were developed by charring in 10% molybdophosphoric acid. In panel E, * and ** indicate species that accumulate in the *lpqN* mutant.

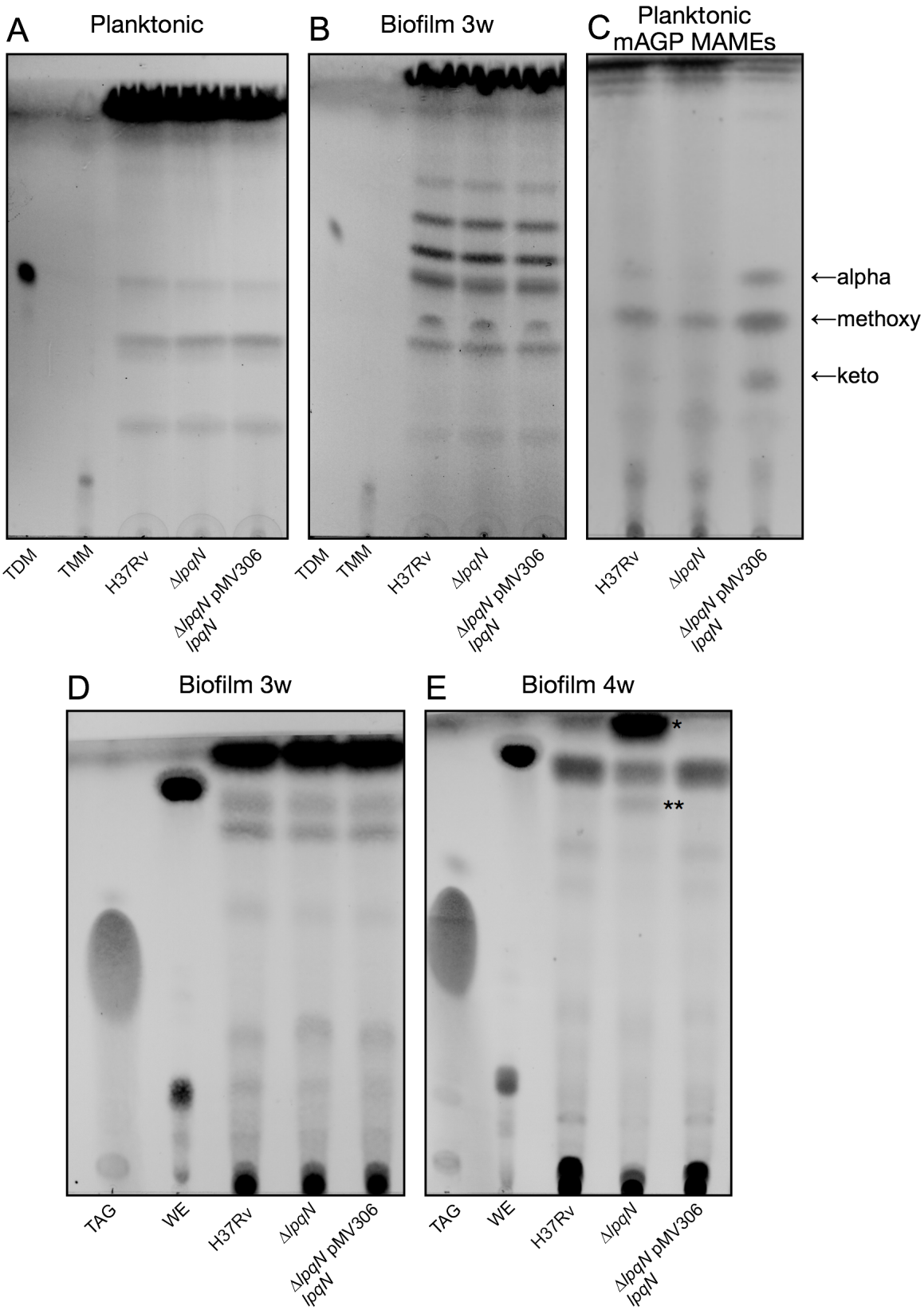
A
Planktonic
B
Biofilm 3w
C
Planktonic
mAGP MAMEs
←alpha
←methoxy
←keto
TDM
TMM
H37Rv
ΔlpqN
ΔlpqN pMV306
lpqN
D
Biofilm 3w
E
Biofilm 4w
*
**
TAG
WE

A **TIC**

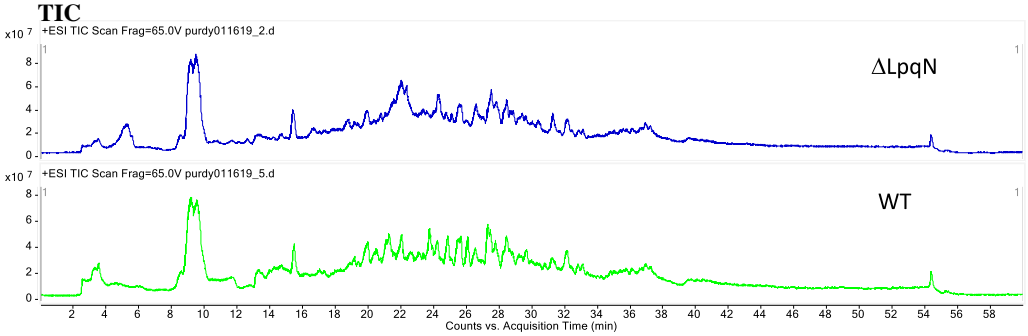

B **TDM**

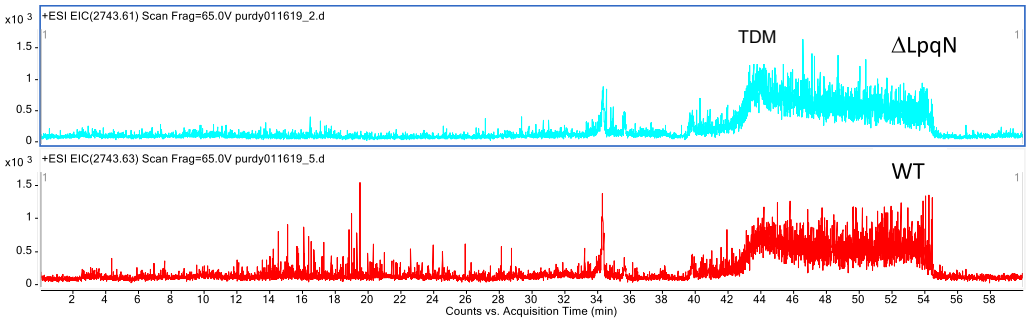

C **TMM**

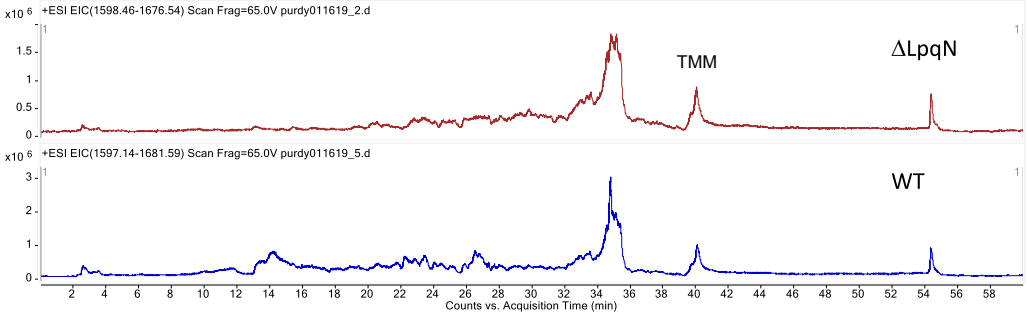

D **TMM** ($[M+NH_4]^+$)

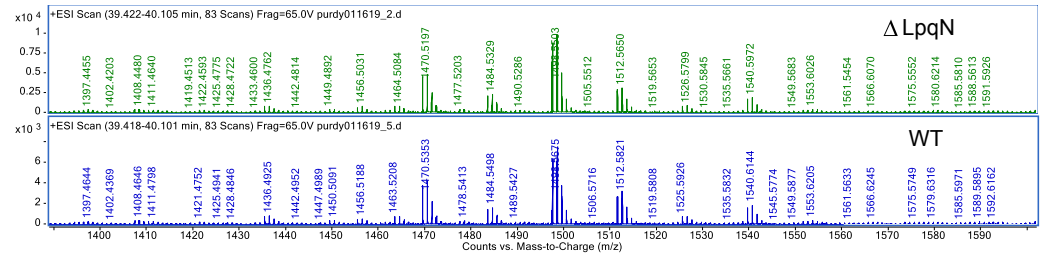

TDM ($[M+NH_4]^+$)

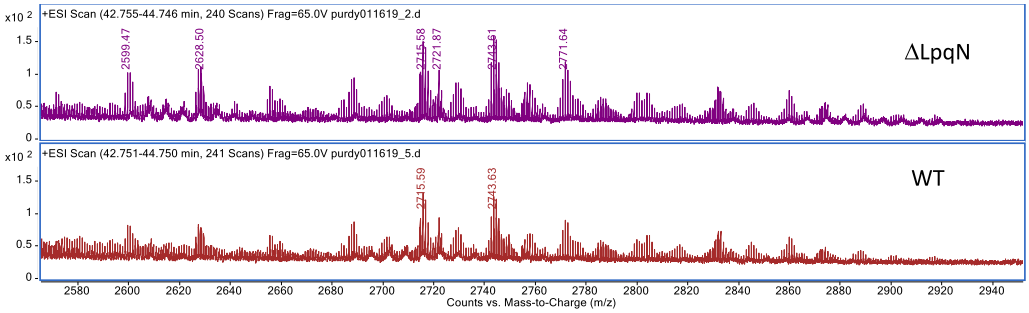

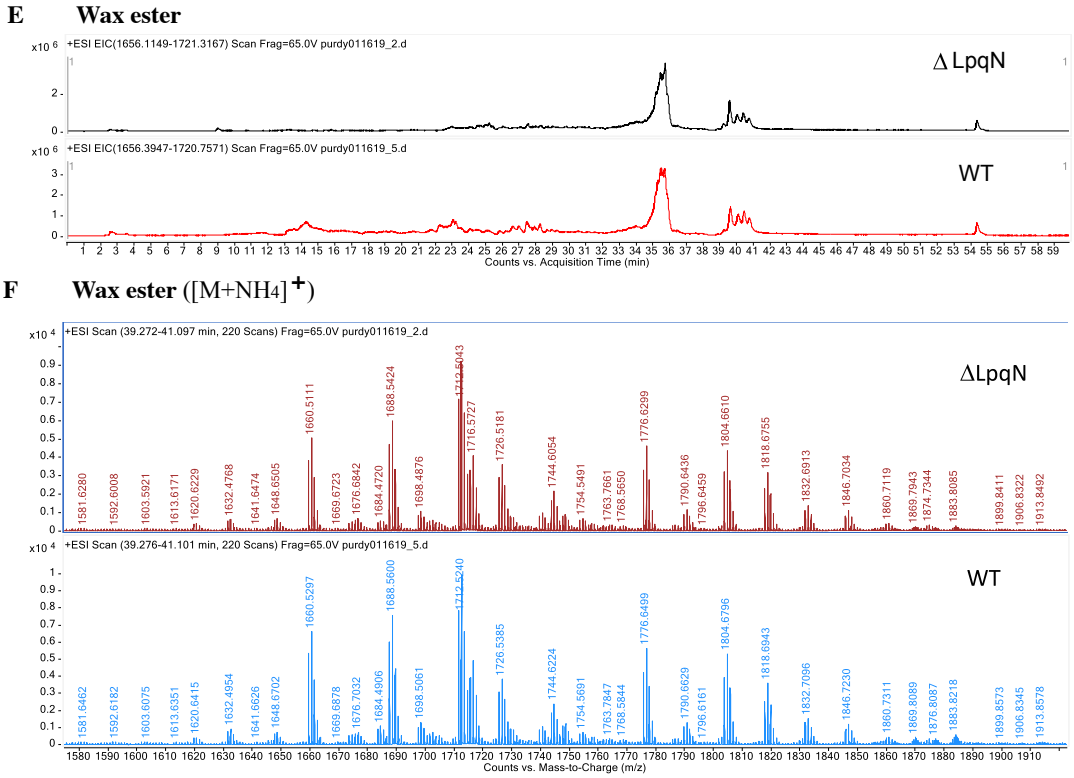

Figure 2.5. Positive-ion ESI HPLC/MS analysis of lipid extracts from wild type *M. tuberculosis* H37Rv and the *lpqN* mutant. **(A)** ESI HPLC/MS Total ion chromatogram (TIC) in the positive ion mode, **(B)** Selected ion chromatogram of TDM (elution time: 43-45.3 min), **(C)** Selected ion chromatogram of TMM (elution time: 39.5-40.5 min), **(D)** The ESI mass spectra of TMM $[M + NH_4]^+$ ions (top panels) and TDM $[M + NH_4]^+$ ions (bottom panels), **(E)** Selected ion chromatograms of wax ester (elution time: 39.5-41 min), **(F)** ESI MS spectra of the $[M+ NH_4]^+$ ions of wax esters. *MS analyses were performed by Dr. Fong-Fu Hsu (Washington University; St. Louis, MO).*

A TIC

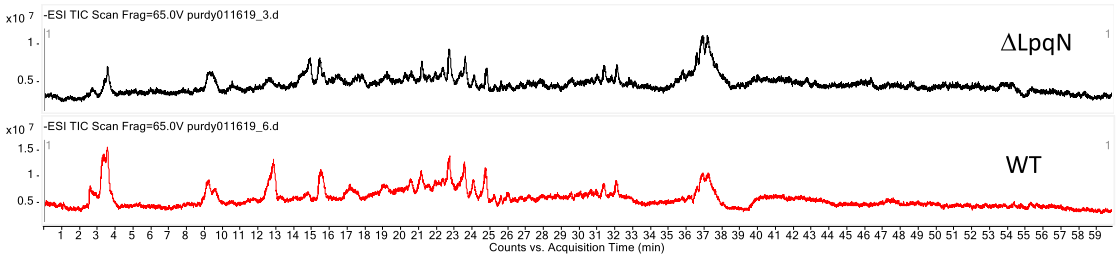

B mycolic acids

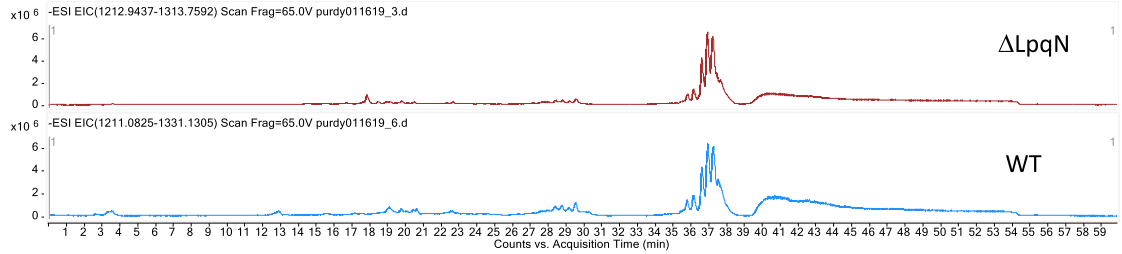

C mycolic acids [M - H]⁻

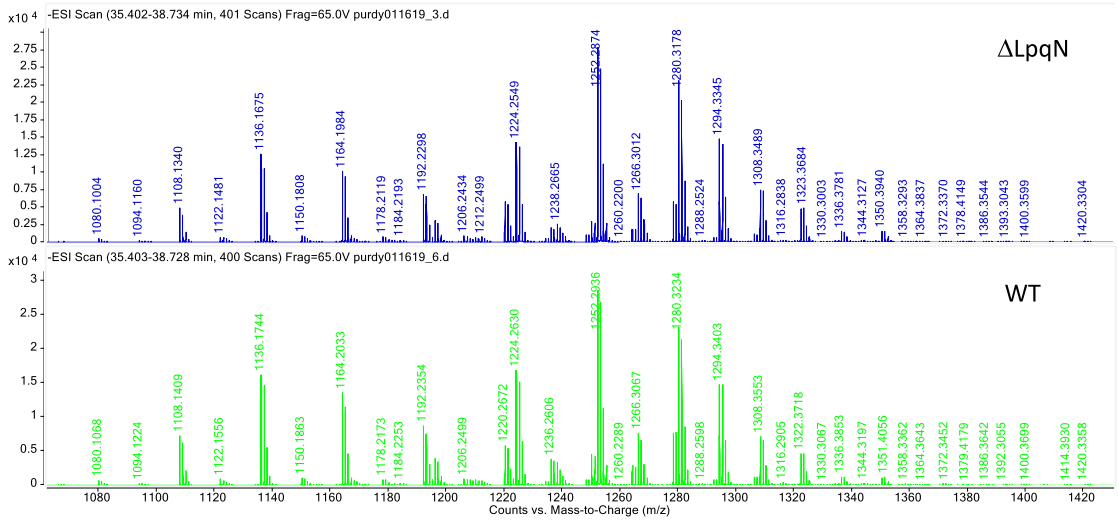

Figure 2.6. Negative-ion ESI HPLC/MS analysis of lipid extracts from wild type *M. tuberculosis* H37Rv and the *lpqN* mutant. **(A)** ESI HPLC/MS Total ion chromatogram (TIC) in the negative ion mode, **(B)** Selected ion chromatogram of mycolic acids (elution time: 35.5-38 min), **(C)** ESI MS spectra of the [M – H]⁻ ions of mycolic acids. *MS analyses were performed by Dr. Fong-Fu Hsu (Washington University; St. Louis, MO).*

cell envelope lipid turnover or remodeling during the course of biofilm development.

The LpqN Crystal Structure Suggests that LpqN May Directly Bind Lipids - To gain additional insight into LpqN function, the crystal structure of *apo*-LpqN was determined at a resolution of 1.65 Å using single anomalous dispersion (**Table 2.4** and **Figure 2.7**). Because LpqN might play a role in cell envelope biogenesis, we also determined structures of LpqN in complexes with dodecyl trehalose (6LT) and trehalose 6-decanoate (T6D) to resolutions of 1.37 Å and 1.74 Å, respectively. We resolved these two ligand-bound LpqN structures by using molecular replacement and utilizing the *apo*-LpqN structure as a search model (**Table 2.4** and **Figure 2.7**). Both 6LT and T6D are water-soluble compounds that are structurally similar to the insoluble lipid molecule TMM in that they contain a two-ring system of the trehalose moiety. Therefore, 6LT and T6D are ideal compounds to mimic TMM with respect to the interaction with LpqN. The crystals of *apo*-LpqN, LpqN-6LT and LpqN-T6D took the space groups C121, I4 and I4, respectively. A single molecule of LpqN was found in the asymmetric unit of each crystal. The molecule of LpqN consists of three α-helices and seven ß-strands. These helices and strands are designated numerically from the N- to C-termini: α1 (61-68), ß1 (84-86), ß2 (104-108), ß3 (120-124), α2 (134-147), ß4 (170-176), ß5 (179-182), ß6 (184-192), ß7 (195-206) and α3 (210-222). Based on the orientation of *apo*-LpqN within the asymmetric unit, the dimensions of this protein can be measured to be 45 Å x 40 Å x 35 Å. Accordingly, ß4, ß5,

Table 2.4 Data collection, phasing and structural refinement statistics. *Crystallography was performed in the lab of Dr. Edward Yu (Case Western Reserve University; Cleveland, OH).*

	Apo-LpqN (6E5D)	LpqN-6LT (6E5F)	LpqN-T6D (6MNA)	SeMet-LpqN
Wavelength (Å)	0.9792	0.9792	0.9792	0.9792
Resolution(Å)	48.11-1.65 (1.71-1.65)	56.57-1.37 (1.41-1.37)	56.25-1.74 (1.85-1.74)	48.59-2.20 (2.32-2.20)
Unit cell parameters				
(a b c) (Å)	99.3 55.5 44.6	80.0 80.0 59.2	79.5 79.5 60.0	99.0 56.4 44.5
(α β γ) (°)	90.0 103.9 90.0	90.0 90.0 90.0	90.0 90.0 90.0	90.0 104.8 90.0
Space Group	C121	I4	I4	C121
Total no. of reflections	187,144	334,562	337,062	155,435
Total no. of unique reflections	27,327	39,223	19,157	12,099
Wilson B factor (Å^2)	24.2	20.73	27.5	42.6
Completeness (%)	96.1 (87.3)	99.7 (98.0)	99.3 (98.5)	99.6 (98.2)
Multiplicity	6.9 (5.3)	8.4 (3.2)	17.6 (17.6)	12.8 (13.3)
$CC_{1/2}$ (%)	99.9 (95.6)	99.9 (64.5)	99.9 (64.3)	99.8 (98.2)
$I/\sigma(I)$	19.0 (2.9)	18.2 (1.9)	11.1 (1.5)	15.3 (5.1)
Phasing				
No. of sites				2
Figure of merit				0.305
Refinement				
R_{work} (%) ‡	18.57	17.8	18.45	
R_{free} (%)§	20.85	20.35	21.75	
No. of. atoms				
Protein	2654	2661	2559	
Water	140	107	101	
Ligand		81	74	
B. factors (Å^2)				
Protein	35.17	30.96	34.88	
Water	41.72	37.98	40.13	
Ligand		70.05	69.63	
r.m.s. deviations				
Bond lengths (Å)	0.002	0.004	0.012	
Bond angle (°)	0.545	0.764	1.242	
Ramachandran Plot (%)				
Favored regions	96.84	98.14	100	
Allowed regions	3.2	1.8	0	
Outliers	0	0	0	

‡ $R_{work} = \Sigma_{hkl} \; || F_{obs} - F_{calc} || \; / \; \Sigma_{hkl} | F_{obs} |$

§ R_{free} was calculated as for R_{work} but using 5% of the data that were excluded from the refinement calculation.

Figure 2.7. Structures of the *M. tuberculosis* LpqN protein. **(A)** Representative section of electron density of *apo*-LpqN. The solvent-flattened electron density (50-1.65 Å) is contoured at 1.0 σ and superimposed with the final refined model (green, carbon; red, oxygen; blue, nitrogen). **(B)** Ribbon diagram of a protomer of LpqN. The secondary structural elements of LpqN are colored green. **(C)** Surface representation of the electrostatic surface potentials of LpqN colored by charged (red, negative -15 kT/e; blue, positive +15 kT/e). **(D)** Representative section of electron density of LpqN-6LT. The solvent-flattened electron density (50-1.37 Å) is contoured at 1.0 σ and superimposed with the final refined model (orange, carbon; red, oxygen; blue, nitrogen). **(E)** Ribbon diagram of a protomer of LpqN-6LT. The secondary structural elements of LpqN are colored orange. The bound 6LT is in cyan. **(F)** Surface representation of the electrostatic surface potentials of LpqN-6LT colored by charged (red, negative -15 kT/e; blue, positive +15 kT/e). The bound 6LT is in cyan. A specific deep binding pocket, which was not observed in *apo*-LpqN, was found to create on the LpqN-6LT surface. **(G)** Representative section of electron density of LpqN-T6D. The solvent-flattened electron density (50-1.74 Å) is contoured at 1.0 σ and superimposed with the final refined model (skyblue, carbon; red, oxygen; blue, nitrogen). **(H)** Ribbon diagram of a protomer of LpqN-T6D. The secondary structural elements of LpqN are colored sky blue. The bound T6D is in yellow. **(I)** Surface representation of the electrostatic surface potentials of LpqN-T6D colored by charged (red, negative -15 kT/e; blue, positive +15 kT/e). The bound T6D is in yellow. A specific deep binding pocket, which was not observed in *apo*-LpqN, was found to create on the LpqN-T6D surface. *Crystallography was performed in the lab of Dr. Edward Yu (Case Western Reserve University; Cleveland, OH).*

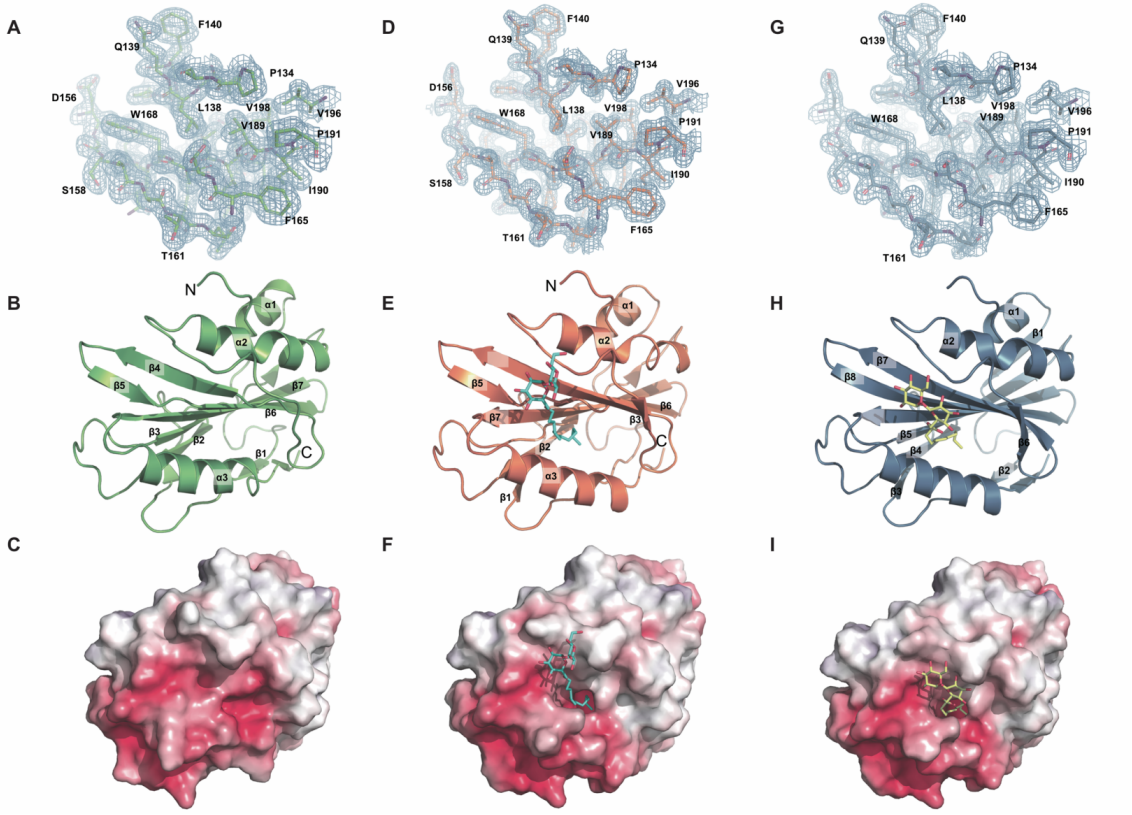
A
F140
Q139
P134
D156
L138
V198
V196
W168
V189
P191
S158
I190
F165
T161
B
N
α1
α2
β4
β5
β7
β6
β3
β2
β1
C
α3
D
F140
Q139
P134
V196
D156
L138
V198
W168
V189
P191
I190
S158
F165
T161
E
N
α1
α2
β5
β7
β6
β3
C
β2
α3
β1
G
F140
Q139
P134
L138
V198
V196
W168
V189
P191
I190
F165
T161
H
α1
β1
α2
β7
β8
β5
β4
β2
C
F
I

ß6, ß7 and α3 are involved in forming a shallow cavity, presumably constituting a ligand binding site. The interior wall of this cavity consists mainly of hydrophobic and polar residues including L87, I121, V183, A184, L201, A203 and M214. Superimposition of the structures of *apo*-LpqN and LpqN-6LT results in an overall root-mean square deviation (r.m.s.d.) of 0.8 Å, suggesting that these two structures are similar in conformation. However, detailed inspection indicates that the two structures are quite different. The main difference between the two conformations is the shift in location of α3 and the rearrangement of the secondary structures of several random loops located at the 6LT binding site. These loops, including residues 93-96, 158-160 and 167-170, convert into ß-strands after binding 6LT. These changes result in a larger internal cavity for LpqN-6LT compared to that of *apo*-LpqN. In addition, a specific deep binding pocket, which was not observed in *apo*-LpqN, was found in LpqN-6LT to coordinate with the binding of the carbon chain of the 6LT ligand. As the secondary structure of LpqN-6LT is very different, we reassigned its structural features to facilitate the description of this ligand-bound protein. The secondary structure assignments of 6LT-bound LpqN from the N- to C-termini are: α1 (61-67), ß1 (93-96), ß2 (104-109), α2 (134-147), ß3 (158-160), ß4 (167-176), ß5 (179-185), ß6 (187-192), ß7 (195-206) and α3 (210-223).

In the structure of LpqN-6LT, the 6LT molecule is bound within the cavity surrounded by ß4, ß5, ß7 and α3. The dodecyl tail of 6LT is completely buried inside the LpqN protein, leaving its two sugar rings of the trehalose head group

partially exposed to solvent. Within 6 Å of the dodecyl group of 6LT, 12 amino acids contact and secure the hydrocarbon tail (**Figure 2.8**). Although the trehalose moiety of 6LT only partially contacts the LpqN protein, the binding of this two-ring head group is extensive. S173 of LpqN forms a hydrogen bond with the trehalose head group to anchor this ligand. G153 also donates its backbone oxygen to make another hydrogen bond with the trehalose moiety. S154 and G171 also participate in binding this head group. In addition, Q152 is 3.7 Å from the trehalose head group and interacts with the ligand via electrostatic interaction.

The structure of LpqN-T6D resembles that of LpqN-6LT. Superimposition of these two structures leads to an r.m.s.d. of 0.1 Å, suggesting that these two structures are almost identical. Again, the main difference between the conformation of these two structures is the switch of local secondary structures from random loops to ß-strands. For example, residues 70-74, 84-86, 120-129, 160-162, 165-167, 185-187 and 225-227 are found to form flexible loops in the structure of LpqN-6LT. These residues are all incorporated into different ß-strands. Based on these structures, it appears that the LpqN protein is able to easily switch its secondary structures to accommodate for substrate binding. As a result, the LpqN-6LT forms three α-helices and nine ß-strands: α1 (61-67), ß1 (70-74), ß2 (84-86), ß3 (93-96), ß4 (104-109), ß5 (120-129), α2 (134-147), ß6 (158-162), ß7 (165-176), ß8 (179-192), ß9 (195-206), α3 (210-223) and ß10 (225-227).

Figure 2.8. The LpqN ligand-binding site. **(A)** The F_o-F_c simulated annealing electron density map of the bound 6LT within the LpqN protein. The bound 6LT is shown as a stick model (cyan, carbon; red, oxygen). The simulated annealing F_o-F_c electron density map is contoured at 3.0 σ (gray mesh). **(B)** The $2F_o$-F_c electron density map of the bound 6LT within the LpqN protein. The bound 6LT is shown as a stick model (cyan, carbon; red, oxygen). The $2F_o$-F_c electron density map is contoured at 1.0 σ (blue mesh). **(C)** Schematic representation of the LpqN and 6LT interactions. Amino acid residues within 3.5 Å from the bound 6LT are included. Dotted lines depict the hydrogen bonds. The hydrogen-bonded distances are also indicated in this figure. **(D)** The F_o-F_c simulated annealing electron density map of the bound T6D within the LpqN protein. The bound T6D is shown as a stick model (yellow, carbon; red, oxygen). The simulated annealing F_o-F_c electron density map is contoured at 3.0 σ (gray mesh). **(E)** The $2F_o$-F_c electron density map of the bound T6D within the LpqN protein. The bound T6D is shown as a stick model (yellow, carbon; red, oxygen). The $2F_o$-F_c electron density map is contoured at 1.0 σ (blue mesh). **(F)** Schematic representation of the LpqN and T6D interactions. Amino acid residues within 3.5 Å from the bound T6D are included. Dotted lines depict the hydrogen bonds. The hydrogen-bonded distances are also indicated in this figure. *Crystallography was performed in the lab of Dr. Edward Yu (Case Western Reserve University; Cleveland, OH).*

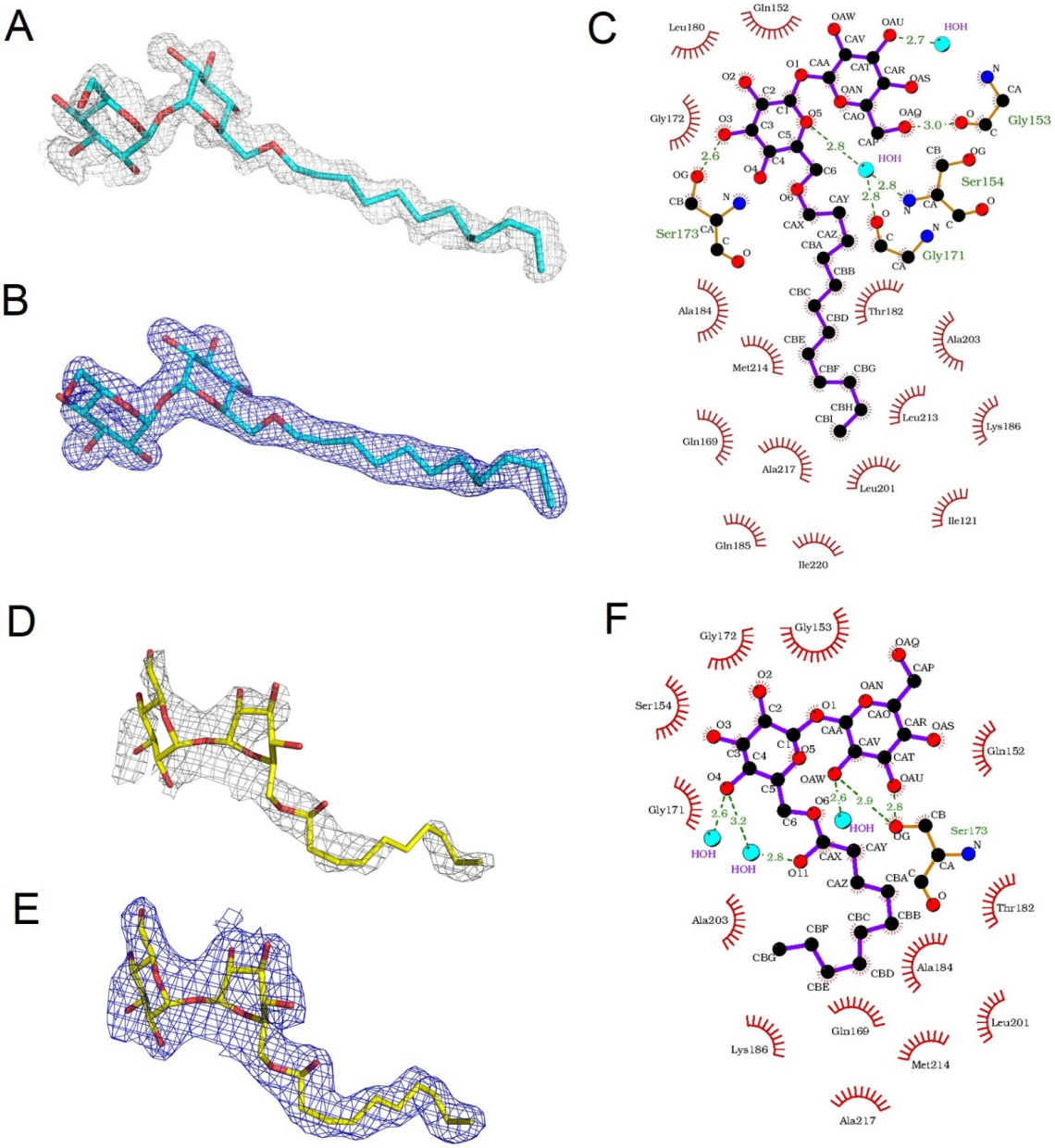
A
B
C
D
E
F
Gln152
Leu180
OAW
OAU
HOH
CAV
2.7
O1
CAA
CAT
CAR
OAS
O2
C2
OAN
N
CA
C1
O5
CAO
Gly172
O3
C3
C5
OAQ
3.0
O
C
Gly153
CAP
2.6
2.8
HOH
CB
OG
O4
C4
C6
OG
Ser154
2.8
2.8
CB
O6
CAY
N
CA
O
CAX
N
C
CAZ
Ser173
CA
CBA
O
N
Gly171
C
CA
O
CBB
CBC
Ala184
Thr182
CBD
CBE
Ala203
Met214
CBF
CBG
CBH
CBI
Leu213
Lys186
Gln169
Ala217
Leu201
Ile121
Gln185
Ile220
Gly172
Gly153
OAQ
CAP
O2
Ser154
OAN
C2
O1
CAO
CAR
OAS
O3
C1
CAA
CAV
Gln152
C3
O5
C4
CAT
O4
OAW
OAU
C5
2.6
2.9
2.8
Gly171
O6
CB
2.6
3.2
HOH
HOH
HOH
OG
Ser173
2.8
CAX
CAY
N
O11
CA
CAZ
CBA
C
O
Thr182
Ala203
CBC
CBB
CBF
CBG
Ala184
CBD
CBE
Leu201
Gln169
Lys186
Met214
Ala217

Like the binding of 6LT, the decanoate tail of T6D is completely buried in the binding cavity formed by LpqN. Within 6 Å of this hydrocarbon chain, at least eight amino acids are actively involved in anchoring the bound T6D. The trehalose head group of T6D is partially exposed to solvent and is surrounded by six amino acids. S173 also participates by forming two hydrogen bonds with the sugar-ring system of T6D to secure the ligand (**Figure 2.8**). The crystal structures of LpqN indeed support the idea that this lipoprotein is capable of binding cell envelope lipids, such as TMM.

DISCUSSION

Using genetic methods, we demonstrated that LpqN interacts with the periplasmic D2 loop domains of the mycolate transporters MmpL3 and MmpL11. As such, LpqN may act as an MFP to facilitate substrate transport by MmpL3 and MmpL11. The outcome of this interaction is likely proper maturation of lipid substrates and/or the correct localization of these lipids within the cell envelope. We hypothesize that LpqN accomplishes these functions through direct binding of MmpL-transported lipids, as our structural data suggest.

Several observations suggest that there is substantial redundancy in this system. The cell envelope lipid profile of planktonic and 3-week biofilm-grown *Mtb* Δ*lpqN* mutant did not differ from the wild-type, implying that the absence of LpqN does not affect the cell envelope lipid composition during these growth phases.

Moreover, *Mtb* Δ*lpqN* does not exhibit attenuated growth in planktonic culture (**Figure 2.3C-D**). Since mycolic acid biosynthesis and MmpL3 are essential, we would expect that perturbing mycolic acid incorporation within the cell envelope would impact *Mtb* growth or viability. Given that *lpqN*-deficient *Mtb* grows at a normal rate and has a normal cell envelope lipid profile, LpqN is unlikely to be the sole facilitator of periplasmic mycolic acid transport in *Mtb*. In support of this, we note that the protein family to which LpqN belongs (PF10738) contains other secreted *Mtb* proteins such as the lipoprotein LpqT (Rv1016c) and the secreted proline-rich Mtc28 (Rv0040c) (El-Gebali et al., 2019).

Lipid binding may be a shared feature of the LpqN protein family. The published structure of Mtc28 exhibits structural homology to eukaryotic lipid binding proteins such as CERT and STARD13, as assessed by the DALI server (Holm and Rosenström, 2010; Kudo et al., 2008; Kundu et al., 2016; Thorsell et al., 2011). Both LpqT and Mtc28, as well as the unrelated lipoprotein LprG (Rv1411c), interact with the MmpL11 D2 domain, but not the MmpL3 D2 domain, via M-PFC (**Table 2.3**). Whether LpqT or Mtc28 are capable of binding lipids is unknown, but LprG binds phosphatidylinositol-containing glycolipids and interacts with Ag85A (Drage et al., 2010; Touchette et al., 2017). Thus, there are presumably multiple interconnected and redundant pathways of cell envelope biogenesis operating in the periplasm that are mediated by lipoproteins and other secreted proteins. Some periplasmic lipid mediators, like LpqN, appear capable of interacting with both MmpL3 and MmpL11. Other potential mediators, like

LpqT, Mtc28, and LprG, appear to preferentially interact with MmpL11. While MmpL3 and MmpL11 both export mycolic acid-containing lipids, MmpL3 is essential and therefore more crucial to cell envelope physiology. Since *lpqN*-deficient *Mtb* is physiologically unimpaired, there are likely additional MmpL3-interacting periplasmic lipid mediators that remain to be identified. The recent characterization of the MmpL3-associated protein TtfA in *M. smegmatis* supports the hypothesis that MmpLs function in concert with accessory proteins to transport their lipid substrates (Fay et al., 2019). LpqN and LpqN family proteins are therefore likely redundant periplasmic mediators of lipid transport.

Our work raises a number of questions regarding the function of LpqN. An M-PFC screen performed in *M. smegmatis* initially identified LpqN as an interacting partner of MmpL11. We also used this system to show LpqN interaction with MmpL3. However, we were unable to demonstrate a direct biochemical interaction between LpqN and MmpL11 when heterologously co-expressed in *M. smegmatis*, suggesting a weak interaction (**Figure 2.1**). We also cannot exclude the possibility that the LpqN-MmpL3/11 interaction is indirect, and that some putative mycobacterial adaptor protein or molecule is required for LpqN to associate with these transporters. LpqN also appeared to preferentially interact with Ag85A when incubated with purified *Mtb* culture filtrate proteins. Similarly, we could not successfully co-purify these two proteins when heterologously co-expressed in *M. smegmatis* (**Figure 2.2**). Again, this may reflect an indirect interaction with a species-specific adaptor protein. The observation that *Mtb* Δ*lpqN* biofilms appear to mature differently than wild-type *Mtb* biofilms potentially

suggests temporal modulation of LpqN function, and is the focus of ongoing investigation.

Recent work demonstrated that LpqN contributes to *Mtb* virulence in a manner apart from its role in cell envelope biogenesis. LpqN appears to interact with the host ubiquitin ligase Cbl that downregulates antibacterial immunity and potentiates *Mtb* growth during *ex vivo* macrophage infection (Penn et al., 2018). While this capacity of LpqN to function as a virulence factor is ostensibly unrelated to its apparent role in cell envelope biogenesis, this finding underscores the critical importance of the mycobacterial cell envelope and its components to pathogenesis.

EXPERIMENTAL PROCEDURES

Bacterial strains and growth conditions - The *Mtb* wild-type strain H37Rv was obtained from the ATCC. Mycobacterial strains were routinely maintained in Middlebrook 7H9 liquid medium (Difco) with 0.05% Tween-80, or on Middlebrook 7H10 agar (Difco), both supplemented with albumin dextrose salts (ADS) containing 8.1 mg/mL NaCl, 50 mg/mL bovine serum albumin (BSA), and 20 mg/mL dextrose. Glycerol was added to liquid 7H9 to a final concentration of 0.5%. Kanamycin (25 μg/mL) and hygromycin (50 μg/mL) were used to maintain bacterial selection when required.

The *Mtb* Δ*lpqN* mutant was created via allelic exchange. Upstream and downstream regions of *lpqN* homology (ROH) were amplified by PCR using Δ*lpqN* 5'/3' Forward/Reverse primers (see **Table 2.5**) and cloned to flank the hygromycin resistance gene in pYUB854-*rpsL* (Bardarov et al., 2002). The resulting linear ROH-flanked hygromycin product was amplified by PCR, purified, concentrated, and used to transform electrocompetent H37Rv/pJV53 (van Kessel and Hatfull, 2007). Transformants were selected on 7H10 agar containing ADS and hygromycin (75 μg/mL). Individual colonies were transferred to 7H10 agar containing hygromycin (50 μg/mL). Deletion of *lpqN* was confirmed via PCR using flanking primers. Loss of the pJV53 recombineering plasmid was accomplished through iterative culturing on 7H10 agar in the absence of kanamycin and confirmed by susceptibility to kanamycin (25 μg/mL). For complementation, *lpqN* + ~1000 bp upstream sequence was amplified via PCR with *lpqN* -865/+1637 primers and cloned into the integrative vector pMV306 (Stover et al., 1991). The resulting complementation plasmid was transformed into the *Mtb* Δ*lpqN* mutant and transformants selected on 7H10 agar containing ADS and kanamycin (25 μg/mL), and confirmed via PCR (**Figure 2.3A-B**).

Mycobacterial biofilms were grown in Sauton's medium containing 0.5 g/L K_2HPO_4, 0.5g/L $MgSO_4$, 4.0 g/L L-asparagine, 0.05 g/L ferric ammonium citrate, 4.76% glycerol, and 1.0 mg/L $ZnSO_4$, with a final pH of 7.0. *Mtb* biofilms were inoculated to OD_{600} = 0.05 in Sauton's medium and incubated at 37ºC/ 5% CO_2

in tightly sealed polystyrene bottles. At 2 weeks, the lids were loosened to permit gas exchange.

Lipid isolation and analyses - *Mtb* lipids were harvested by collecting and centrifuging planktonic or biofilm cultures in 50 mL conical vials, washing once with PBS, then moving to glass test tubes containing 3 mm glass beads. Surface lipids were extracted by shaking with hexanes (~5 mL) for 2 min, followed by pelleting (1000xg/10 min). Supernatants were removed into fresh glass tubes and treated with HPLC-grade $CHCl_3$:MeOH (2:1, v:v) prior to removal from biosafety containment. For total lipid extraction, bacterial pellets were autoclaved prior to removal from biosafety containment, then extracted with ~5 mL $CHCl_3$:MeOH (2:1, v:v) and 1 mL HPLC-grade H_2O by shaking and bath sonication. The organic layer was separated by centrifugation (1000xg/10 min), transferred to pre-weighed vial, and dried under inert N_2 gas. mAGP was isolated as previously described (Daffe et al., 1990). Mycolic acid methyl esters (MAMEs) were obtained by incubating mAGP in 15% tetrabutylammonium hydroxide (overnight, 100ºC) followed by iodomethane (4 hours, room temperature) and extraction with dichloromethane (DCM). Extracted lipids were resuspended in $CHCl_3$ or DCM (MAMEs) and loaded onto aluminum-backed silica plates (EMD Millipore) for TLC analysis. Solvent systems used were chloroform:methanol:ammonium hydroxide (80:20:2, v:v:v), hexanes:ethyl acetate (99:5, v:v, three developments) and toluene:acetone (99:1, v:v) (Fisher). Lipids were visualized via spraying with 12-molybdophosphoric acid (Alfa Aesar;

10%, w/v in EtOH) and charring. The extracted lipids were also subjected to LC/MS analysis using Agilent 6550A QTOF system in conjunction with Agilent 1290 HPLC. HPLC separation and MS data acquisition were performed as described previously (Howard et al., 2018).

Mycobacterial protein fragment complementation assay - The M-PFC screen was previously described and relies on the reconstitution of two domains of the DHFR protein, which confers resistance to trimethoprim (Singh et al., 2006). The MmpL3 and MmpL11 D1 and D2 periplasmic domains were amplified by PCR, and the products subcloned into pGEM-T Easy (Promega). Once confirmed by sequencing, the pUAB200 integrative plasmids were constructed such that the D1 and D2 domains were in-frame with the DHFR [F3] fragment. The pUAB200 was then transformed into *M. smegmatis* mc^2155 generating "bait" strains. An H37Rv *Mtb* "prey" library of over 10^6 independent clones was generated in pUAB300. Briefly, H37Rv genomic DNA was partially digested with *Hpa*I and fragments between 0.5 and 2 kb were cloned into the *Cla*I site of pUAB300. Library DNA was generated by a MaxiPrep (Qiagen). To screen the library, electrocompetent "bait" strains were transformed with the *Mtb* library DNA, and plated to $kan_{25}/hyg_{50}/trim_{50}$ plates. Screens were considered successful if they resulted in 10^6 $kan^R hyg^R$ transformants. Clones that grew on trimethoprim were screened by PCR to eliminate those that grew due to the presence of pUAB300 plasmids containing the *Mtb dfrA* (*rv2763c*) gene. Sequencing of the "prey" *Mtb* genomic library plasmid identified the genes fused to DHFR [F1,2]. The MmpL11

D2-LpqN interaction was confirmed by direct cloning of LpqN lacking its signal sequence into pUAB300 to generate in frame fusions with the DHFR [F1,2] fragment. The MmpL D1 and D2-LpqN interactions were measured by determining the trimethoprim MIC_{90}. Similarly, LpqT, LprG, and Mtc28 were cloned without their signal sequences into pUAB300 in order to assess their interaction with MmpL3/11 D2 domains. A pUAB300 plasmid containing the *Mtb dfrA* (*rv2763c*) gene was used as a positive control. Strains were serially diluted onto 7H11 agar containing 2-fold dilutions of trimethoprim from 6.25 ug/mL to 200 ug/mL.

Protein purification - The *E. coli* LpqN expression construct was created by amplifying *lpqN* lacking its signal sequence via PCR with primers *lpqN*.61/687 followed by subcloning into pGEM-T Easy. Upon sequence confirmation, the product was cloned into pET-15b (Novagen) in frame with an N-terminal 6x-histidine tag. This construct was transformed into *E. coli* BL21-DE3, and protein production was induced at OD_{600} = ~0.5 with 0.4 mM IPTG (~1 hour/37ºC). Bacteria were harvested via centrifugation and lysed via sonication. Protein was affinity purified over HisPur Cobalt Superflow Agarose resin (Thermo) and confirmed by Western analysis.

LpqN – CFP pull-downs - Recombinantly-expressed LpqN and culture filtrate proteins (CFP; BEI Resources, NR-14825, lot# 610560541) (500 µg each) were incubated overnight at 4ºC in buffer A (300 mM NaCl, 50 mM $NaPO_4$). Cross-linking was performed using 1% formaldehyde for 30 min at room temperature,

followed by quenching with 225 mM glycine for 5 min. Cross-linked samples were buffer exchanged back into buffer A prior to LpqN purification on HisPur Cobalt Superflow Agarose resin (Thermo). LpqN from the non-cross-linked sample was similarly purified. Background CFP binding was assessed by flowing 500 µg of CFP alone over the cobalt resin. All resin-immobilized samples were washed (2x buffer A, 1x buffer A + 10 mM imidazole) and eluted in buffer A + 200 mM imidazole. LpqN-interacting proteins and CFP background were identified by mass spectrometry at the OHSU Proteomics Shared Resource.

Protein Mass Spectrometry - 0.5 mL of each eluate was concentrated and buffer exchanged with Amicon Ultra 3kDa MWCO filter. Samples were solubilized in 0.05% ProteaseMAX, reduced with dithiothreitol, alkylated with iodoacetamide, digested with trypsin overnight and dried. Each sample was dissolved in 20 µL of 5% formic acid and 20 µL/sample injected into Orbitrap Fusion. Sample digests were loaded onto an Acclaim PepMap 0.1 x 20 mm NanoViper C18 peptide trap (Thermo Scientific) for 5 min at a 5 µL/min flow rate in a 2% acetonitrile, 0.1% formic acid mobile phase and peptides separated using a PepMap RSLC C18, 2 µm particle, 75 µm x 25 cm EasySpray column (Thermo Scientific) using a 7.5–30% acetonitrile gradient over 60 min in mobile phase containing 0.1% formic acid and a 300 nL/min flow rate using a Dionex NCS-3500RS UltiMate RSLC nano UPLC system. Tandem mass spectrometry data was collected using an Orbitrap Fusion Tribrid mass spectrometer configured with an EasySpray NanoSource (Thermo Scientific). Survey scans were performed in the Orbitrap

mass analyzer at 120,000 resolution, and data-dependent MS2 scans in the linear ion trap using HCD following isolation with the instrument's quadrupole. Comet (version 2015.01, revision 1) was used to search MS2 Spectra against an April 2017 version of the uniprot_Mycobacterium.tuberculosis_h37rv_both.fasta (8352 entries) FASTA protein database, with concatenated sequence-reversed entries to estimate error thresholds and 179 common contaminant sequences and their reversed forms (Wilmarth et al., 2009). The database processing was performed with Python scripts available at http://www.ProteomicAnalysisWorkbench.com. Comet searches for all samples were performed with trypsin enzyme specificity. Average parent ion mass tolerance was 2.5 Da. Monoisotopic fragment ion mass tolerance was 1.005 Da. A static modification of +57.02146 Da was added to all cysteine residues. A variable modification of +15.99491 Da on methionine residues was also allowed.

LpqN expression and purification for crystallization studies - Briefly, the LpqN protein containing a 6xHis tag at the C-terminus was overproduced in *E. coli* BL21(DE3) cells possessing pET15bΩ*lpqN*. Cells were grown in 2 L of Luria Broth (LB) medium with 100 μg/ml ampicillin at 37°C. When the OD_{600} reached 0.5, the culture was treated with 0.2 mM isopropyl-β-D-thiogalactopyranoside (IPTG) to induce LpqN expression, and cells were harvested within 3 h. The collected bacterial cells were suspended in 100 ml ice-cold buffer containing 20 mM Na-HEPES (pH 7.2) and 200 mM NaCl, 10 mM $MgCl_2$ and 0.2 mg DNase I (Sigma-Aldrich). The cells were then lysed with a French pressure cell. Cell

debris was removed by centrifugation for 45 min at 4°C and 20,000 rev/min. The crude lysate was filtered through a 0.2 μm membrane and was loaded onto a 5 ml Hi-Trap Ni^{2+}-chelating column (GE Healthcare Biosciences, Pittsburgh, PA) pre-equilibrated with 20 mM Na-HEPES (pH 7.2) and 200 mM NaCl. To remove unbound proteins and impurities, the column was first washed with six column volumes of buffer containing 50 mM imidazole, 250 mM NaCl, and 20 mM Na-HEPES (pH 7.2). The LpqN protein was then eluted with four column volume of buffer containing 300 mM imidazole, 250 mM NaCl, and 20 mM Na-HEPES (pH 7.2). The purity of the protein was judged using 12.5% SDS-PAGE stained with Coomassie Brilliant Blue. The purified protein was extensively dialyzed against buffer containing 20 mM Na-HEPES (pH 7.5), and concentrated to 15 mg/ml.
For the 6xHis selenomethionyl-substituted (SeMet)-LpqN protein expression, a 1 ml LB broth overnight culture containing *E. coli* BL21(DE3)/pET15bΩ*lpqN* cells was transferred into 20 ml of LB broth containing 100 μg/ml ampicillin and grown at 37°C. When the OD_{600} value reached 1.2, cells were harvested by centrifugation at 3,000 g/min for 10 min, and then washed two times with 10 ml of M9 minimal salts solution. The cells were re-suspended in 20 ml of M9 media and then transferred into a 2 L pre-warmed M9 solution containing 100 μg/ml ampicillin. The cell culture was incubated at 37°C with shaking. When the OD_{600} reached 0.4, 100 mg/l of lysine, phenylalanine and threonine, 50 mg/l isoleucine, leucine and valine, and 60 mg/l of L-selenomethionine were added. The culture continued to incubate at 37°C with shaking for 15 min. Protein expression was the induced with 0.2 mM IPTG, and cells were harvested within 3 h after

induction. The procedures for purifying 6xHis SeMet-LpqN were identical to those of native LpqN.

Crystallization of LpqN - All crystals of the 6xHis LpqN protein were obtained using hanging-drop vapor diffusion. The LpqN crystals were grown at room temperature in 24-well plates with the following procedures. A 2 μl protein solution containing 15 mg/ml LpqN protein in 20 mM Na-HEPES (pH 7.5) was mixed with a 2 μl of reservoir solution containing 0.1 M Na-citrate (pH 6.0) and 1.9 M $(NH_4)_2SO_4$. The resultant mixture was equilibrated against 500 μl of the reservoir solution. Crystals grew to a full size in the drops within two weeks. Cryoprotection was achieved by raising the glycerol concentration stepwise to 25% with a 5% increment in each step.

Crystals of SeMet-LpqN were prepared using similar procedures. The reservoir solution for crystallizing SeMet-LpqN is the same as that for native LpqN. These SeMet crystals grew to a full size in the drops within two weeks. Cryoprotection was achieved by raising the glycerol concentration stepwise to 25% with a 5% increment in each step.

The LpqN-6LT or LpqN-T6D crystals were prepare by incubating the purified LpqN protein (15 mg/ml) with 0.1% 6LT or 0.1% T6D for 2 hours at 4^{o}C before crystallization. Crystals of LpqN-6LT and LpqN-T6D were then prepared using similar procedures as above. Their crystallization conditions are identical to each

other. The reservoir solution for these complex crystals is the same as that for *apo*-LpqN (0.1 M Na-citrate (pH 6.0) and 1.9 M $(NH_4)_2SO_4$). Both crystals of LpqN-6LT and LpqN-T6D grew to a full size in the drops within two weeks. Cryoprotection was achieved by raising the glycerol concentration stepwise to 25% with a 5% increment in each step.

Data collection, structural determination and refinement - All diffraction data were collected at 100K at beamline 24ID-C located at the Advanced Photon Source, using a Pilatus 6M detector (Dectris Ltd., Switzerland). Diffraction data were processed using DENZO and scaled using SCALEPACK (Otwinowski and Minor, 1997). Crystals of LpqN, LpqN-6LT, LpqN-T6D and SeMet-LpqN belong to space groups C121, I4, I4 and C121, respectively (**Table 2.4**).

The LpqN protein contains two methionines (excluding the N-terminal methionine). Within the asymmetric unit of SeMet-LpqN, these two selenium sites were identified using SHELXC and SHELXD (Schneider and Sheldrick, 2002) as implemented in the HKL2MAP package (Pape and Schneider, 2004). Single anomalous dispersion (SAD) was employed to obtain experimental phases using the program Autosol (Terwilliger et al., 2009) in PHENIX (Adams et al., 2002). The resulting phases were then subjected to density modification and NCS averaging using the program PARROT (Cowtan, 2010) using the native structure factor amplitudes. The SeMet sites were also used to trace the molecule by anomalous difference Fourier maps, where we could ascertain the proper registry

of SeMet residues. The initial model of LpqN was constructed manually using program Coot (Emsley and Cowtan, 2004). Then the model was refined using PHENIX, leaving 5% of reflections in the Free-R set. Iterations of refinement were performed using PHENIX. Model buildings were done using Coot, which led to the current model (**Table 2.4**).

The crystal structures of LpqN-6LT and LpqN-T6D were determined by molecular replacement (MR), utilizing the final structure of LpqN as a search model. The procedures for structural refinement and model building were the same as those of LpqN (**Table 2.4**).

LpqN-MmpL11/Ag85A Interaction - HA-tagged LpqN was amplified by PCR using *lpqN* -570.F/+HA.R primers and the resulting product cloned into the pOLYG plasmid to generate pOLYG *lpqN* HA where LpqN is expressed from its native promoter. MmpL11 was amplified using *mmpL11* TAP.F/R primers and ligated in-frame with the Tandem affinity-tagged (TAP; 6xHistidine and FLAG-tag) tag into pOLYG-TAP plasmid to generate pOLYG *mmpL11*-TAP plasmid. MmpL11 expression in the pOLYG *mmpL11* TAP is driven by its native promoter. The *lpqN*-HA fragment was ligated into the pOLYG*mmpL11*-TAP plasmid to generate the pOLYG*lpqN*-HA/*mmpL11*-TAP co-expression plasmid. HIS-tagged Ag85A was amplified using Ag85A.F/R primers and ligated into the pOLYG plasmid via NEBuilder (New England Biolabs) to generate pOLYG*ag85A*-HIS. The *lpqN*-HA fragment was ligated into the pOLYG*ag85a*-HIS plasmid to

generate the pOLYG*lpqN*-HA/*ag85A*-HIS co-expression plasmid, as above. To test the LpqN/MmpL11 interaction, *M. smegmatis* mc^2155 was transformed with either pOLYG*lpqN*-HA or pOLYG*lpqN*-HA/*mmpL11*-TAP, and grown in 7H9 liquid medium, as above. Protein cross-linking was induced by adding formaldehyde to a final concentration of 1% for 30 minutes at room temperature. All samples were quenched with 2.5 M glycine, washed with 1x PBS, and lysed in urea lysis buffer (8 M urea, 300 mM NaCl, 0.5% NP-40, 50 mM NaH_2PO_4, 50 mM Tris, Roche Complete Protease Inhibitor, pH 7.0) via sonication. Lysates were incubated on buffer-equilibrated HisPur Cobalt Superflow Agarose Resin (Thermo Scientific), washed extensively, and eluted in urea lysis buffer adjusted to 300 mM imidazole. Resin flow through and elutions were separated via SDS-PAGE (10%) and analyzed by Western blot (1:2500 mouse monoclonal α-FLAG/α-HA; Thermo Scientific). To test the LpqN/Ag85A interaction, *M. smegmatis* was transformed with pOLYG*ag85a*-HIS or pOLYG*lpqN*-HA/*ag85A*-HIS, and cross-linked as above. Washed cell pellets were lysed in 1X PBS + Roche Complete Protease Inhibitor via sonication, and incubated on Pierce HA Epitope Tag Antibody Agarose conjugate (Thermo Scientific). Resin-bound proteins were extensively washed in lysis buffer, eluted in 50 mM NaOH and immediately quenched with 1.0 M Tris pH 8.5. Lysates, resin flow through, and elutions were separated via SDS-PAGE (15%) and analyzed by Western blot (1:1000 rabbit polyclonal α-HIS/α-HA; Thermo Scientific).

ACKNOWLEDGMENTS

This project was funded by R21 AI113074 to GEP, and R01 AI123148 to GEP and EWY. GCM was funded by 5T32AI007472. Protein mass spectrometric analysis was performed by the OHSU Proteomics Shared Resource with partial support from NIH core grants P30EY010572, P30CA069533 and S10OD012246. Lipid mass spectrometric analysis was performed by the Washington University Biomedical Mass Spectrometry Research Resource which is supported by NIH grants P41-GM103422. P60-DK-20579, and P30-DK56341.

CONFLICT OF INTEREST

The authors declare that they have no conflicts of interest with the contents of this article.

Table 2.5. Primers used in this study.

Name	Primer (5'-3')
ΔlpqN 5' F	tataagatcttagtcgtagccggcgtagtt
ΔlpqN 5' R	tataaagcttgctgtcggtcttgatgttga
ΔlpqN 3' F	tatatctagagcagaagacggtggtgattc
ΔlpqN 3' R	agctggtaccatgtggtagcggaactcgac
lpqN -865	aggtgccatacgagctgaac
lpqN +1637	tcaagggaatcgagaagtgc
lpqN +367	gcgatcctctccaaactcac
hyg primer 22	tggctaaaatgtatcctaaatcag
hyg primer 3500	tgttataacagacactgcttg
mmpL3D1.102	atcaattggcaagcacgtcacgcagagc
mmpL3D1.573	atatcgatcaacggcagcgccagcacttc
mmpL3D2.990	tacaattgcaatcctgggcaaacacgt
mmpL3D2.1185	taatcgatcatcacccggttaaccagcttg
mmpL11D1.90	atcaattgcgatgacgcagtcggggaatc
mmpL11D1.349	atatcgatgcgttcggcgttggcaatatc
mmpL11D2.1172	aattcatatggtgctgggcaacagcttg
mmpL11D2.1587	ataggatcctcacggttgcgtcgcggacac
lpqN.61	atatcatatgagtttcaacatcaagaccgacag
lpqN.687	atatggatccttagggcgtgatggtcgtctc
lpqN qRT.Forward	gcgatcctctccaaactcac
lpqN qRT.Reverse	ggaatcaccaccgtcttctg
lpqN.pUAB300.F	aaggatccagtttcaacatcaagaccgacag
lpqN.pUAB300.R	ttatcgatttagggcgtgatggtcgtctg
lpqT.pUAB300.F	taggatcctgcggaccgaaatcgcctg

lpqT.pUAB300.R	ataagctttactttgccgcgacgacg
lprG.pUAB300.F	cggtggaggtggtgggtccggatcctgctcgtcgggctcgaag
lprG.pUAB300.R	tacgtcgacatcgataagcttcagctcaccgggggcttc
mtc28.pUAB300.F	taggatccgatcccctgctgccaccg
mtc28.pUAB300.R	ataagcttctagcgcggcgggactgg
lpqN -570.F	atgatatcgacctcggtgtcgtcgtg
lpqN +HA.R	taaagcttttaagcgtaatctggaacatcgtatgggtagggcgtgatggtcgtctg
lpqN TAP.F	atggatccggcaacatcgagatgtcgccga
lpqN TAP.R	tcaatgatgatgatgatgatgtcctcctcctcccttgtcgtcatcgtctttgtagtcggatccgggcgtgatggtcgtctgct
mmpL11 TAP.F	atggatcccgcctcgaaatgggccttca
mmpL11 TAP.R	atggatcccctcgcctcctccaacatcg
Ag85A.F	agtggatccccccgggctgcagcgcaagccgaagcggccctg
Ag85A.R	agtggtggtggtggtggctagcggcgccctggggcgcggg

CHAPTER 3

MMPL11 LIPID TRANSPORTER FUNCTION IS MODULATED BY C-TERMINAL PHOSPHORYLATION

Geoff C. Melly[1], Haley Stokas[1], Patrick M. Davidson[1], José Santinni Roma[1], and Georgiana E. Purdy[1]

[1]Oregon Health & Science University, Department of Molecular Microbiology & Immunology, Portland, OR, 97239, United States

Contributions: That MmpL11 is phosphorylated was originally reported by Prisic et al. Based on this, GM proposed the analyses of MmpL11 phosphorylation, in addition to domain deletions. Optimization of MmpL11 purification and *in vitro* kinase assays were performed by GM. Other experiments were performed as a collaborative effort between many Purdy Lab members. Specific contributions are noted in the figure legends.

This manuscript is pending submission (November 2019).

ABSTRACT - The *Mycobacterium tuberculosis* (*Mtb*) cell envelope is a critical interface between the host and pathogen and provides a protective barrier against the immune response and antibiotics. Cell envelope lipids are mycobacterial virulence factors that influence the host immune response. The mycobacterial membrane protein Large (MmpL) proteins transport cell envelope lipids and siderophores that are important for the basic physiology and pathogenesis of *Mtb*. We recently identified MmpL11 as a conserved transporter of mycolic acid containing lipids including monomeromycolyl diacylglycerol (MMDAG), mycolate wax ester (MWE), and long-chain triacylglycerols (LC-TAGs). These lipids contribute to biofilm formation in *Mtb* and *M. smegmatis*, and persistence in *Mtb*. In this report, we identified MmpL11 domains and residues that are essential for lipid transporter activity. Specifically, we show that the D1 periplasmic loop and a conserved tyrosine are essential for MmpL11 function. Intriguingly, we found that MmpL11 levels are regulated by phosphorylation of the cytoplasmic C-terminal domain. To our knowledge, this study is the first direct evidence of phospho-regulation of MmpL transporter activity in *Mtb* and *M. smegmatis*. Our results offer further insight into the function of MmpL transporters and regulation of mycobacterial cell envelope biogenesis.

INTRODUCTION

Mycobacterium tuberculosis (*Mtb*), the causative agent of the human disease tuberculosis (TB), remains a major public health concern. In 2017, there were approximately 10 million new cases and 1.3 million deaths due to TB (World Health Organization, 2018). The *Mtb* cell envelope and associated lipids play a crucial role at the host-pathogen interface to promote bacterial survival. The lipid-rich mycobacterial cell envelope is a robust physical barrier to host antimicrobial defenses and antibiotics. This intrinsic resistance is largely conferred by mycolic acids, extremely long chain (C_{60-90}) α-alkyl-β-hydroxy fatty acids that are major constituents of the mycobacterial cell envelope (Barry et al., 1998). Mycolic acids and their derivatives form an outer layer termed the mycomembrane that consists of an inner leaflet of mycolylated arabinogalactan (AG) anchored to peptidoglycan (the mAGP complex) and an outer leaflet of non-covalently associated lipids such as phthiocerol dimycocerosate (PDIM), sulfolipids, and trehalose 6,6'-dimycolate (TDM) (Chiaradia et al., 2017; Marrakchi et al., 2014). In addition to acting as a passive physical barrier, some cell envelope components can directly interfere with host immune responses (Camacho et al., 2001; Cambier et al., 2014; Indrigo, 2003).

The biogenesis of the mycobacterial cell envelope is incompletely described despite decades of research. Recent work showed that the MmpL family of proteins transports cell envelope constituents from the bacterial cytoplasm to the

periplasmic space where they are subsequently incorporated into the cell envelope (reviewed in (Melly and Purdy, 2019)). MmpL proteins are considered members of the resistance-nodulation-cell division (RND) superfamily of integral membrane transporters. Typically, RND transporters utilize energy derived from the proton motive force (PMF) to export their substrates (Domenech et al., 2005; Owens et al., 2013; Ruggerone et al., 2013), and this appears to be the case for at least one MmpL family member (Bernut et al., 2016). While MmpL proteins share some properties with the well-studied RND proteins from Gram-negative bacteria, it appears that their structure and function are unique. The structure of MmpL3 from *M. smegmatis* was recently solved, revealing that the protein is distinct from RND proteins in that it functions as a monomer rather than the expected trimer (Su et al., 2019; Zhang et al., 2019). As mentioned, MmpL proteins export bulky hydrophobic substrates, whereas many RND family proteins are notable for their drug efflux properties (Delmar et al., 2014). Therefore, further research into the structure and function of the MmpL proteins may reveal additional novel features.

A number of MmpL-exported substrates have been identified. Importantly, MmpL3 transports trehalose monomycolate (TMM) into the periplasm (Grzegorzewicz et al., 2012; Xu et al., 2017). Mycolic acid transfer catalyzed by members of the periplasmic antigen 85 (Ag85) enzyme complex generates AG-anchored mycolic acids and free TDM from TMM. Together, AG-anchored and trehalose-esterified mycolic acids form the inner and outer leaflets, respectively,

of the mycomembrane (Backus et al., 2014; Belisle et al., 1997; Grzegorzewicz et al., 2012). MmpL3 is therefore an essential *Mtb* protein, and an attractive target for therapeutic development (Degiacomi et al., 2017; Li et al., 2016). MmpL4, MmpL5, MmpL7, MmpL8, MmpL10 and MmpL11 are required for full *Mtb* virulence, indicating that their substrates are important in the context of infection (Domenech et al., 2005; Lamichhane et al., 2005). This has been conclusively shown for a number of MmpL substrates. For example, MmpL7 transports PDIM, which masks activators of host pattern recognition receptors (PRRs), and MmpL8 transports sulfolipids, which antagonize innate immune signaling (Blanc et al., 2017; Cambier et al., 2014).

We identified MmpL11 as a conserved transporter of lipids that contribute to biofilm formation in *M. smegmatis* and *Mtb*. The *M. smegmatis mmpL11* mutant makes monomeromycolyl diacylglycerol (MMDAG) and mycolate wax ester (MWE), but fails to transport them to the bacterial surface, indicating that these lipids are substrates for MmpL11 (Pacheco et al., 2013). We subsequently showed that long-chain triacylglycerols (LC-TAGs) and MWE are the MmpL11 substrates in *Mtb* where they also contribute to intracellular growth and non-replicating persistence (Wright et al., 2017). Because MmpL11 and its substrate lipids are important for the maintenance *of Mtb* infection, we sought to further characterize MmpL11 function. We report the identification of protein domains and residues that are essential to MmpL11 transporter activity, and show that phosphorylation of the MmpL11 cytoplasmic C-terminus is important for

regulating transporter levels. To our knowledge, this study provides the first direct evidence of phospho-regulation of MmpL transporter activity. Together, these findings offer further insight into the physiological processes underlying the biogenesis of the *Mtb* cell envelope.

RESULTS

Identification of Critical Residues and Domains for MmpL11 Function - $MmpL11_{TB}$ is predicted to contain 12 transmembrane (TM) helices, two major periplasmic loop domains (D1 = 150 and D2 = 136 aa) and a 277-aa cytoplasmic C-terminal tail (**Figure 3.1A**) (Sonnhammer et al., 1998). We previously reported that heterologous expression of $MmpL11_{TB}$ via the pVV16 vector complements the *M. smegmatis mmpL11* mutant, indicating that MmpL11 function is conserved (Pacheco et al., 2013). We therefore used complementation of the *M. smegmatis mmpL11* mutant with $MmpL11_{TB}$ point and deletion mutants followed by biofilm formation and lipid analysis as a tractable system for rapidly determining the contribution of specific residues and domains to $MmpL11_{TB}$ function.

A previous study noted strict conservation of a TM10 tyrosine residue amongst *Mtb* MmpL family members and showed that this residue was essential for MmpL3 function in *M. smegmatis* (Bernut et al., 2016). We hypothesized that this residue was important for MmpL11 function as well. To address this, we

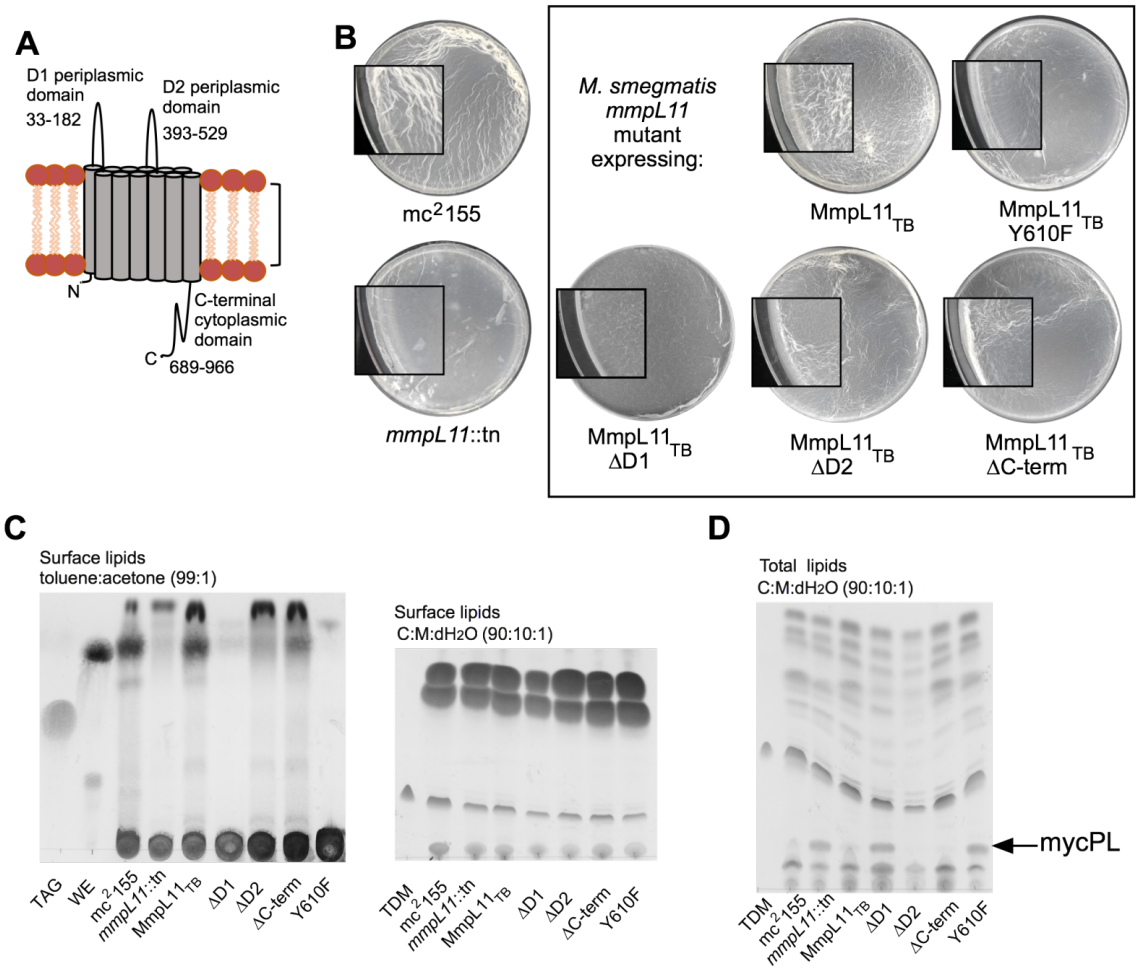

Figure 3.1. Identification of MmpL11 residues important for biofilm formation. (**A**) Schematic diagram of MmpL11 structural domains. (**B**) Wild-type mc^{2}155, *mmpL11*-deficient, and MmpL11$_{TB}$-variant-expressing *M. smegmatis* biofilms were grown in petri dishes and imaged at 4 days post-inoculation. (**C**) Hexanes-extractable surface lipids of 4-day old biofilms were resolved via TLC in 99:1, v:v, toluene:acetone (left) or chloroform: methanol:dH2O (90:10:1) (right). TAG: triacylglycerol standard, WE: wax ester standard, TDM: TDM standard (Sigma). (**D**) Total lipids of 4-day old biofilms were resolved via TLC in chloroform:methanol:dH2O (90:10:1). *These data were collected by Dr. Georgiana Purdy and Patrick Davidson (Purdy Lab).*

assessed the ability of a Y610F point-substituted MmpL11$_{TB}$ mutant to complement the *M. smegmatis mmpL11* mutant. The biofilm phenotype of the *M. smegmatis mmpL11* mutant expressing MmpL11$_{TB}$(Y610F) resembled that of the *M. smegmatis mmpL11* mutant in that it was weaker and less reticulated than biofilms formed by wild-type *M. smegmatis* (**Figure 3.1B**). Thin-layer chromatography (TLC) analysis of biofilm surface lipids verified the inability of point-substituted MmpL11$_{TB}$(Y610F) to reconstitute the wild-type *M. smegmatis* biofilm lipid profile (**Figure 3.1C**). These observations confirm the essentiality of residue Y610 to MmpL11 function. As a control to demonstrate that other surface lipids are not impacted, we analyzed the same lipid extracts using a different solvent system. There were no significant differences observed in the surface lipid profiles using the chloroform:methanol:water (90:10:1) solvent system, indicating that the MmpL11$_{TB}$(Y610F) point substitution specifically inhibited transport of MmpL11 lipid substrates (**Figure 3.1C**).

Domain-dependent interactions may also be important for MmpL11 transporter function. A recent report described an interaction between recombinantly-expressed MmpL11$_{TB}$ D1 and D2 periplasmic domains (Chim et al., 2015). These large periplasmic domains are thought to be analogous to the porter/docking domains of canonical RND transporters that permit substrate release during transport. In addition, the C-terminal cytoplasmic domain may act as a scaffold to enable co-localization of cell envelope biosynthetic and transport machinery, as suggested for MmpL7 (Jain and Cox, 2005). To investigate the contribution of

these domains to MmpL11 lipid transport, we created separate expression constructs for MmpL11$_{TB}$ lacking the D1 or D2 periplasmic loop domain [MmpL11$_{TB}$(ΔD1), MmpL11$_{TB}$(ΔD2)] or the C-terminal cytoplasmic tail [MmpL11$_{TB}$(ΔC-term)]. *M. smegmatis mmpL11* mutant biofilms expressing the ΔD1 domain deletion mutant resembled the *mmpL11* mutant (**Figure 3.1B**). Consistent with the visual biofilm phenotype, the ΔD1 domain deletion construct failed to complement the *mmpL11* mutant surface lipid phenotype (**Figure 3.1C**). *M. smegmatis mmpL11* mutants expressing either the ΔD2 or the ΔC-term MmpL11 domain deletion mutants formed biofilms, although they exhibited an intermediate visual phenotype relative to the *mmpL11* mutant and *mmpL11* mutant complemented with wild-type MmpL11$_{TB}$ (**Figure 3.1B**). Furthermore, the surface lipid profiles of the ΔD2 or the ΔC-term domain mutant biofilms did not differ from the wild-type *M. smegmatis* biofilm (**Figure 3.1C**). These results suggest that the periplasmic MmpL11$_{TB}$ D1 loop, but not the D2 loop or C-terminal domains, is required for optimal transport of lipid substrates in *M. smegmatis*. In our previous study, we found that the M. *smegmatis mmpL11* mutant accumulated the mycolic acid biosynthetic intermediate mycPL in total lipid extracts (Pacheco et al., 2013). Consistent with our observations, we found that *mmpL11* mutants expressing the point-substituted MmpL11$_{TB}$(Y610F) and MmpL11$_{TB}$(ΔD1) also accumulated mycPL (**Figure 3.1D**). To confirm that the observed biofilm defects were the result of specific lipid deficiencies, and not due to impaired bacterial growth during biofilm formation, we quantified bacteria in the wells from which biofilms were harvested. In all biofilm assays, the number of M.

smegmatis mmpL11 mutant bacteria carrying *mmpL11* variant alleles was the same as wild-type (data not shown). This result is consistent with our previous observation that the lack of functional MmpL11 in *M. smegmatis* or *Mtb* does not impact bacterial replication in biofilm medium (Pacheco et al., 2013; Wright et al., 2017).

To confirm that $MmpL11_{TB}$ expression and stability in the *M. smegmatis mmpL11* mutant were not impacted by the D1 domain deletion or Y610F mutation, we evaluated the protein levels of these $MmpL11_{TB}$ variants via Western analysis. Protein levels of the two non-functional $MmpL11_{TB}$ variants were higher in these complemented strains than in the wild-type $MmpL11_{TB}$ complemented strain (**Figure 3.2**). Therefore, the inability of these mutant alleles to complement the *M. smegmatis mmpL11* mutant phenotype is due to deficient protein function and not a result of diminished protein expression or stability. The increased protein levels in the ΔD1 and Y610 expression strains suggest that the bacterium responds to the lack of functional protein by upregulating or stabilizing MmpL11. Together, these data reveal that the periplasmic D1 domain and residue Y610 are absolutely critical for $MmpL11_{TB}$ transporter function.

$MmpL11_{TB}$ function and stability is modulated by phosphorylation - Serine/threonine protein kinases (STPKs) modulate the function of many *Mtb* proteins, including cell envelope biosynthetic enzymes, via phosphorylation of specific residues (Molle et al., 2010; Veyron-Churlet et al., 2010). Intriguingly,

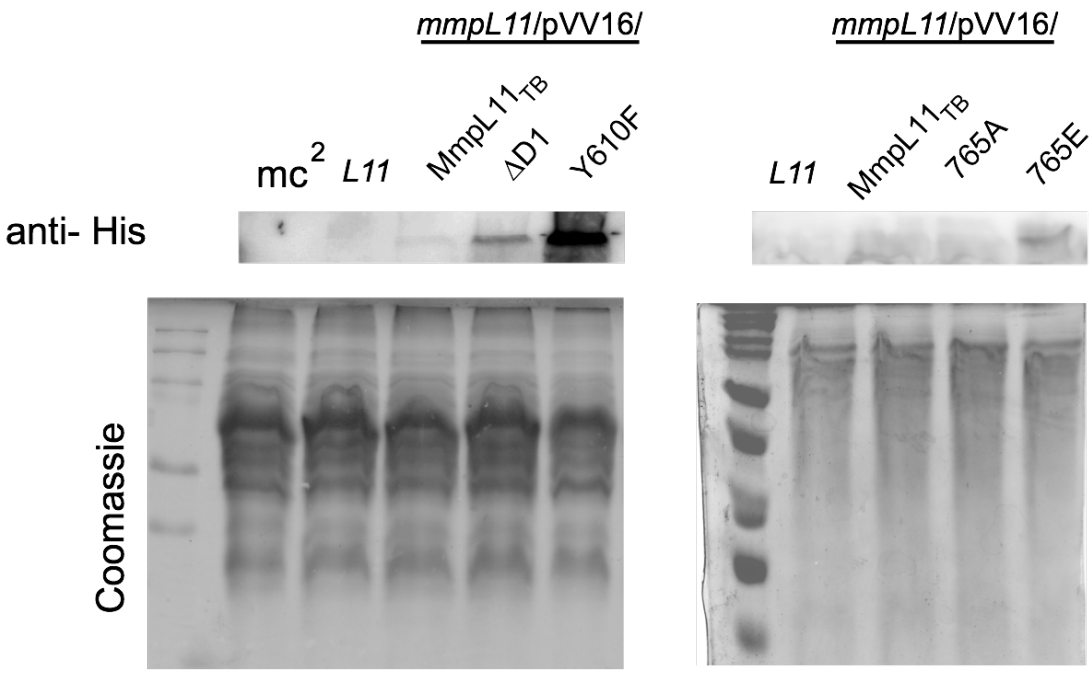

Figure 3.2. $MmpL11_{TB}$ levels in heterologous complementation strains. Whole-cell lysates of *M. smegmatis mmpL11* mutant expressing 6xHistidine-tagged $MmpL11_{TB}$ variants from the pVV16 vector were harvested. Samples were normalized to protein amounts, separated via SDS-PAGE, and probed with anti-Histidine antibody. Coomassie-stained total protein is shown as a loading control. *This analysis was performed by Haley Stokas (Purdy Lab).*

Prisic et al. reported that MmpL11$_{TB}$ was phosphorylated at residue T765 when grown in planktonic culture with acetate as the sole carbon source (Prisic et al., 2010). This observation suggests that MmpL11 function could be modulated by phosphorylation at T765 in response to metabolic cues. We created phospho-ablative [MmpL11$_{TB}$(T765A)] and phospho-mimetic [MmpL11$_{TB}$(T765E)] expression constructs in the pVV16 expression vector, and took advantage of our *M. smegmatis mmpL11* mutant complementation system to determine if MmpL11T$_B$ transporter activity is regulated by protein phosphorylation at this residue. MmpL11-deficient *M. smegmatis* expressing the phospho-ablative MmpL11$_{TB}$(T765A) point-substituted allele formed reticulated biofilms that resembled wild-type *M. smegmatis* biofilms both visually and in surface lipid profile (**Figure 3.3A-B**). However, the phospho-mimetic MmpL11$_{TB}$(T765E) allele failed to complement either the visual biofilm phenotype or the surface lipid profile of the *M. smegmatis mmpL11* mutant (**Figure 3.3A-B**). This result demonstrates that phosphorylation at T765 negatively regulates either MmpL11$_{TB}$ function or stability. There were no significant differences observed in the surface lipid profiles using the chloroform:methanol:water (90:10:1) solvent system, indicating that the MmpL11$_{TB}$(T765E) point substitution specifically inhibited transport of MmpL11 lipid substrates (**Figure 3.3B**). Western analysis of the pVV16 *mmpL11$_{TB}$*(T765A) and phospho-mimetic pVV16 *mmpL11$_{TB}$*(T765E) expression strains confirmed that constitutive expression resulted in adequate protein expression (**Figure 3.2**). Thus, phosphorylation of residue T765 inhibits MmpL11$_{TB}$-mediated lipid export in *M. smegmatis.*

Figure 3.3. Identification of MmpL11 phosphorylated residues important for biofilm formation in *M. smegmatis*. (**A**) Wild-type mc^2155, *mmpL11*-deficient, and $MmpL11_{TB}$-variant-expressing *M. smegmatis* biofilms were grown in petri dishes and imaged at 4 days post-inoculation. (**B**) Hexanes-extractable surface lipids of 4-day old biofilms were resolved via TLC (99:1, v:v, toluene:acetone) or chloroform: methanol:dH2O (90:10:1). TAG: triacylglycerol standard, WE: wax ester standard (Sigma), TDM: TDM standard (Sigma). *These analyses were performed by Dr. Georgiana Purdy.*

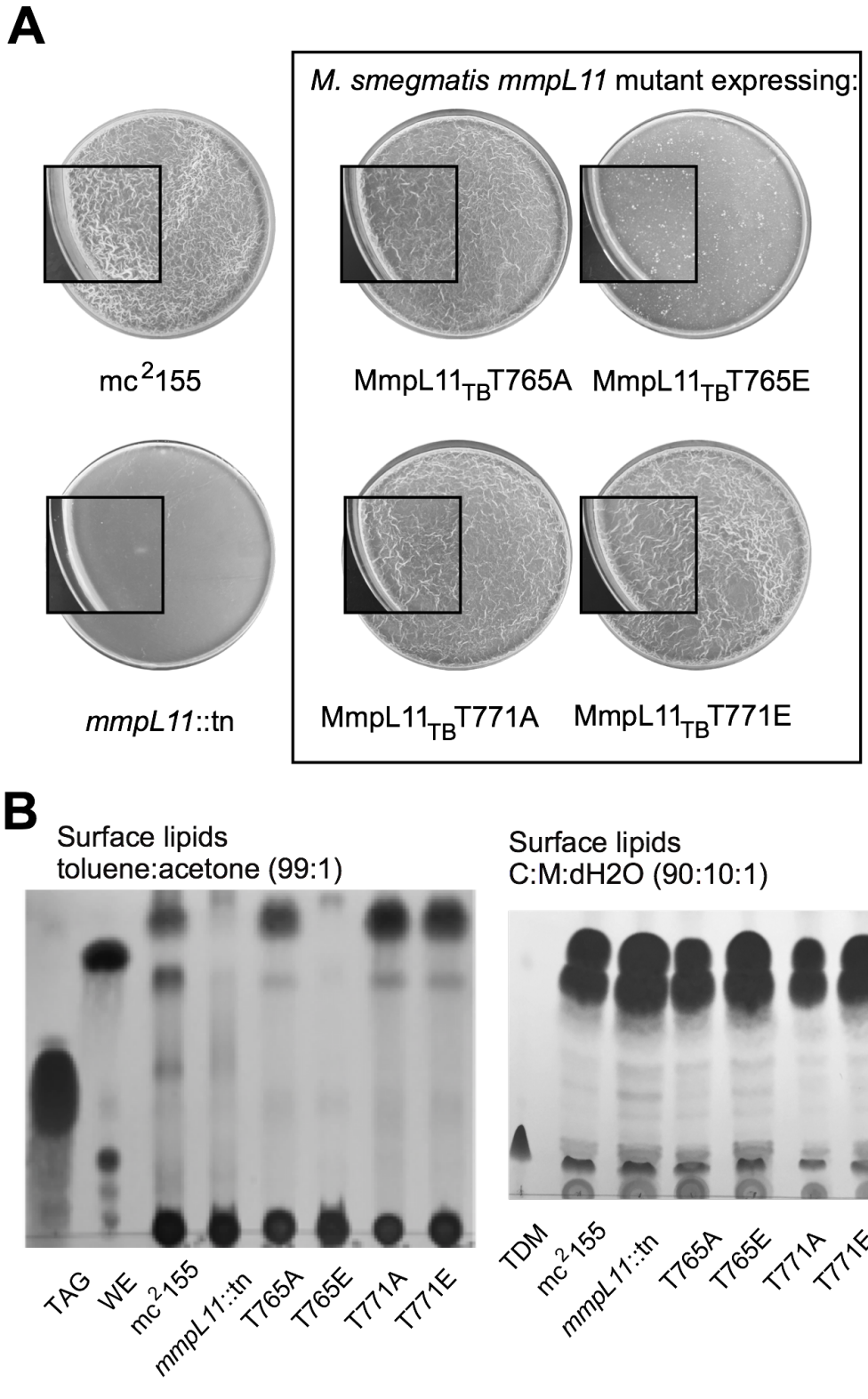
A
M. smegmatis mmpL11 mutant expressing:
mc2155
MmpL11TBT765A
MmpL11TBT765E
mmpL11::tn
MmpL11TBT771A
MmpL11TBT771E
B
Surface lipids
toluene:acetone (99:1)
TAG
WE
mc2155
mmpL11::tn
T765A
T765E
T771A
T771E
Surface lipids
C:M:dH2O (90:10:1)
TDM
mc2155
mmpL11::tn
T765A
T765E
T771A
T771E

The previous phospho-proteomic study reported by Prisic was performed on *Mtb* planktonic cultures grown with different carbon sources (Prisic et al., 2010). Given that the phosphorylation state of T765 impacted MmpL11$_{TB}$ function in *M. smegmatis*, we examined the *in vivo* phosphorylation state of MmpL11$_{TB}$ purified from *M. smegmatis*. Initial protein purification attempts from the constitutive pVV16 expression constructs were unsuccessful, so MmpL11$_{TB}$ was cloned with its native promoter in the mycobacterial shuttle vector pOLYG with a C-terminal FLAG- 6X-His affinity tag. Expression of MmpL11$_{TB}$ in *M. smegmatis* was followed over time, and we observed increased levels of MmpL11$_{TB}$ when bacterial cultures were in stationary and late stationary phase (**Figure 3.4**).

MmpL11$_{TB}$ was purified under denaturing conditions from *M. smegmatis mmpL11*//pOLYG *mmpL11$_{TB}$* biofilm cultures. Using mass spectrometry analysis, we identified 6 phosphorylation sites when MmpL11$_{TB}$ was harvested from biofilm cultures, two of which had sites that were ambiguously identified due to a lack of fragment ions in the regions of interest (**Table 3.1**). The peptide containing T765 and T771 was one of these ambiguously assigned peptides, and phosphorylation could occur at either of these sites. To determine if residue T771 was also important for MmpL11$_{TB}$ function in *M. smegmatis* biofilms, we created phospho-ablative (T771A) and –mimetic (T771E) MmpL11$_{TB}$ expression constructs. Both the phospho-ablative and phospho-mimetic MmpL11$_{TB}$(T771) constructs complemented the *M. smegmatis mmpL11* mutant biofilm and surface lipid phenotype to that of wild-type (**Figure 3.3B**), indicating that the phosphorylation

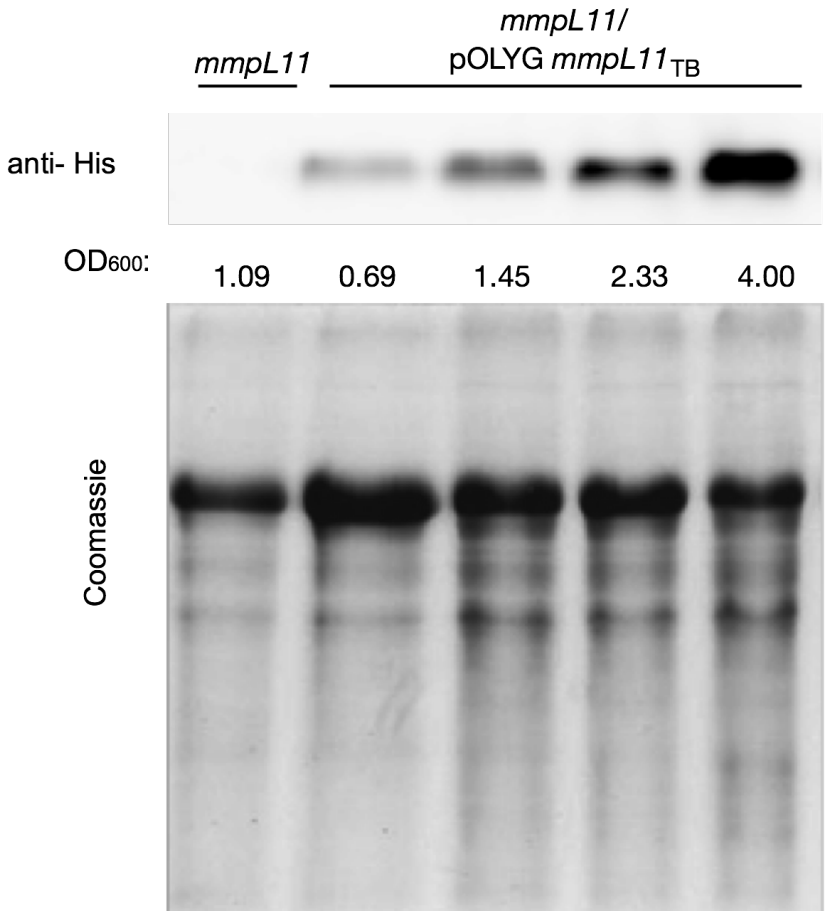

Figure 3.4. MmpL11$_{TB}$ accumulates in late stationary phase culture. Whole-cell lysates of *M. smegmatis* expressing 6xHistidine-tagged MmpL11$_{TB}$ under control of its native promoter were harvested at the indicated optical densities. Samples were normalized to protein amounts, separated via SDS-PAGE, and probed with anti-Histidine antibody. Coomassie-stained total protein is shown as a loading control. *This analysis was performed by José Santinni Roma (Purdy Lab).*

Table 3.1. Phosphorylated MmpL11$_{TB}$ residues (#) in biofilms of the *M. smegmatis mmpL11* mutant expressing MmpL11$_{TB}$. *MmpL11 protein was purified by José Santinni Roma, with technical assistance provided by the OHSU Proteomics Shared Resource.*

MmpL11 Peptide	Start AA
R.GAPALALVAAPRPDAS#Y#QDIDNAVALLR.Q*	64
R.VAGAAQVDVGGPT#ALIKDFDDR.V	502
R.LAPDAICVT#DPLAFT#GCGCDGKALDQVQLAYR.N*	757
K.RLAVALDALQT#TTWECGGVQTHR.A	811
R.LAVALDALQT#T#TWECGGVQTHR.A	812
R.RCLS#VAVAMLEEAR.-	953

*Singly phosphorylated, but site could not be localized from observed fragment ions.

status of T771 does not impact MmpL11$_{TB}$ function in *M. smegmatis*. While we were unable to confirm the presence or absence of phospho-T765 in MmpL11$_{TB}$ harvested from *M. smegmatis* biofilms, its absence would be consistent with the contribution that functionally active MmpL11 lipid transporter makes to biofilm formation in the organism.

Phosphorylation of residue T765 inhibited MmpL11$_{TB}$ transporter activity when heterologously expressed *in M. smegmatis*. To determine the relative importance of T765 phosphorylation status in the native *Mtb* environment, we transformed the *Mtb mmpL11* mutant (*Mtb mmpL11*::hyg) with the phospho-ablative and –mimetic MmpL11$_{TB}$ point-substituted expression constructs and analyzed biofilm formation. The *Mtb mmpL11* mutant expressing the phospho-ablative MmpL11$_{TB}$(T765A) phenocopied the visual biofilm phenotype of wild-type *Mtb*, while the phospho-mimetic MmpL11$_{TB}$(T765E) failed to complement the *Mtb mmpL11* mutant (**Figure 3.5A**). Consistent with these results, the lipid profile of the MmpL11$_{TB}$(T765A)-expressing strain resembled that of wild-type *Mtb*, whereas the MmpL11$_{TB}$(T765E)-expressing strain failed to complement (**Figure 3.5B).** Again, there were no significant differences observed in the surface lipid profiles using the chloroform:methanol:water (90:10:1) solvent system, indicating that only MmpL11 substrates were impacted. Taken together, these data suggest that the phosphorylation status of T765 in the C-terminal domain modulates the lipid transporter activity of MmpL11$_{TB}$ in both *M. smegmatis* and *Mtb*.

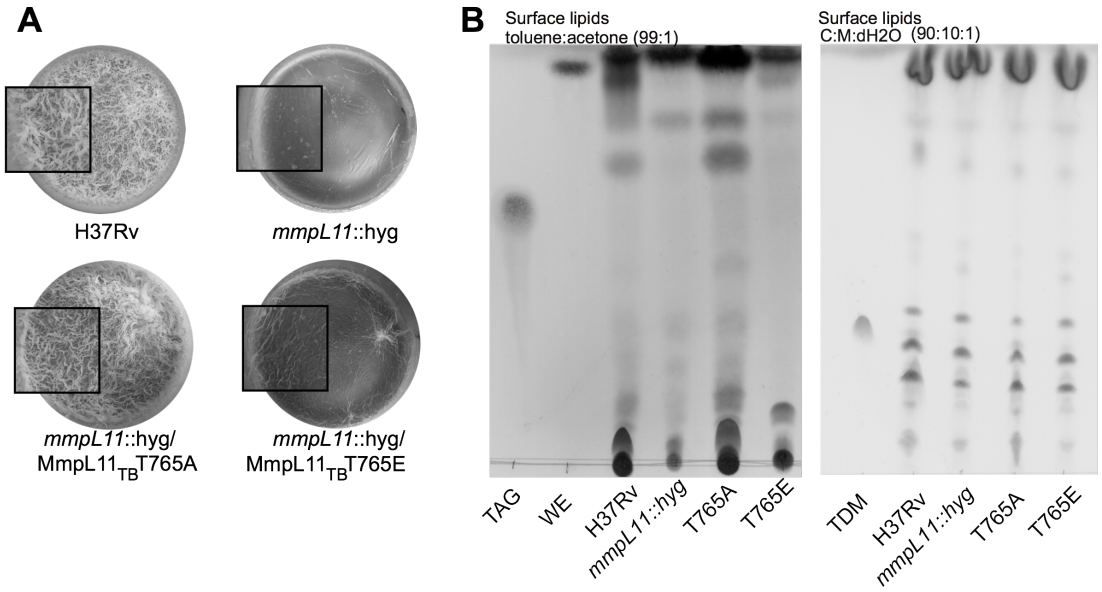

Figure 3.5. Identification of MmpL11 phosphorylated residues important for biofilm formation in *Mtb*. (**A**) Wild-type H37Rv, *mmpL11* mutant, and $MmpL11_{TB}$-variant-expressing biofilms were grown in culture bottles and imaged at 3 weeks post-inoculation. (**B**) Hexanes-extractable surface lipids of 3-week old biofilms were resolved via TLC (99:1, v:v, toluene:acetone) or chloroform:methanol:dH2O (90:10:1). TAG: triacylglycerol standard, WE: wax ester standard (Sigma), TDM: TDM standard (Sigma). *This analysis was performed by Dr. Georgiana Purdy.*

We were interested in whether protein expression levels of the non-functional phospho-mimetic MmpL11 variant would be altered relative to the functional wild-type MmpL11 protein. To investigate protein expression levels, we transformed the *M. smegmatis mmpL11* mutant with the pOLYG phospho-ablative (T765A) and –mimetic (T765E) $MmpL11_{TB}$ expression constructs where MmpL11 expression is controlled via its native promoter. We followed protein levels over time as done with the wild-type $MmpL11_{TB}$ above. While the phospho-ablative $MmpL11_{TB}$(T765A) protein accumulated over time, as did wild-type $MmpL11_{TB}$, the phospho-mimetic $MmpL11_{TB}$(T765E) protein did not (**Figure 3.6**). These data suggest that protein expression of wild-type functional MmpL11 increases over time, while that of non-functional MmpL11 does not.

This observation implies that phosphorylation post-translationally regulates MmpL11 protein levels. However, MmpL11 levels may also be regulated transcriptionally. To address this possibility, we used qRT-PCR to examine the expression of the *mmpL11* gene *in vitro* under conditions relevant to growth phase, hypoxia, and reaeration. We did not observe significant transcriptional regulation of *mmpL11* in *Mtb* upon exposure to any of these conditions, indicating that expression of *mmpL11* is not transcriptionally responsive to in vitro growth condition (**Figure 3.7**).

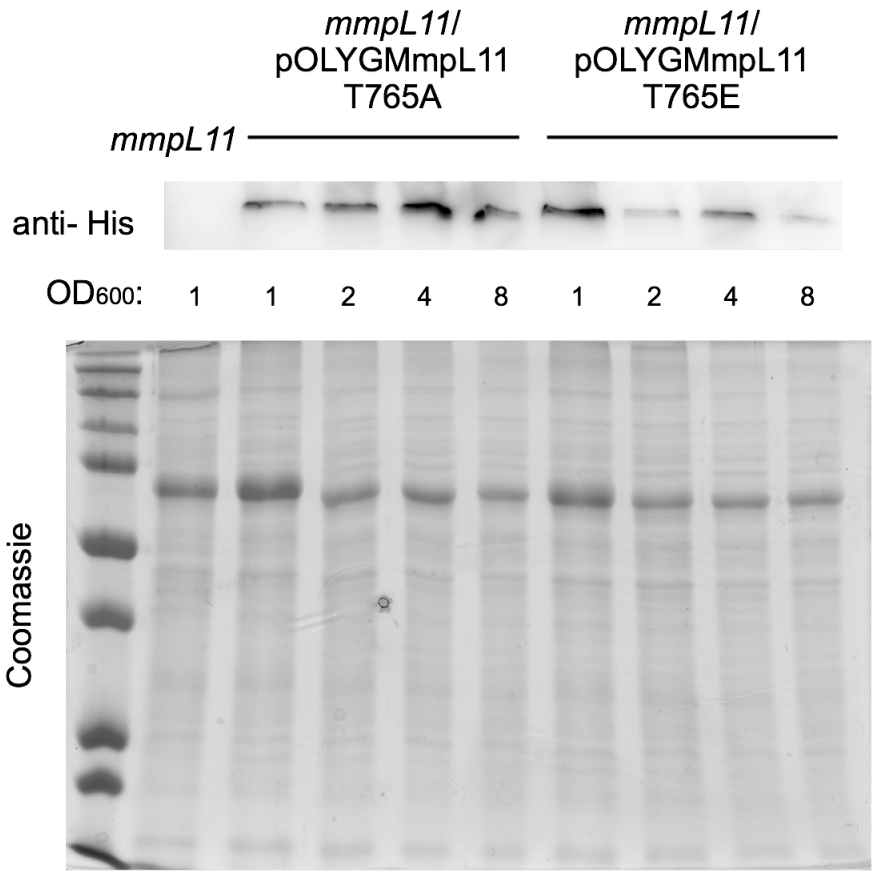

Figure 3.6. Phosphorylation regulates MmpL11 levels. Whole-cell lysates of *M. smegmatis* expressing 6xHistidine-tagged MmpL11$_{TB}$ phospho-ablative (T765A) and –mimetic (T765E) alleles under control of the native promoter were harvested at the indicated optical densities. Samples were normalized to protein amounts, separated via SDS-PAGE, and probed with anti-Histidine antibody. Coomassie-stained total protein is shown as a loading control. *This analysis was performed by Haley Stokas (Purdy Lab).*

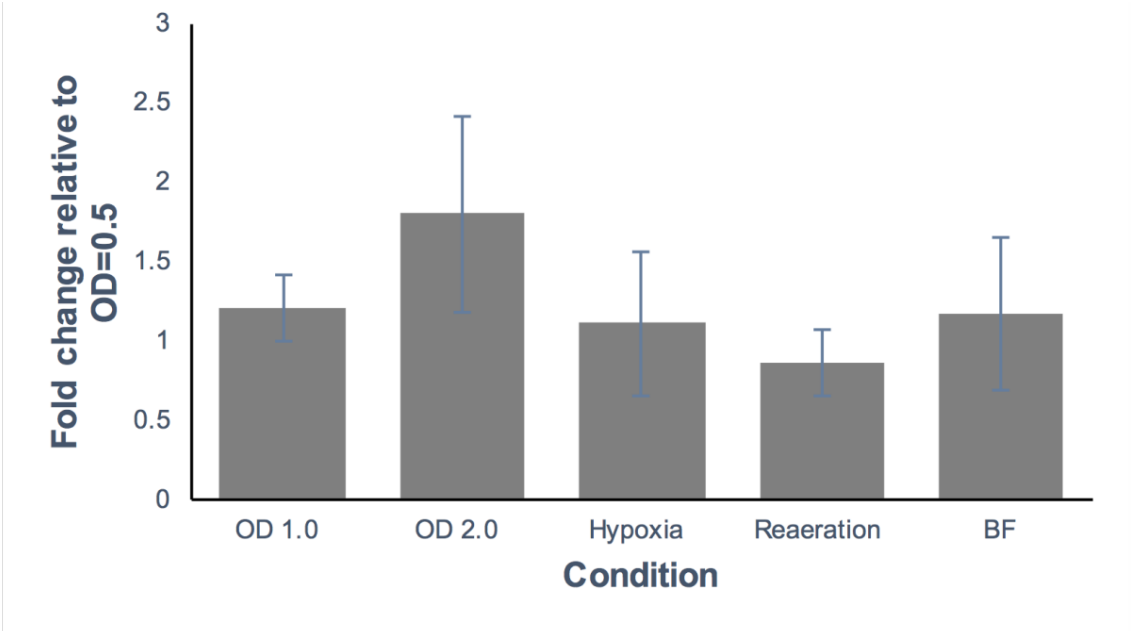

Figure 3.7. *mmpL11* expression in different *in vitro* growth conditions. Expression of *mmpL11* in *Mtb* was normalized to expression of the constitutively expressed gene *sigA*. Changes in *mmpL11* expression relative to expression at an OD_{600} = 0.05 were calculated as: fold change $2^{-\Delta\Delta CT}$. qRT- PCR was performed in triplicate on three biological replicates. Mean expression and standard deviation of all biological replicates is shown. Differences in *mmpL11* expression were not significant. *This analysis was performed by José Santinni Roma (Purdy Lab).*

Affinity purification of MmpL11 in *Mtb* identifies potential interacting partners - Protein-protein interactions may be a means by which MmpL transporters coordinate the synthesis and transport of their substrates (Jain and Cox, 2005). To identify *Mtb* proteins that interact with $MmpL11_{TB}$ *in vivo,* we used wild-type *Mtb* carrying the pOLYG $mmpL11_{TB}$ expression vector grown planktonically. Purification of MmpL11 from biofilm cultures was unsuccessful. Formaldehyde was added to induce protein cross-linking, and affinity-tagged MmpL11 from cross-linked and un-cross-linked samples was purified in denaturing conditions by metal affinity chromatography. Since purification occurred under denaturing conditions, the un-cross-linked samples served to identify background binding of *Mtb* proteins to the affinity resin. Mass spectrometry was performed to identify proteins co-purified with MmpL11. Proteins that were identified as enriched in 3 out of 3 experiments are summarized in **Table 3.2**. Proteins involved in mycolic acid biosynthesis, such as DesA1 and AcpM were enriched when crosslinked to $MmpL11_{TB}$. This result is consistent with our prediction that MmpL11 interacts with cell envelope biosynthetic enzymes. Intriguingly, PknD also co-purified with MmpL11 in all three experiments, though it was also present in the background. However, we were unable to show phosphorylation of the $MmpL11_{TB}$ C-terminus by PknD or other *Mtb* STPK kinases via *in vitro* kinase assays (**Figure 3.8**). The identity of the kinase or kinases that phosphorylate MmpL11 is currently under investigation.

Table 3.2. Proteins that co-purified with MmpL11 from *Mtb*.[a] *Technical assistance was provided by the OHSU Proteomics shared resource.*

Functional annotation[b]	**Protein**
Cell wall and Cell wall processes	Rv2625c, Rv2969c
Lipid metabolism	DesA1, AccA3, AccD5, AcpM
Regulatory proteins	DevR
Intermediary metabolism, respiration	MetE, Rv3273, AtpA, AceE, Icd2, DlaT, GlnA2, LldD, AtpB, IlvC LpdC, GltA2, Icl, Rv0338c
Chaperones	GroEL1, GroEL2, DnaK, GroS
Information pathways	Tuf, RplB, PcnA
Virulence, adaptation	Cfp29, HspX, Rv3134c
Conserved hypotheticals	Rv1265, Rv2744c

[a] Proteins identified in 3/3 experimental replicates.

[b] Functional categories from https://mycobrowser.epfl.ch

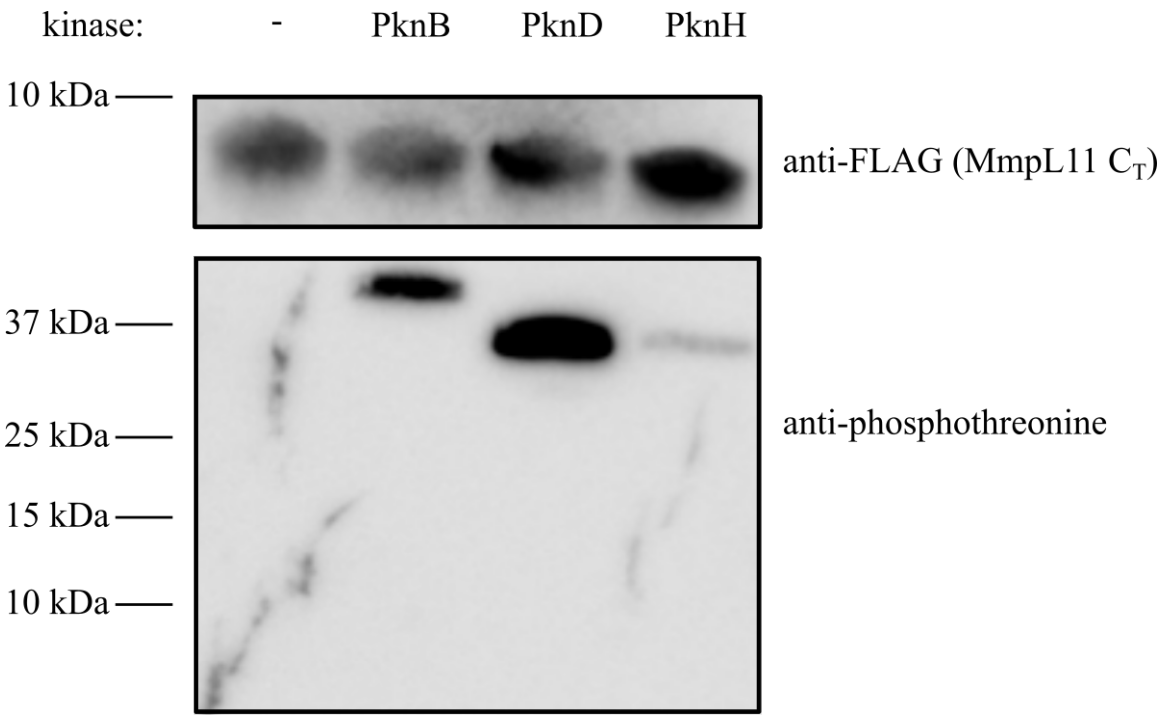

Figure 3.8. *In vitro* MmpL11$_{TB}$ C-terminal kinase assay. A FLAG-tagged peptide containing the putative MmpL11 C-terminal T765 phosphosite (residues 754-778; MmpL11 C_T) was incubated with the indicated recombinant *Mtb* kinase domains (1 μM:25 μM, kinase:substrate) in the presence of 1 mM ATP for 60 minutes at 37º C. Reactions were separated on 12% SDS Tricine and probed with α-FLAG and α-phosphothreonine antibodies to detect MmpL11 C_T and phosphorylated threonine residues, respectively.

DISCUSSION

In this study, we identified residues and domains required for optimal MmpL11 transporter activity. Amino acid residue Y610 is indispensable for MmpL11 function, presumably because it enables utilization of the PMF for substrate transport. This tyrosine is conserved in the TM10 regions of all known *Mtb* MmpL transporters. Thus, PMF coupling likely represents the ultimate biophysical foundation for MmpL substrate transport (Bernut et al., 2016). Furthermore, our data suggest that the D1 periplasmic domain plays a critical role in MmpL11-mediated lipid transport, since the $MmpL11_{TB}(\Delta D1)$ construct fails to complement the biofilm and lipid phenotypes of the *M. smegmatis mmpL11* mutant. In contrast, the expression of $MmpL11_{TB}(\Delta D2)$ or $MmpL11_{TB}(\Delta C\text{-term})$ in the *M. smegmatis mmpL11* mutant partially restored the visual biofilm phenotype, and lipids were similar to wild-type. The incomplete complementation of the visual biofilm phenotype by these domain-deletion variants implies that these domains might be required for optimal MmpL11 lipid export.

To our knowledge, our study is the first direct evidence of phospho-regulation of MmpL transporter activity in *Mtb* and *M. smegmatis*. MmpL7 was reported to be a potential substrate of PknD, although the functional outcome of this phosphorylation is unclear (Pérez et al., 2006). Similarly, Prisic et al. identified phosphorylated residues of MmpL3, MmpL10, and MmpL11 in their seminal work (Prisic et al., 2010). The phospho-residues of MmpL3 and MmpL11 are

exclusively located in the C-terminal cytoplasmic domain, compatible with the cytoplasmic localization of most *Mtb* STPK kinase domains. We generated phospho-ablative and phospho-mimetic point-substituted constructs to determine whether MmpL11 function is modulated *in vivo* by phosphorylation at T765, and found that the ability of $MmpL11_{TB}$ alleles to complement biofilm phenotypes depended on the phosphorylation state of T765. Furthermore, when expressed under control of the native $MmpL11_{TB}$ promoter, phospho-mimetic $MmpL11_{TB}$(T765E) protein levels fail to accumulate over time, suggesting that non-functional MmpL11TB is unstable. Residue T765 is phosphorylated in *Mtb* grown planktonically with acetate as the sole carbon source (Prisic et al., 2010). This is consistent with our data that show that MmpL11 levels are low during logarithmic growth in planktonic culture. That T765 was not definitively phosphorylated in $MmpL11_{TB}$ harvested from *M. smegmatis* biofilms is consistent with the accumulation of MmpL11 during this growth state and the importance of functional MmpL11 to biofilm formation. Taken together, these data suggest a model in which MmpL11 transporter function and stability is binarily modulated via phosphorylation at residue T765.

We also gained further insight into MmpL11 lipid transport by identifying proteins that interact with MmpL11. We hypothesized that MmpL11 might act as a scaffold to recruit cytoplasmic lipid biosynthetic enzymes in order to couple synthesis and efficient transport of its substrates. The precedent for enzyme-transporter interaction was established by the characterization of the interaction

between the PDIM transporter MmpL7 and PpsE, which is involved in PDIM biosynthesis (Jain and Cox, 2005). Membrane proteins are inherently difficult to study. Nevertheless, we were able to express epitope-tagged MmpL11 in *Mtb* and perform crosslinking and co-purification from planktonic *Mtb* cultures. In so doing, we identified several MmpL11-interacting proteins involved in *Mtb* lipid metabolism. These include proteins that contribute to mycolic acid biosynthesis, including DesA1, AcpM, and AccA3. This is in agreement with our observation that MmpL11 transports mycolate wax ester in *Mtb* (Wright et al., 2017). In addition, the triacylglycerol synthase Tgs1 was present in two of the crosslinked samples, suggesting that it may contribute to the biosynthesis of the LC-TAG. This possibility is the subject of future investigation. As a whole, these data support the hypothesis that MmpL proteins recruit biosynthetic enzymes to co-localize substrate production and transport.

Together, these data suggest a model in which the phospho-status of T765 regulates $MmpL11_{TB}$-mediated lipid transport and protein stability. Given that the C-terminus of MmpL11 is dispensable for lipid transport (**Figure 3.1B-C**), we hypothesize that phosphorylation at this site recruits an inhibitory interacting partner that prevents lipid export. Sustained inhibition appears to decrease MmpL11 protein stability (**Figure 3.6**), likely through the activation of protein degradation mechanisms. Expression of *mmpL11* mRNA is relatively constant regardless of growth conditions (**Figure 3.7**), yet MmpL11 is only active during specific growth phases. Post-translational regulation of MmpL11 lipid export via a

phosphorylation status-dependent inhibitory interacting partner is therefore the simplest model suggested by our data. Future work will be directed toward identifying this putative inhibitor of lipid transport by evaluating phospho-dependent differences in the MmpL11 interactome. We are also actively working to determine the kinase or kinases responsible for MmpL11 phosphorylation and decipher the different metabolic cues that trigger phosphorylation or dephosphorylation of MmpL11.

EXPERIMENTAL PROCEDURES

Bacterial strains and growth conditions - Bacterial strains and growth conditions. The *Mtb* wild-type strain H37Rv and *M. smegmatis* mc^2155 were obtained from the ATCC. Construction of the *M. smegmatis* and *Mtb mmpL11* mutants was previously described (Pacheco et al., 2013; Wright et al., 2017). Mycobacterial strains were routinely maintained in Middlebrook 7H9 liquid medium (Difco) with 0.05% Tween-80, or on Middlebrook 7H10 agar (Difco), both supplemented with albumin dextrose salts (ADS) containing 8.1 mg/mL NaCl, 50 mg/mL bovine serum albumin (BSA), and 20 mg/mL dextrose. Glycerol was added to liquid 7H9 to a final concentration of 0.5%. Kanamycin (25 μg/mL) and hygromycin (50 μg/mL) were used for bacterial selection when required.

Mycobacterial biofilms were grown in Sauton's medium containing 0.5 g/L K2HPO4, 0.5g/L MgSO4, 4.0 g/L L-asparagine, 0.05 g/L ferric ammonium citrate,

4.76% glycerol, and 1.0 mg/L ZnSO4, with a final pH of 7.0. *M. smegmatis* biofilms were grown by inoculating bacteria to an initial OD_{600} of 0.05 with Sauton's medium in polystyrene Petri dishes (Fisher). Biofilms were incubated at 30º C for 4 days prior to imaging or use in subsequent assays. *Mtb* biofilms were inoculated to OD_{600} = 0.05 in Sauton's medium and incubated at 37º C/ 5% CO2 in tightly sealed polystyrene bottles (Corning). At 3 weeks, the lids were loosened to permit gas exchange.

Cloning and expression of MmpL11 point mutants and domain deletion mutants - The pVV16 *mmpL11*$_{TB}$ expression construct was previously described (Pacheco et al., 2013). MmpL11 point substitution constructs (T765A, T765E, and Y610F) were generated via splice overlap PCR (primers are indicated in **Supplemental Table 3**). The C-terminal tail deletion mutant (ΔC-term) was generated using the *mmpL11* forward cloning primer and a ΔCT_698 Reverse primer. PCR products were subcloned into pGEM-T Easy (Promega). Once confirmed by sequencing, the mutated alleles were cloned into the pVV16 expression vector in frame with a C-terminal 6x-histidine tag. The deletion of the MmpL11 periplasmic D1 and D2 loops (ΔD1 and ΔD2) was achieved using the NEBuilder HiFi DNA Assembly System (NEB). Primers flanking the D1 or D2 loop were used to amplify *mmpL11* lacking amino acids 46-182 and 398-524, respectively. Following the confirmation of all mutant sequences, the plasmids were transformed into electrocompetent *M. smegmatis* mc^2155 *mmpL11::tn* and grown under kanamycin and hygromycin dual selection.

Western analyses - Western analyses were performed to confirm MmpL11 protein expression. Samples were normalized to protein amount and proteins separated by 10% SDS-PAGE at 150 V for 90 min and transferred to PVDF membrane. The membrane was blocked overnight at 4º C using BSA Block [PBS, 0.2% Tween-20 (v/v), 3% BSA (w/v)]. Primary (1:1,000 Anti-His) and secondary (1:10,000 GOXMO-Hrp) antibodies were used to probe for His-tagged MmpL11 variants. The Western blot was developed with Super Signal West Femto Maximum Sensitivity Substrate (Thermo Scientific, 34095) and imaged using an ImageQuant LAS 4000 (GE).

Lipid isolation and analyses - *M. smegmatis* biofilm lipids were harvested by collecting biofilm material into glass tubes containing 3 mm glass beads. Bacteria were treated with HPLC-grade hexanes to isolate surface lipids or $CHCl_3$:MeOH (2:1, v:v) to isolate total lipids, shaken, and sonicated for 15 minutes in a 50º C water bath. Tubes were centrifuged at 2000xg for 10 min to separate aqueous and organic phases and pellet cell debris. The organic phase from each extraction was transferred to a clean, pre-weighed vial and dried under inert N_2 gas. Extracted lipids were resuspended in $CHCl_3$ and loaded onto aluminum-backed silica plates (EMD Millipore) for TLC analysis. Solvent systems used were toluene:acetone (99:1, v:v) and chloroform:methanol:water (90:10:1) (Fisher). Lipids were visualized via spraying with 12-molybdophosphoric acid (Alfa Aesar; 10%, w/v in EtOH) and charring.

Mtb biofilm lipids were harvested by collecting biofilm material into 50 mL conical vials, resuspended in PBS, and transferred to glass test tubes containing 3 mm glass beads. Surface lipids were extracted by shaking with 5 mL hexanes for 2 min, followed by pelleting at 1000xg for 10 min. Supernatants were removed into fresh glass tubes and treated with HPLC-grade $CHCl_3$:MeOH (2:1, v:v) prior to removal from biosafety containment. For total lipids, bacteria were pelleted in glass tubes and spent media removed. Bacterial pellets were autoclaved prior to removal from biosafety containment, then extracted with ~ 5 mL CHCl3:MeOH (2:1, v:v). A Folsch wash was performed and the organic layer was separated by centrifugation at 1000xg for 10 min, transferred to pre-weighed vial, and dried under inert N_2 gas.

Protein purification - To purify $MmpL11_{TB}$ from *M. smegmatis*, mc^2155 and mc^2155*mmpL11*/pOLYG *mmpL11*$_{TB}$ cultures were grown to an OD_{600} = 2 or as biofilms. All strains were normalized to OD_{600} prior to pelleting. Bacteria were harvested by centrifugation and pellets were resuspended in 1 mL of Buffer 1 [8M Urea, 300mM NaCl, 0.5% NP-40 (v/v), 50mM NaH_2PO_4, 50mM Tris pH 7.0, 10% Glycerol (v/v), pH 7.0] containing Pierce EDTA-Free Protease Inhibitor. Cells were lysed by sonication and proteins affinity purified over HisPur Cobalt Superflow Agarose resin (Thermo Scientific) and confirmed by Western analysis.

MmpL11 from *Mtb* proved remarkably recalcitrant to purification, and a number of issues complicated the envisioned experimental strategy. A significant effort was

directed towards optimizing the purification of affinity-tagged, cross-linked MmpL11 from H37Rv *Mtb*. A constitutive expression strategy involving expression in the pVV16 vector was able to complement the *mmpL11* mutant but produced very little tagged protein. MmpL11 expression was most successful when expressed under its native promoter in the pOLYG vector. Purification was most successful from mid-log phase (OD_{600} ~ 0.5) cultures. Attempts to purify MmpL11 protein from *Mtb* biofilms were unsuccessful. Purification was only possible under strict denaturing conditions and in the presence of detergent, conditions that were achieved with 8M urea and 0.5% NP-40 (v/v). We hypothesize that this is primarily due to the nature of MmpL11 as a polytopic integral membrane protein. However, a contributing factor may be the potential inaccessibility of the C-terminal 6xHis affinity tag under native conditions, perhaps due to oligomerization between MmpL11 proteins, interactions with other protein interacting partners, or to unique, tag-obscuring, protein folding within the C-terminal domain. Surprisingly, the inclusion of glycerol in the lysis buffer also appeared to inhibit downstream protein purification, for unknown reasons. Additionally, the protein cross-linking process severely reduced the amount of purified protein obtained. Three- to six-fold excesses of cross-linked relative to un-cross-linked cultures were required to obtain roughly equivalent amounts of purified protein as evaluated by Western blot. Finally, protein purification was maximized when filtered lysates were incubated on lysis buffer-equilibrated affinity resin overnight at 4º C. Given these empirically-determined

considerations, the following protocol proved to be the most successful means of obtaining purified MmpL11 protein from *Mtb*:

To purify $MmpL11_{TB}$ from *Mtb*, H37Rv/pOLYG $mmpL11_{TB}$ cultures were grown to mid-logarithmic phase (OD_{600} = 0.5). Protein crosslinking was performed using a final concentration of 1% formaldehyde for 30 minutes at room temperature, and quenched with 2.5 M glycine. Bacteria were harvested by centrifugation, pellets were washed in 1X PBS and resuspended in 1 mL of Buffer 1 (as above, but lacking glycerol) containing Pierce EDTA-Free Protease Inhibitor. Cells were lysed by bead beating and the lysates filter-sterilized prior to removal from biosafety containment. Protein lysates were incubated on buffer-equilibrated HisPur Cobalt Superflow Agarose Resin (Thermo Scientific) and washed extensively. His-tagged MmpL11 was eluted in Buffer 1 (lacking glycerol) adjusted to 300 mM imidazole.

Protein Mass Spectrometry - The samples used to identify MmpL11-binding proteins were run for 6 minutes at 200 V into a 10% BisTris gel. A brief staining was done with Imperial Protein Stain (Thermo Scientific) to verify protein presence and estimate amount. The top of each gel lane including the tracking dye was excised and digested using the “In-Gel Digestion Protocol for Low Protein Amounts” procedure described in section 5 of the Promega ProteaseMax Surfactant, Trypsin Enhancer Technical Manual. Each sample was then dissolved in 20 µL of 5% formic acid and analyzed using an Orbitrap Fusion

mass spectrometer configured with an EasySpray NanoSource (Thermo Scientific). Digests were loaded onto an Acclaim PepMap 0.1 x 20 mm NanoViper C18 peptide trap (Thermo Scientific) for 5 min at a 5 µL/min flow rate in a 2% acetonitrile, 0.1% formic acid mobile phase and peptides separated using a PepMap RSLC C18, 2 µm particle, 75 µm x 25 cm EasySpray column (Thermo Scientific) using a 7.5–30% acetonitrile gradient over 30 or 60 min in mobile phase containing 0.1% formic acid and a 300 nL/min flow rate using a Dionex NCS-3500RS UltiMate RSLC nano UPLC system. Survey scans from 400-1600 m/z were performed in the Orbitrap mass analyzer at 120,000 resolution, AGC target of 4×10^5, maximum injection time of 50 ms, and a m/z= 445.12 polysiloxane ion lock mass. Data-dependent MS2 scans were performed in the linear ion trap using HCD following isolation with the instrument's quadrupole. Data-dependent MS/MS scans used a cycle time of 3 sec between survey scans, a mono isotopic peak determination filter with a peptide setting, intensity threshold of 5×10^3, dynamic exclusion of 30 sec with a +/- 10 ppm mass tolerance, charge state filter to ignore +1 ions, quadrupole isolation window of 1.6 m/z, HCD collision energy of 30%, rapid scan rate, AGC target of 1×10^4, and maximum injection time of 35 ms.

Mass spectrometry was also used for MmpL11 phosphorylation site determination. $MmpL11_{TB}$ was purified from *M. smegmatis mmpL11*/pOLYG *mmpL11*$_{TB}$ biofilm cultures. Gel bands containing MmpL11 were Coomassie stained, excised and digested as above and peptides separated using the same

nano UPLC conditions as above using a 60 min gradient, except a Symmetry C18 trap and 75 µm x 250 BEH 130 C18 column with 1.7 µm particles (Waters) was used and peptides analyzed using a Q-Exactive HF mass spectrometer and Nano Flex Ion Spray Source (Thermo Scientific) fitted with a 20 µm stainless steel nano-bore emitter spray tip. Survey mass spectra were acquired in m/z 375−1400 at 120,000 resolution, AGC target of 3 x 10^6, maximum injection time of 50 ms, and a m/z= 445.12 polysiloxane ion lock mass. Data-dependent MS/MS acquisition selected the top 10 most abundant precursor ions using an isolation width of 1.2 m/z, normalized collisional energy of 30, AGC setting of 1 x 10^5, maximum ion time of 100 ms, minimum AGC target of 5 x 10^3, exclusion of +1 ions, and dynamic exclusion in auto mode.

Comet (version 2016.01, revision 1) was used to search MS2 spectra against a June 2018 version of the uniprot_Mycobacterium.tuberculosis_h37rv database or March 2017 version of the Swissprot *M. smegmatis* protein database, with the *M. tuberculosis* H37RV MmpL11 sequence added. Databases also contained concatenated sequence-reversed entries to estimate error thresholds and 179 common contaminant sequences and their reversed forms (Wilmarth et al., 2009). The database processing was performed with python scripts available at https://github.com/pwilmart/fasta_utilities.git and Comet results processing used the PAW pipeline from https://github.com/pwilmart/PAW_pipeline.git. Comet searches for all samples were performed with trypsin enzyme specificity. Average parent ion mass tolerance was 1.25 Da to improve estimates of peptide

false discovery. Monoisotopic fragment ion mass tolerance was 1.0005 Da. A static modification of +57.02146 Da was added to all cysteine residues. A variable modification of +15.9949 Da on methionine residues was also allowed, with an additional variable modification of 79.9663 on Serine, Threonine, and Tyrosine residues during the analysis of MmpL11 phosphorylation. The PAW pipeline (Wilmarth et al., 2009) transforms Comet scores into linear discriminant function scores (Keller et al., 2002), and separate target and decoy score histograms were created for each peptide charge state (2+, 3+, and 4+) for all peptides of 7 amino acids or longer. Scores for forward and reversed entry phosphopeptides were also processed separately from non-modified peptides to better control false discovery rate (FDR) for this class of peptides. The overall peptide FDR for the analysis was 1.65%, and the overall protein FDR was 1.9%. Numbers of assigned MS/MS spectra to each protein entry across 3 separate experiments detecting MmpL11 binding proteins were used to identify proteins that were more abundant in cross-linked versus non-crosslinked control samples, and full results appear in **Table S1**. All phosphopeptide spectra were loaded into the Interactive Peptide Spectral Annotator (Brademan et al., 2019) for manual data validation.

***In vitro* kinase assay –** A FLAG-tagged peptide corresponding to the MmpL11 C-terminal region containing the putative T765 phosphosite (MmpL11 C_T 754-778 –FLAG) was synthesized commercially (Life Technologies; Carlsbad, CA). PknB, PknD, and PknH kinase domains were cloned into the pet24a vector in-

frame with the C-terminal 6xHistidine tagged and purified from BL21 *E. coli* via affinity chromatography (HisPur resin, Thermo Scientific). Kinases and substrate were incubated in a 1:25 μM ratio in kinase buffer (25 mM Tris pH 7.0, 5 mM $MgCl_2$, 1 mM EDTA, 1 mM DTT, 1 mM ATP) for 60 minutes at 37º C. Reactions were separated on 12% SDS-Tricine gels, transferred to PVDF membrane, blocked with BSA blocking buffer, and probed with mouse α-FLAG (1:2500; Thermo Scientific, MA1-9178) or rabbit α-phosphothreonine (1:1000; Abcam, ab9337). Blots were developed with Femto or Pico Western visualization reagents (Thermo Scientific).

Statistical analyses - Data were analyzed and statistics generated using GraphPad PRISM.

ACKNOWLEDGMENTS

This project was funded by NIH NIAID R01 AI087840 and R21 AI113074 to GEP and T32 AI007472 to GM. Mass spectrometric analysis was performed by the OHSU Proteomics Shared Resource with partial support from NIH core grants P30EY010572, P30CA069533 and S10OD012246

CONFLICT OF INTEREST

The authors declare that they have no conflicts of interest with the contents of this article.

Table 3.3. Primers used in this study.

Name	5'-Primer-3'
mmpL11 cloning primer Forward	catatgatgcgcttgagccgcaac
mmpL11 cloning primer Reverse	aagcttcctcgcctcctccaacatcgc
T765A mutation 5'Reverse	ggcgagcggatcggcaacgcaaatggc
T765A mutation 3'Forward	gccatttgcgttgccgatccgctcgcc
T765E mutation 5'Reverse	ggcgagcggatcttcaacgcaaatggc
T765E mutation 3'Forward	gccatttgcgttgaagatccgctcgcc
Y610F mutation 5'Reverse	agcaggaagatttcaaagtccatcgacaa
Y610F mutation 3'Forward	ttgtcgatggactttgaaatcttcctgct
ΔCT_698 Reverse	aagcttccatcggtcaaacatcgccat
pVV16NdeI-5'mmpL11 Forward	atccggaggaatcacttccatatgatgcgcttgagccgcaac
mmpL11ΔD1 Loop_46 Reverse	ggttccagcgggcgacttcgaaaccgcc
mmpL11ΔD1 Loop_182 Forward	cgaagtcgcccgctggaacctgcctatc
mmpL11ΔD2 Loop_398 Reverse	gcgtcgcggacagcaagctgttgcccag
mmpL11ΔD2 Loop_524 Forward	cagcttgctgtccgcgacgcaaccgctg
pVV16HindIII-3'mmpL11 Reverse	agtggtggtggtggtggtgaagcttcctcgcctcctccaacatcgc
T771A mutation 5' Reverse	atccacacccggcgaaggcgagc
T771A mutation 3' Forward	gctcgccttcgccgggtgtggat
T771E mutation 5' Reverse	atccacaccttcgaaggcgagc
T771E mutation 3' Forward	gctcgccttcgaagggtgtggat
PknB kinase domain NEBuilder Forward	ctttaagaaggagatatacatatgATGACCACCCCTTCCCACC
PknB kinase domain NEBuilder Reverse	ggtgctcgagtgcggccgcaagcttGCCCACCGAACCGAACCGATGCT

PknD kinase domain NEBuilder Forward	ctttaagaaggagatatacatatgGTGAGCGATGCCGTTCCG
PknD kinase domain NEBuilder Reverse	agtggtggtggtggtggtgctcgagGCGCCGCAGAATCGTCGT
PknH kinase domain Forward	ctttaagaaggagatatacatatgATGAGCGACGCACAGGACTCG
PknH kinase domain Reverse	ggtgctcgagtgcggccgcaagcttGTCGGGGTCGCTGAGCGC

CHAPTER 4

SUMMARY AND CONCLUSIONS

I. Cell Envelope Biogenesis in the Periplasm

Our investigations identified LpqN as a periplasmic protein that is involved with cell envelope biosynthetic processes in *Mtb*. Through complementary biochemical and genetic techniques, we showed that LpqN interacts with the D2 periplasmic domains of the MmpL3 and MmpL11 transporters. These transporters are responsible for export of mycolic acid-containing lipids, which are essential for generating the mycobacterial outer membrane and for potentiating bacterial persistence in the host. In so doing, they make critical contributions to the virulence of *Mtb*. Additionally, we have evidence that supports the hypothesis that LpqN interacts with members of the Ag85 enzyme complex, particularly Ag85A, enzymes that use MmpL-transported lipids as substrates for mycomembrane biogenesis. These data strongly implicate LpqN as a periplasmic intermediary between mycolic acid transport and extracytoplasmic envelope biogenesis. In support of this role for LpqN, our structural studies confirmed that LpqN is capable of binding analogues of TMM, the MmpL3 and Ag85 substrate. Thus, we postulate that LpqN functions as a quasi-MFP to facilitate substrate delivery of envelope lipid precursors from

MmpL3/MmpL11 to the secreted Ag85 enzymes that synthesize mature mycomembrane lipids.

Genetic and biochemical data suggest that LpqN is not the only mycobacterial lipoprotein that performs this role. The other secreted members of the LpqN family, LpqT and Mtc28, are also likely involved with transport of mycolic acids in the periplasm. Although there is no structural information for LpqT, the crystal structure of Mtc28 is homologous to proteins of known lipid-binding function, such as the ceramide-binding eukaryotic protein CERT (Holm and Rosenström, 2010; Kudo et al., 2008). This further corroborates the hypothesis that lipid binding is a conserved feature of the LpqN family. However, while LpqN appears to promiscuously interact with both MmpL3 and MmpL11, Mtc28 and LpqT appear to preferentially interact with MmpL11. Since the importance of MmpL3 and MmpL11 substrates varies according to the physiological and replicative state of the bacteria, these other LpqN-family proteins may play a more active role during dormancy and biofilm formation when transport of MmpL11 substrates is more important. This possibility could be investigated through examining the biofilm lipid profiles of *lpqT*- and *mtc28*-deficient mycobacterial strains.

LpqN was the only protein we examined that interacted with the essential mycolic acid transporter MmpL3 in the M-PFC system. *Mtb* lacking LpqN protein grows at the same rate as wild-type *Mtb* and exhibits no discernible cell envelope lipid

differences during planktonic and early biofilm growth. This demonstrates that MmpL3-mediated mycolic acid transport is unaffected in the *lpqN* mutant. These observations suggest two possible interpretations: either there are other functionally redundant lipid-binding periplasmic proteins that compensate for the absence of LpqN, or periplasmic lipid binding is not essential for the biogenesis of the mycobacterial cell envelope. Of these two possibilities, the former seems more probable. From a purely chemical standpoint, mycolic acids are highly hydrophobic and would not be expected to freely diffuse across the approximately 15 nm wide aqueous periplasmic space. The *Mtb* genome contains >90 genes that are predicted to encode lipoproteins (Cole et al., 1998; Sutcliffe and Harrington, 2004). Redundancy in periplasmic lipid transport pathways is consistent with this hypothesis, and could explain why the *lpqN*-deficient *Mtb* does not exhibit a gross defect in cell envelope biogenesis. Functional redundancy of envelope lipid export also suggests that cell envelope biogenesis and metabolism is robust and resistant to perturbation. This model aligns with the fundamental role that the *Mtb* cell envelope plays in modulating and resisting host immune defenses. Redundancy of LpqN family members could be investigated by the construction and characterization of double mutants in *Mtb* H37Rv.

Additionally, there are a multitude of other secreted proteins of unknown function in the *Mtb* genome, including the proline-glutamate/proline-proline-glutamate (PE/PPE) proteins, many of which are secreted and may play a role in cell

envelope biogenesis and virulence (Ates et al., 2016; Singh et al., 2016). Thus, it is possible that the hypothesized lipid binding/transfer function of LpqN is redundantly shared with other secreted proteins of the PE/PPE family. The abundance of PE/PPE protein-coding genes has frequently been posited as a source of antigenic variation, although this has yet to be conclusively demonstrated (reviewed in (Akhter et al., 2012; Sampson, 2011)). From an evolutionary perspective, this hypothesis is attractive because secreted *Mtb* proteins, especially lipoproteins, are frequently potent immunogens (Boesen et al., 1995; Young and Garbe, 1991). Therefore, one can speculate that it may be evolutionarily advantageous for *Mtb* to undergo antigenic variation of exposed surface proteins to counter cell-mediated host immune mechanisms.

A number of issues complicate the characterization of LpqN as a periplasmic MFP interacting partner of MmpL3 and/or MmpL11. For instance, attempts to co-purify LpqN and MmpL11 in a heterologous *M. smegmatis* co-expression system were unsuccessful. It is possible that the interaction between full-length, membrane-inserted MmpL11 and membrane-anchored LpqN requires the presence of an additional adaptor protein or molecule. This putative adaptor may be superfluous for the M-PFC interaction, which consists of fusion proteins constitutively expressed in the cytoplasm. An alternative possibility may be that interactions in the periplasm require post-translational modifications such as glycosylation. Mycobacterial proteins, especially lipoproteins, are frequently glycosylated (Becker et al., 2017; Mehaffy et al., 2019). *M. smegmatis* might lack

the requisite glycosyltransferases that would enable glyco-dependent protein-protein interactions.

These same considerations underlie the observation the LpqN and Ag85A also failed to co-purify using the *M. smegmatis* heterologous co-expression strategy. These *Mtb* proteins (e.g. LpqN, MmpL11, and Ag85) were expressed under control of their native promoters, in the genetic context of *M. smegmatis*, a non-pathogenic mycobacterial species that possesses its own homologues of each of these recombinantly-expressed *Mtb* proteins. Many cell envelope biogenesis proteins are conserved between *M. smegmatis* and *Mtb*, as exemplified by the observation that $MmpL11_{TB}$ can complement an *M. smegmatis mmpL11* mutant. Therefore, we cannot rule out interactions between the tagged *Mtb* proteins and their untagged *M. smegmatis* interacting partner homologues, which could interfere with detection following co-purification.

Regardless of the failure to directly demonstrate biochemical interaction of full-length proteins in *M. smegmatis*, abundant evidence in Chapter 2 clearly implicates LpqN in periplasmic lipid transport. Further characterization of LpqN, e.g. via lipid transfer assays, would validate the identification of LpqN as a periplasmic MFP and further define its precise lipid ligands.

LpqN appears to play a specific role during biofilm maturation, given that a highly non-polar lipid accumulates in the 4-week Δ*lpqN* biofilm relative to wild-type *Mtb*.

Comparing the 3-week to the 4-week wild-type *Mtb* lipid profiles demonstrates that biofilm lipids change over the course of biofilm maturation, with some early abundant lipid bands depleting at the later time point and vice-versa. These lipid shifts are presumably the result of cell envelope metabolic processes. The 4-week Δ*lpqN*-accumulating lipid **(***, **Figure 2.4F**) is highly represented in all *Mtb* strains at the 3-week time point. However, the apparent intensity of this lipid band dramatically decreases at the 4-week time point in the wild-type and complemented mutant *Mtb* biofilms, while it is maintained in the Δ*lpqN* mutant. While the significance of this observation is unknown, it does not appear to have a deleterious effect on the biofilm formation of the Δ*lpqN* mutant, given that wild-type and Δ*lpqN Mtb* biofilms are visually indistinguishable at both 3- and 4-week time points. Despite the obvious TLC phenotype, and to our great consternation, examination of 4-week biofilm lipids via mass spectrometry did not reveal any differences between wild-type and Δ*lpqN* lipids, thereby precluding us from definitively identifying this Δ*lpqN*-associated lipid. That the 4-week Δ*lpqN* mutant biofilm maintains this lipid presents the possibility that LpqN may have a non-redundant role in the catabolism of cell envelope lipids. A precedent for lipoproteins contributing to metabolic recycling is LpqY, which cooperates with the SugABC importer to recycle trehalose disaccharide into the cytoplasm for subsequent reuse in mycolic acid metabolism (Kalscheuer et al., 2010).

Canonical RND transporters work together with MFPs in the periplasm and OMFs in the outer membrane to export substrates across the inner and outer

membranes of bacteria (**Figure 4.1**). We identified LpqN and potentially other LpqN family proteins as interacting partners of MmpL transporters and other extracellular biosynthetic proteins in *Mtb*. Therefore, LpqN and LpqN family proteins resemble MFPs. Our structural data showing that LpqN can bind analogues of the lipid substrates of MmpL3 and MmpL11 further corroborates the characterization of LpqN as an MFP. Whether MmpL-mediated substrate export also requires the presence of an OMF is unknown. *Mtb* has markedly fewer experimentally-determined outer membrane proteins than *E. coli* (Song et al., 2008). Our mass spectrometry-based approach to identify LpqN interacting proteins did not identify any putative OMF proteins. However, this experiment was performed with *Mtb* culture filtrate proteins, the majority of which are actively secreted, with smaller amounts of cytoplasmic proteins present as a result of bacterial lysis or unintended secretion. Thus, it is unlikely that this experimental strategy would identify a putative integral mycomembrane protein and we are unable to exclude the possibility that MmpL-mediated substrate export also requires an as-yet unidentified OMF.

Two lines of reasoning suggest that MmpL-mediated lipid transport differs significantly from canonical RND substrate export. First, the majority of identified MmpL substrates are cell envelope lipids that comprise the mycomembrane. Therefore, an outer membrane factor may not be required for MmpL substrate transport, given that these cell envelope lipids are incorporated into, and not transported through, the mycobacterial outer membrane. Second, structural

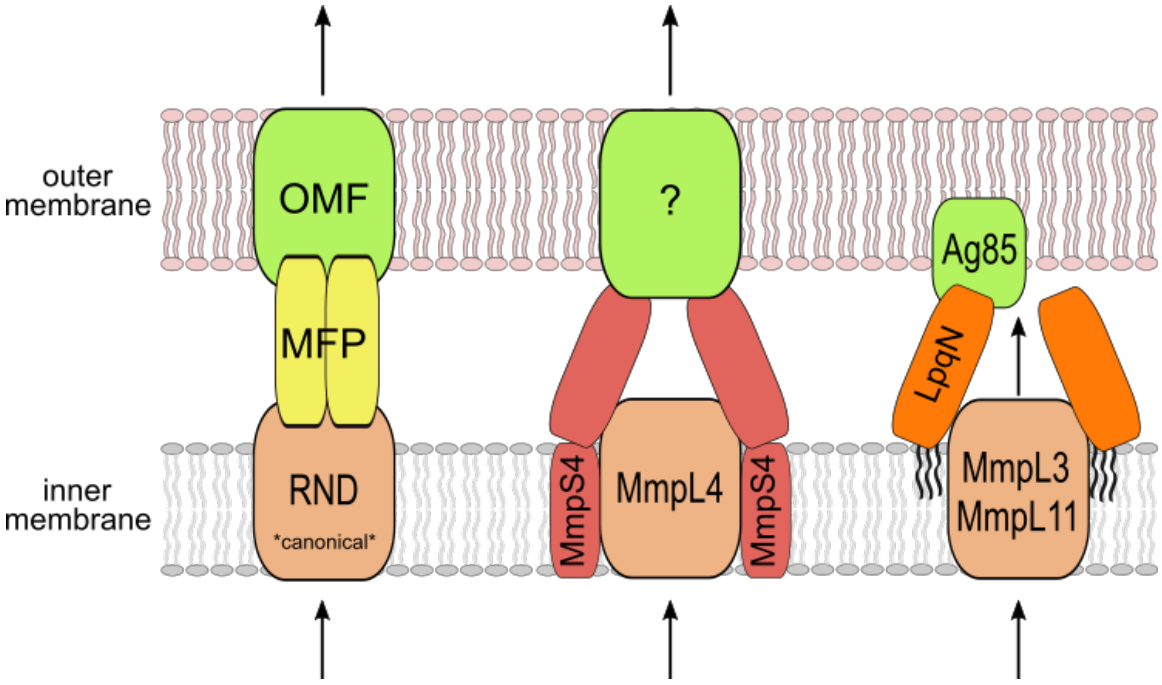

Figure 4.1. RND proteins work in concert with adaptor proteins to export substrates. Canonical RND proteins (e.g. *E. coli* AcrB) interact with membrane fusion proteins (MFP) and outer membrane factors (OMFs) to directly transport substrates across both the inner and outer membranes. Some MmpL proteins (e.g. MmpL4/5) have accessory integral membrane MmpS proteins that are required for substrate export, and thus likely function as MFPs. Lipoprotein LpqN likely functions as a redundant MFP for MmpL3 and MmpL11. Mycolic acids are likely incorporated into the mycomembrane through the association of LpqN with members of the Antigen 85 mycolyltransferase complex. How other MmpL substrates are incorporated into, or transported through, the mycomembrane is unknown.

data suggest that MmpL proteins function as monomers, in contrast to most other RND proteins which typically function as homo-dimers and –trimers. Together, these considerations indicate that while MmpL proteins nominally belong to the RND family, their higher-order transport mechanisms are fundamentally dissimilar to those of most other RND proteins.

Intriguingly, the extracellular domain (ECD) of the *Mtb* STPK PknH (Rv1266c) is also categorized as an LpqN family member. Many *Mtb* STPKs function as sensor kinases, coupling detection of extracellular signals to phosphorylation of cytoplasmic target proteins. As phosphorylation frequently alters protein functionality, these STPKs are a means by which *Mtb* can rapidly respond to environmental cues. For example, the PASTA-domains of the PknB ECD couple phosphorylation of substrate proteins to recognition of PG-fragments in the periplasm (Barthe et al., 2010; Kang et al., 2005a; Kaur et al., 2019; Mir et al., 2011). That the PknH ECD resembles LpqN suggests that PknH may bind cell envelope lipids, then subsequently phosphorylate its target proteins. Defining the putative PknH activating signal, identifying target substrates, and characterizing the functional consequences of PknH-mediated phosphorylation will undoubtedly prove to be a fruitful area for future research and has the potential to reveal undescribed mechanisms of metabolic adaptation in *Mtb*.

II. Insight into MmpL Transporter Structure/Function

In Chapter 3, we described further insight into the structural requirements of MmpL11 lipid export. These findings confirm the prediction that the PMF is the energetic foundation of MmpL-mediated substrate transport. Additionally, we evaluated the contributions to lipid transport made by the larger structural elements of MmpL11, namely the D1 and D2 periplasmic domains, and the C-terminal cytoplasmic region. In this manner, we discovered that the D1 domain is critical for transporter function, while the D2 and C-terminal domains were dispensable.

The importance of the D1 domain for substrate transport is supported by the structural observations derived from the reported ligand-bound crystal structure of the *M. smegmatis* MmpL3 lipid transporter (Su et al., 2019). This study showed manifold interactions between the co-crystallized phosphatidylethanolamine (PE) ligand and numerous amino acid side chains in the D1 domain, specifically residues Q40, S41, F43, Y44, D64, T66, S67, V70, V109, T121, M125, F134, S136, D144, L171, L174, A175, S428, E429, F445, F452, and R453. However, ligand-residue interactions between D2 residues I427, T454, P456, R501, P502, A503, N504, Q517, and T549 were observed as well, belying the dispensability of the D2 domain for lipid transport (Su et al., 2019).

Certain protein-ligand interactions are likely more important than others. Interestingly, Belardinelli et al. reported that a Q40C mutation in MmpL3 rendered *M. smegmatis* susceptible to growth inhibition by the thiol-reactive compound ebselen, implicating this D1 amino acid residue in the physiologically critical transport of mycolic acids (Belardinelli et al., 2016). The Q40 side chain was also observed to interact with PE in the ligand-bound crystal structure (Su et al., 2019). These data support the assertion that protein-ligand interactions that occur in the D1 domain are absolutely necessary for MmpL3 transporter function. This is likely also the case for the structurally similar MmpL11 protein, thus reconciling our data showing the requirement of the D1 domain for MmpL11-mediated lipid export. While Q40 is not conserved between $MmpL3_{TB}$ and $MmpL11_{TB}$, this difference likely reflects the distinct substrate preferences of MmpL11. Our $MmpL11_{TB}(\Delta D1)$ domain-deletion mutant is presumably lacking a critical amino acid residue whose side chain is required for ligand binding. A crystal structure of ligand-bound MmpL11 would provide structural verification of the essentiality of MmpL11 D1 residues to MmpL11 transporter activity and conclusively identify ligand-binding residues.

Numerous protein-ligand interactions also occur in the D2 domain of MmpL3, suggesting that these interactions are also important for transporter activity (Su et al., 2019). However, the $MmpL11_{TB}(\Delta D2)$ variant was capable of lipid export, as assessed via TLC, indicating transporter activity was not abrogated by the deletion of the D2 domain. Nevertheless, the qualitative, visual biofilm phenotype

of the *M. smegmatis mmpL11* mutant expressing $MmpL11_{TB}(\Delta D2)$ was intermediate between wild-type and *mmpL11*-deficient *M. smegmatis* (**Figure 3.1**). These observations suggest that while the MmpL11 D2 domain is not absolutely required for transport of specific lipid substrates, its presence may optimize MmpL11 transporter activity. A prediction to reconcile these seemingly paradoxical data could be that the D2 domain stabilizes ligand binding and potentiates lipid export, but does not confer specificity, and is thus not required for MmpL11 function.

Under the structural classification scheme proposed by Chim et al., MmpL3 and MmpL11 belong to MmpL Cluster II (Chim et al., 2015). Thus, our conclusions regarding MmpL11 function can likely be extended to MmpL3. Testing the functionality of MmpL3 variants is a more complicated endeavor due to the essentiality of MmpL3-mediated mycolic acid transport, but can be investigated through conditional depletion strategies (Bernut et al., 2016). Our work suggests that $MmpL3_{TB}(\Delta D1)$ will be unable to rescue MmpL3-depleted *M. smegmatis*. However, expression of $MmpL3_{TB}(\Delta D2)$ might be expected to partially restore growth of MmpL3-depleted *M. smegmatis*, albeit to a slower rate compared to growth of the wild-type strain given the putative ligand stabilization and transport efficiency contributions of the D2 domain.

MmpL Cluster II is characterized by a relatively minimalistic D2 domain, compared to the more ornate periplasmic D2 docking domains exhibited by

Cluster I MmpL proteins (**Figure 1.5**). This structural difference suggests that the D2 domains of Cluster I MmpLs might play a more critical role in substrate transport. It is therefore reasonable to predict that periplasmic domains might play roles of differing importance in the two MmpL clusters. Future work towards investigating structure-function relationships in MmpL Cluster I could reveal a means by which to precisely and selectively target different MmpL transporters. Given that many MmpL substrates are important for virulence, this could present new treatments for TB disease

Another notable distinction between MmpL Clusters I and II is the presence of a substantial C-terminal (Ct) cytoplasmic domain in Cluster II MmpL transporters. This Ct domain is dispensable for MmpL11 lipid export, as assessed by TLC. However, the visual biofilm phenotype indicates that the Ct domain contributes to forming a fully rugose and reticulated wild-type mycobacterial biofilm (**Figure 3.1**). Our mass-spectrometry based study of MmpL11 interacting partners in *Mtb* identified a number of cytoplasmic lipid biosynthetic proteins (**Table 3.2**). The C-terminus is the region of MmpL11 that most likely participates in these interactions. Removal of the Ct domain would thereby uncouple substrate synthesis and export but not completely abrogate substrate transport, consistent with our biofilm lipid TLC and visual data.

The Ct domain may also play a role in the oligomerization of Cluster II MmpL proteins. Although the Ct domains of both MmpL3 and MmpL11 are dispensable

for transporter activity, RND family proteins usually associate as homotrimers, and, less frequently, homodimers (Belardinelli et al., 2016; Kumar et al., 2017; Murakami et al., 2002). It is therefore very surprising that both published crystal structures of *M. smegmatis* MmpL3 concurred in that MmpL3 exists in a monomeric state (Su et al., 2019; Zhang et al., 2019). However, both groups purified protein truncations of MmpL3 that lack a substantial portion of the C-terminal residues. Thus, if the Ct domain is required for the oligomerization of MmpL3, the crystal structure of C-terminally truncated MmpL3 would be that of a monomer. While the investigators examined the oligomerization status of full-length MmpL3 via mass spectrometry and native gel electrophoresis, concluding that MmpL3 is indeed monomeric, these experiments necessitated the presence of the membrane-solubilizing detergent dodecyl maltoside. If inter-MmpL3 interactions require protein integration in the plasma membrane or hydrophobic interactions between Ct domains, then the observed MmpL3 monomers would not be representative of the physiologically-active MmpL protein. Another possibility is that oligomerization might be dependent on subcellular localization given that the accumulation of MmpL3 at the mycobacterial poles is abrogated by truncating the protein after the 10^{th} transmembrane domain (Carel et al., 2014). Thus, although the C-terminal domain is not required for transporter activity, we cannot exclude the possibility that Cluster II MmpL proteins function as oligomeric complexes in their native state.

The Ct region of Cluster II MmpLs is also a potential point of post-translational regulation. It is becoming increasingly apparent that post-translational modulation of protein function is a rapid means by which *Mtb* can respond and adapt to its external environment. This seems to be especially true in the case of MmpL11, given that MmpL11 substrates are important during specific growth phases, yet expression of *mmpL11* mRNA appears to be relatively constant regardless of *in vitro* culture conditions (**Figure 3.7**). Phosphorylation sites were identified in the Ct domains of both MmpL3 and MmpL11 (Prisic et al., 2010). The phosphorylation patterns varied according to culture conditions, strongly suggesting protein kinase-mediated phosphorylation events as a mechanism of MmpL post-translational regulation. In this study, a single phospho-site was identified in the MmpL11 Ct domain. This site was only identified when *Mtb* was cultured with acetate as the sole carbon source. We predicted that phosphorylation at this site would serve as a binary regulator of MmpL11 transporter activity. Our experiments with phospho-mimetic and phospho-ablative $MmpL11_{TB}$ confirmed that phosphorylation at this residue negatively regulates MmpL11 function (**Figures 3.3** and **3.5**). The mechanism of inhibition appears to be protein destabilization which leads to degradation of MmpL11, as shown by comparing the expression of phospho-mimetic and phospho-ablative $MmpL11_{TB}$ variants (**Figure 3.6**).

Phospho-regulation of MmpL11 appears to be a simple on/off binary mechanism, given that only a single phospho-residue regulates MmpL11 function. Intriguingly,

six phospho-sites were identified in the MmpL3 Ct region (Prisic et al., 2010). Phosphorylation at these sites appeared to be highly responsive to culture conditions, suggesting that phospho-regulation of MmpL3 is more finely tuned than a simple on/off mechanism. The essentiality of MmpL3-mediated mycolic acid export is consistent with the prediction that finer gradations of control of MmpL3 transporter function are necessary to modulate cell envelope biogenesis in response to external conditions. Future research should be directed at ascertaining how phosphorylation impacts MmpL3 function and protein levels.

Eukaryotic-like STPKs are responsible for protein phosphorylation in *Mtb*. Phosphorylation of the Ct regions of Cluster II MmpLs is in agreement with the cytoplasmic localization of most STPK kinase domains. Since Cluster I MmpLs do not have a large Ct domain, it is unclear whether these proteins are similarly regulated by phosphorylation. MmpL10 was the only other MmpL protein identified as being phosphorylated in the *Mtb* phosphoproteome study, in a linking region between two TMDs (Prisic et al., 2010). It is unknown whether phosphorylation at this residue impacts MmpL10 transporter function, or if other Cluster I MmpL proteins might be phosphorylated under different conditions than those used in the Prisic study.

One report identified MmpL7 as a potential substrate of the PknD kinase (Pérez et al., 2006). Interestingly, the phospho-sites identified in this study lie in what was predicted by TMHMMpred to be the D2 periplasmic domain of MmpL7

(Sonnhammer et al., 1998). Since the PknD kinase domain is cytoplasmic, it was originally unclear how phosphorylation at this domain might occur. Since we now have a *bona fide* structure of a mycobacterial MmpL protein, we constructed homology models of *Mtb* MmpL3, MmpL11, and MmpL7 based on the crystal structure of *M. smegmatis* MmpL3 using the Phyre2 web server [**Figure 4.2**, (Kelley et al., 2015)]. The MmpL3 and MmpL11 models were highly similar, and validated the initial topology predictions. However, the MmpL7 model predicted opposite membrane topology compared to TMHMMpred, with the MmpL7 D1 and D2 domains localized to the cytoplasm (Kelley et al., 2015). If our model is accurate, then phosphorylation of the MmpL7 D2 domain is reasonable. Together, these observations suggest that MmpL7 has divergent membrane topology relative to other MmpL proteins.

Other evidence suggests that MmpL7 is fundamentally dissimilar to the other *Mtb* MmpL proteins. Transport of the MmpL7 substrate PDIM is dependent on the DrrABC transporter (Camacho et al., 2001). No other MmpL transporter requires the presence of an ABC transporter for substrate translocation, suggesting that MmpL7 utilizes a different transport mechanism compared to other MmpL proteins. The dependence of MmpL7-mediated transport on DrrABC suggests that ATP hydrolysis is the energetic basis of MmpL7-mediated transport, rather than the PMF. Thus, mutation of the conserved TM10 tyrosine residue (Y837 in the case of MmpL7), which is critical for MmpL3- and MmpL11-mediated transport, might not abrogate substrate transport in the same manner as it does

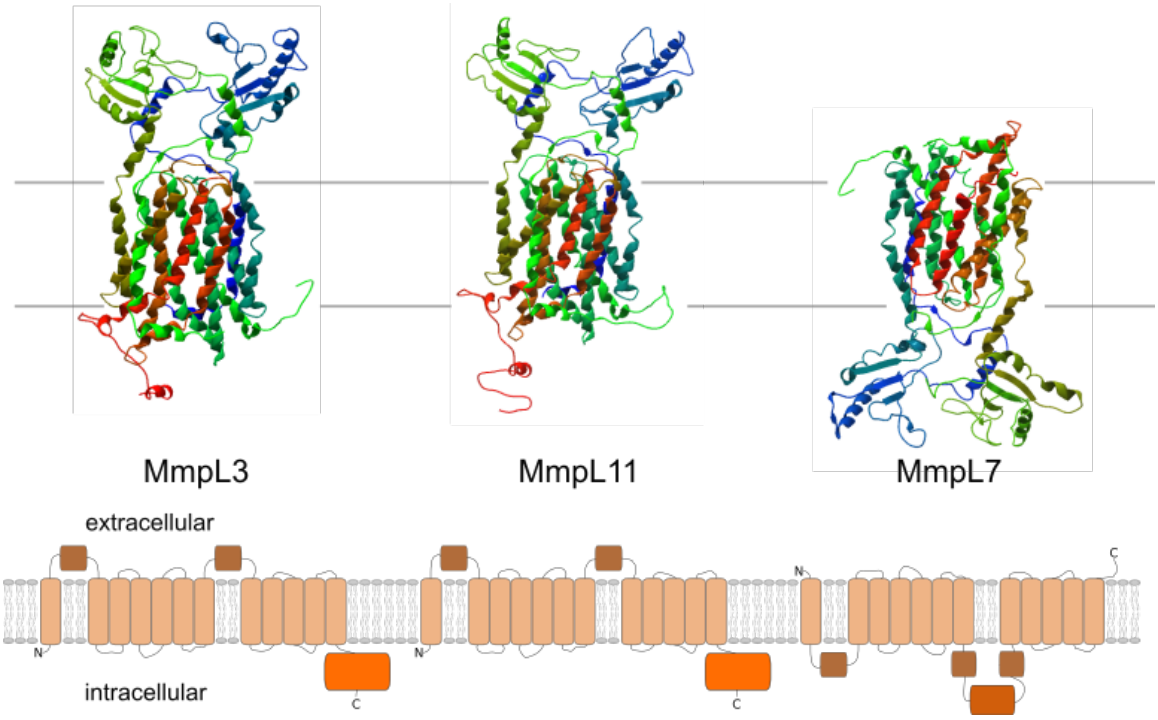

Figure 4.2. Homology structures of *Mtb* MmpL proteins constructed via the Phyre2 web portal. The highest confidence template structure for all three proteins was *M. smegmatis* MmpL3 in complex with the small molecule inhibitor ICA38 (3Zhang et al., 2019; PDB: 6AJJ). The Phyre2 topology predictions are illustrated underneath each model structure. N. B. The MmpL3 and MmpL11 model structures do not contain their respective cytoplasmic domains, given that the template *M. smegmatis* MmpL3 structure is C-terminally truncated.

for other MmpL transporters [(Bernut et al., 2016); Chapter 3)]. Future work has the potential to elucidate the seemingly unique transport mechanism of MmpL7.

A further question regarding phospho-regulation of MmpL-mediated transport concerns the identity of the kinases that perform the phosphorylation(s). In the case of MmpL11, a likely candidate was PknD, given that we identified PknD via mass spectrometry in two out of three cross-linked MmpL11 pull-down experiments. However, initial attempts to demonstrate *in vitro* phosphorylation of the MmpL11 C-terminal domain by PknD and other kinases were unsuccessful (**Figure 3.8**). The crystal structure of the extracellular sensor domain of PknD revealed a symmetric, six-bladed β-propeller (Good et al., 2004). The identity of the ligand bound by this structure is unknown. Further research should be directed towards confirming the identity of the kinase that phosphorylates MmpL11, and defining the stimulus that initiates this signal. In a broader sense, identifying the influence of other STPK signal transduction pathways on MmpL-mediated transport of cell envelope components is of interest. Dissecting these pathways has the potential to facilitate new ways to manipulate *Mtb* adaptive processes, particularly in the context of infection, in order to more efficaciously treat TB disease.

REFERENCES

Adams, P.D., Grosse-Kunstleve, R.W., Hung, L.-W., Ioerger, T.R., McCoy, A.J., Moriarty, N.W., Read, R.J., Sacchettini, J.C., Sauter, N.K., and Terwilliger, T.C. (2002). PHENIX: building new software for automated crystallographic structure determination. Acta Crystallogr. D Biol. Crystallogr. *58*, 1948–1954.

Akhter, Y., Ehebauer, M.T., Mukhopadhyay, S., and Hasnain, S.E. (2012). The PE/PPE multigene family codes for virulence factors and is a possible source of mycobacterial antigenic variation: perhaps more? Biochimie *94*, 110–116.

Alderwick, L.J., Harrison, J., Lloyd, G.S., and Birch, H.L. (2015). The Mycobacterial Cell Wall--Peptidoglycan and Arabinogalactan. Cold Spring Harb Perspect Med *5*, a021113.

Alderwick, L.J., Radmacher, E., Seidel, M., Gande, R., Hitchen, P.G., Morris, H.R., Dell, A., Sahm, H., Eggeling, L., and Besra, G.S. (2005). Deletion of Cg-emb in corynebacterianeae leads to a novel truncated cell wall arabinogalactan, whereas inactivation of Cg-ubiA results in an arabinan-deficient mutant with a cell wall galactan core. Journal of Biological Chemistry *280*, 32362–32371.

Algood, H.M.S., Lin, P.L., and Flynn, J.L. (2005). Tumor necrosis factor and chemokine interactions in the formation and maintenance of granulomas in tuberculosis. Clin. Infect. Dis. *41 Suppl 3*, S189–S193.

Algood, H.M.S., Lin, P.L., Yankura, D., Jones, A., Chan, J., and Flynn, J.L. (2004). TNF Influences Chemokine Expression of Macrophages In Vitro and That of CD11b+ Cells In Vivo during Mycobacterium tuberculosis Infection. The Journal of Immunology *172*, 6846–6857.

Arumugam, P., Shankaran, D., Bothra, A., Gandotra, S., and Rao, V. (2018). The MmpS6-MmpL6 Operon Is an Oxidative Stress Response System Providing Selective Advantage to Mycobacterium tuberculosis in Stress. J Infect Dis *367*, 850.

Astarie Dequeker, C., Le Guyader, L., Malaga, W., Seaphanh, F.-K., Chalut, C., Lopez, A., and Guilhot, C. (2009). Phthiocerol Dimycocerosates of M. tuberculosis Participate in Macrophage Invasion by Inducing Changes in the Organization of Plasma Membrane Lipids. PLoS Pathog *5*, e1000289.

Ates, L.S., van der Woude, A.D., Bestebroer, J., van Stempvoort, G., Musters, R.J.P., Garcia-Vallejo, J.J., Picavet, D.I., Weerd, R.V. de, Maletta, M., Kuijl, C.P., et al. (2016). The ESX-5 System of Pathogenic Mycobacteria Is Involved In Capsule Integrity and Virulence through Its Substrate PPE10. PLoS Pathog *12*, e1005696.

Augenstreich, J., Arbues, A., Simeone, R., Haanappel, E., Wegener, A., Sayes, F., Chevalier, F.L., Chalut, C., Malaga, W., Guilhot, C., et al. (2017). ESX-1 and phthiocerol dimycocerosates of Mycobacterium tuberculosis act in concert to cause phagosomal rupture and host cell apoptosis. Cell Microbiol.

Baba, T., Natsuhara, Y., Kaneda, K., and Yano, I. (1997). Granuloma formation activity and mycolic acid composition of mycobacterial cord factor. Cell. Mol. Life Sci. *53*, 227–232.

Babu, M.M., Priya, M.L., Selvan, A.T., Madera, M., Gough, J., Aravind, L., and Sankaran, K. (2006). A database of bacterial lipoproteins (DOLOP) with functional assignments to predicted lipoproteins. Journal of Bacteriology *188*, 2761–2773.

Backus, K.M., Dolan, M.A., Barry, C.S., Joe, M., McPhie, P., Boshoff, H.I.M., Lowary, T.L., Davis, B.G., and Barry, C.E. (2014). The three Mycobacterium tuberculosis antigen 85 isoforms have unique substrates and activities determined by non-active site regions. J. Biol. Chem. *289*, 25041–25053.

Balcewicz-Sablinska, M.K., Keane, J., Kornfeld, H., and Remold, H.G. (1998). Pathogenic *Mycobacterium tuberculosis* evades apoptosis of host macrophages by release of TNF-R2, resulting in inactivation of TNF-alpha. The Journal of Immunology *161*, 2636–2641.

Bardarov, S., Bardarov, S., Jr, Pavelka, M.S., Jr, Sambandamurthy, V., Larsen, M., Tufariello, J., Chan, J., Hatfull, G., and Jacobs, W.R., Jr (2002). Specialized transduction: an efficient method for generating marked and unmarked targeted gene disruptions in Mycobacterium tuberculosis, M. bovis BCG and M. smegmatis. Microbiology (Reading, Engl.) *148*, 3007–3017.

Barry, C.E., Lee, R.E., Mdluli, K., Sampson, A.E., Schroeder, B.G., Slayden, R.A., and Yuan, Y. (1998). Mycolic acids: structure, biosynthesis and physiological functions. Prog. Lipid Res. *37*, 143–179.

Barthe, P., Mukamolova, G.V., Roumestand, C., and Cohen-Gonsaud, M. (2010). The structure of PknB extracellular PASTA domain from mycobacterium tuberculosis suggests a ligand-dependent kinase activation. Structure *18*, 606–615.

Becker, K., Haldimann, K., Selchow, P., Reinau, L.M., Dal Molin, M., and Sander, P. (2017). Lipoprotein Glycosylation by Protein-O-Mannosyltransferase (MAB_1122c) Contributes to Low Cell Envelope Permeability and Antibiotic Resistance of Mycobacterium abscessus. Front. Microbiol. *8*, 2123.

Belardinelli, J.M., Larrouy-Maumus, G., Jones, V., Sorio de Carvalho, L.P., McNeil, M.R., and Jackson, M. (2014). Biosynthesis and translocation of unsulfated acyltrehaloses in Mycobacterium tuberculosis. J. Biol. Chem. *289*, 27952–27965.

Belardinelli, J.M., Yazidi, A., Yang, L., Fabre, L., Li, W., Jacques, B., Angala, S.K., Rouiller, I., Zgurskaya, H.I., Sygusch, J., et al. (2016). Structure–Function Profile of MmpL3, the Essential Mycolic Acid Transporter from Mycobacterium tuberculosis. ACS Infect. Dis. *2*, 702–713.

Belisle, J.T., Vissa, V.D., Sievert, T., Takayama, K., Brennan, P.J., and Besra, G.S. (1997). Role of the major antigen of *Mycobacterium tuberculosis* in cell wall biogenesis. Science *276*, 1420–1422.

Bernut, A., Viljoen, A., Dupont, C., Sapriel, G., Blaise, M., Bouchier, C., Brosch, R., de Chastellier, C., Herrmann, J.-L., and Kremer, L. (2016). Insights into the smooth-to-rough transitioning in Mycobacterium bolletii unravels a functional Tyr residue conserved in all mycobacterial MmpL family members. Molecular Microbiology *99*, 866–883.

Blanc, L., Gilleron, M., Prandi, J., Song, O.-R., Jang, M.-S., Gicquel, B., Drocourt, D., Neyrolles, O., Brodin, P., Tiraby, G., et al. (2017). Mycobacterium tuberculosis inhibits human innate immune responses via the production of TLR2 antagonist glycolipids. Proc. Natl. Acad. Sci. U.S.a. *4*, 201707840.

BLOCH, H. (1950). Studies on the virulence of tubercle bacilli; isolation and biological properties of a constituent of virulent organisms. Journal of Experimental Medicine *91*, 197–218–pl.

Boesen, H., Jensen, B.N., Wilcke, T., and Andersen, P. (1995). Human T-cell responses to secreted antigen fractions of Mycobacterium tuberculosis. Infect. Immun. *63*, 1491–1497.

Bowdish, D.M.E., Sakamoto, K., Kim, M.-J., Kroos, M., Mukhopadhyay, S., Leifer, C.A., Tryggvason, K., Gordon, S., and Russell, D.G. (2009). MARCO, TLR2, and CD14 are required for macrophage cytokine responses to mycobacterial trehalose dimycolate and Mycobacterium tuberculosis. PLoS Pathog *5*, e1000474.

Brademan, D.R., Riley, N.M., Kwiecien, N.W., and Coon, J.J. (2019). Interactive Peptide Spectral Annotator: A Versatile Web-based Tool for Proteomic Applications. Mol. Cell Proteomics *18*, S193–S201.

Braunstein, M., Brown, A.M., Kurtz, S., and Jacobs, W.R. (2001). Two Nonredundant SecA Homologues Function in Mycobacteria. Journal of Bacteriology *183*, 6979–6990.

Braunstein, M., Espinosa, B.J., Chan, J., Belisle, J.T., and Jacobs, W.R. (2003). SecA2 functions in the secretion of superoxide dismutase A and in the virulence of Mycobacterium tuberculosis. Molecular Microbiology *48*, 453–464.

Brennan, P.J., and Nikaido, H. (1995). The envelope of mycobacteria. Annu. Rev. Biochem. *64*, 29–63.

Brosch, R., Gordon, S.V., Marmiesse, M., Brodin, P., Buchrieser, C., Eiglmeier, K., Garnier, T., Gutierrez, C., Hewinson, G., Kremer, K., et al. (2002). A new evolutionary scenario for the Mycobacterium tuberculosis complex. Proc Natl Acad Sci USA *99*, 3684–3689.

Bulut, Y., Michelsen, K.S., Hayrapetian, L., Naiki, Y., Spallek, R., Singh, M., and Arditi, M. (2005). Mycobacterium tuberculosis heat shock proteins use diverse Toll-like receptor pathways to activate pro-inflammatory signals. Journal of Biological Chemistry *280*, 20961–20967.

Camacho, L.R., Constant, P., Raynaud, C., Laneelle, M.A., Triccas, J.A., Gicquel, B., Daffe, M., and Guilhot, C. (2001). Analysis of the Phthiocerol Dimycocerosate Locus of *Mycobacterium tuberculosis*. Journal of Biological Chemistry *276*, 19845–19854.

Camacho, L.R., Ensergueix, D., Perez, E., Gicquel, B., and Guilhot, C. (1999). Identification of a virulence gene cluster of Mycobacterium tuberculosis by signature-tagged transposon mutagenesis. Molecular Microbiology *34*, 257–267.

Cambier, C.J., Takaki, K.K., Larson, R.P., Hernandez, R.E., Tobin, D.M., Urdahl, K.B., Cosma, C.L., and Ramakrishnan, L. (2014). Mycobacteria manipulate macrophage recruitment through coordinated use of membrane lipids. Nature *505*, 218–222.

Carel, C., Nukdee, K., Cantaloube, S., Bonne, M., Diagne, C.T., Laval, F., Daffe, M., and Zerbib, D. (2014). Mycobacterium tuberculosis proteins involved in mycolic acid synthesis and transport localize dynamically to the old growing pole and septum. PLoS ONE *9*, e97148.

Chackerian, A.A., Alt, J.M., Perera, T.V., Dascher, C.C., and Behar, S.M. (2002). Dissemination of Mycobacterium tuberculosis Is Influenced by Host Factors and Precedes the Initiation of T-Cell Immunity. Infect. Immun. *70*, 4501–4509.

Chalut, C. (2016). MmpL transporter-mediated export of cell-wall associated lipids and siderophores in mycobacteria. Tuberculosis (Edinb) *100*, 32–45.

Chen, M., Gan, H., and Remold, H.G. (2006). A Mechanism of Virulence: Virulent Mycobacterium tuberculosis Strain H37Rv, but Not Attenuated H37Ra, Causes Significant Mitochondrial Inner Membrane Disruption in Macrophages Leading to Necrosis. The Journal of Immunology *176*, 3707–3716.

Chiaradia, L., Lefebvre, C., Parra, J., Marcoux, J., Burlet-Schiltz, O., Etienne, G., Tropis, M., and Daffe, M. (2017). Dissecting the mycobacterial cell envelope and defining the composition of the native mycomembrane. Sci Rep *7*, 12807.

Chim, N., Torres, R., Liu, Y., Capri, J., Batot, G., Whitelegge, J.P., and Goulding, C.W. (2015). The Structure and Interactions of Periplasmic Domains of Crucial MmpL Membrane Proteins from Mycobacterium tuberculosis. Chemistry &

Biology *22*, 1098–1107.

Chou, T.H., Delmar, J.A., Wright, C.C., Kumar, N., Radhakrishnan, A., Doh, J.K., Licon, M.H., Bolla, J.R., Lei, H.T., Rajashankar, K.R., et al. (2015). Crystal structure of the Mycobacterium tuberculosis transcriptional regulator Rv0302. Protein Science *24*, 1942–1955.

Cohen, S.B., Gern, B.H., Delahaye, J.L., Adams, K.N., Plumlee, C.R., Winkler, J.K., Sherman, D.R., Gerner, M.Y., and Urdahl, K.B. (2018). Alveolar Macrophages Provide an Early Mycobacterium tuberculosis Niche and Initiate Dissemination. Cell Host and Microbe *24*, 439–446.e4.

Cole, S.T., Brosch, R., Parkhill, J., Garnier, T., Churcher, C., Harris, D., Gordon, S.V., Eiglmeier, K., Gas, S., Barry, C.E., III, et al. (1998). Deciphering the biology of Mycobacterium tuberculosis from the complete genome sequence. Nature *393*, 537–544.

Converse, S.E., Mougous, J.D., Leavell, M.D., Leary, J.A., Bertozzi, C.R., and Cox, J.S. (2003). MmpL8 is required for sulfolipid-1 biosynthesis and *Mycobacterium tuberculosis* virulence. Proc Natl Acad Sci USA *100*, 6121–6126.

Cowley, S.C., and Elkins, K.L. (2003). CD4+ T cells mediate IFN-gamma-independent control of Mycobacterium tuberculosis infection both in vitro and in vivo. The Journal of Immunology *171*, 4689–4699.

Cowtan, K. (2010). Recent developments in classical density modification. Acta Crystallogr. D Biol. Crystallogr. *66*, 470–478.

Cox, J.S., Chen, B., McNeil, M., and Jacobs, W.R. (1999). Complex lipid determines tissue-specific replication of *Mycobacterium tuberculosis* in mice. Nature *402*, 79–83.

Cronan, M.R., and Tobin, D.M. (2014). Fit for consumption: zebrafish as a model for tuberculosis. Disease Models & Mechanisms *7*, 777–784.

Cronan, M.R., Beerman, R.W., Rosenberg, A.F., Saelens, J.W., Johnson, M.G., Oehlers, S.H., Sisk, D.M., Jurcic Smith, K.L., Medvitz, N.A., Miller, S.E., et al. (2016). Macrophage Epithelial Reprogramming Underlies Mycobacterial Granuloma Formation and Promotes Infection. Immunity *45*, 861–876.

D'Avila, H., Melo, R.C.N., Parreira, G.G., Werneck-Barroso, E., Castro-Faria-Neto, H.C., and Bozza, P.T. (2006). Mycobacterium bovis Bacillus Calmette-Guérin Induces TLR2-Mediated Formation of Lipid Bodies: Intracellular Domains for Eicosanoid Synthesis In Vivo. The Journal of Immunology *176*, 3087–3097.

Daffe, M., and Etienne, G. (1999). The capsule of *Mycobacterium tuberculosis* and its implications for pathogenicity. Tubercle and Lung Disease *79*, 153–169.

Daffe, M., Brennan, P.J., and McNeil, M. (1990). Predominant structural features of the cell wall arabinogalactan of Mycobacterium tuberculosis as revealed through characterization of oligoglycosyl alditol fragments by gas chromatography/mass spectrometry and by 1H and 13C NMR analyses. Journal of Biological Chemistry *265*, 6734–6743.

Daffe, M., Quémard, A., and Marrakchi, H. (2017). Mycolic acids: from chemistry to biology. Biogenesis of Fatty Acids, Lipids and Membranes.

Daniel, J., Maamar, H., Deb, C., Sirakova, T.D., and Kolattukudy, P.E. (2011). Mycobacterium tuberculosis Uses Host Triacylglycerol to Accumulate Lipid Droplets and Acquires a Dormancy-Like Phenotype in Lipid-Loaded Macrophages. PLoS Pathog *7*, e1002093.

Danilchanka, O., Pires, D., Anes, E., and Niederweis, M. (2015). The Mycobacterium tuberculosis outer membrane channel protein CpnT confers susceptibility to toxic molecules. Antimicrobial Agents and Chemotherapy *59*, 2328–2336.

Danilchanka, O., Sun, J., Pavlenok, M., Maueröder, C., Speer, A., Siroy, A., Marrero, J., Trujillo, C., Mayhew, D.L., Doornbos, K.S., et al. (2014). An outer membrane channel protein of Mycobacterium tuberculosis with exotoxin activity. Proc Natl Acad Sci USA *111*, 201400136–201406755.

De Angelis, F., Lee, J.K., O'Connell, J.D., Miercke, L.J.W., Verschueren, K.H., Srinivasan, V., Bauvois, C., Govaerts, C., Robbins, R.A., Ruysschaert, J.-M., et al. (2010). Metal-induced conformational changes in ZneB suggest an active role of membrane fusion proteins in efflux resistance systems. Proc. Natl. Acad. Sci. U.S.a. *107*, 11038–11043.

Degiacomi, G., Benjak, A., Madacki, J., Boldrin, F., Provvedi, R., Palù, G., Kordulákova, J., Cole, S.T., and Manganelli, R. (2017). Essentiality of mmpL3 and impact of its silencing on Mycobacterium tuberculosis gene expression. Sci Rep *7*, 43495.

Delmar, J.A., Chou, T.H., Wright, C.C., Licon, M.H., Doh, J.K., Radhakrishnan, A., Kumar, N., Lei, H.T., Bolla, J.R., Rajashankar, K.R., et al. (2015). Structural Basis for the Regulation of the MmpL Transporters of Mycobacterium tuberculosis. Journal of Biological Chemistry *290*, jbc.M115.683797–28574.

Delmar, J.A., Su, C.C., and Yu, E.W. (2014). Bacterial multidrug efflux transporters. Annu Rev Biophys *43*, 93–117.

Dheda, K., Booth, H., Huggett, J.F., Johnson, M.A., Zumla, A., and Rook, G.A.W. (2005). Lung remodeling in pulmonary tuberculosis. J Infect Dis *192*, 1201–1209.

DiGiuseppe Champion, P.A., and Cox, J.S. (2007). Protein secretion systems in Mycobacteria. Cell Microbiol *9*, 1376–1384.

Dinh, T., Paulsen, I.T., and Saier, M.H. (1994). A family of extracytoplasmic proteins that allow transport of large molecules across the outer membranes of gram-negative bacteria. Journal of Bacteriology *176*, 3825–3831.

Domenech, P., Reed, M.B., and Barry, C.E. (2005). Contribution of the *Mycobacterium tuberculosis* MmpL Protein Family to Virulence and Drug Resistance. Infect. Immun. *73*, 3492–3501.

Domenech, P., Reed, M.B., Dowd, C.S., Manca, C., Kaplan, G., and Barry, C.E. (2004). The Role of MmpL8 in Sulfatide Biogenesis and Virulence of *Mycobacterium tuberculosis*. Journal of Biological Chemistry *279*, 21257–21265.

Drage, M.G., Tsai, H.-C., Pecora, N.D., Cheng, T.-Y., Arida, A.R., Shukla, S., Rojas, R.E., Seshadri, C., Moody, D.B., Boom, W.H., et al. (2010). *Mycobacterium tuberculosis* lipoprotein LprG (Rv1411c) binds triacylated glycolipid agonists of Toll-like receptor 2. Nature Publishing Group *17*, 1088–1095.

Dubnau, E., Chan, J., Raynaud, C., Mohan, V.P., Laneelle, M.A., Yu, K., Quémard, A., Smith, I., and Daffe, M. (2000). Oxygenated mycolic acids are necessary for virulence of Mycobacterium tuberculosis in mice. Molecular Microbiology *36*, 630–637.

Dubois, V., Viljoen, A., Laencina, L., Le Moigne, V., Bernut, A., Dubar, F., Blaise, M., Gaillard, J.-L., Guerardel, Y., Kremer, L., et al. (2018). $MmpL8_{MAB}$ controls Mycobacterium abscessus virulence and production of a previously unknown glycolipid family. Proc Natl Acad Sci USA *13*, 201812984–10.

Ehrt, S., and Schnappinger, D. (2009). Mycobacterial survival strategies in the phagosome: defence against host stresses. Cell Microbiol *11*, 1170–1178.

Eiglmeier, K., Parkhill, J., Honoré, N., Garnier, T., Tekaia, F., Telenti, A., Klatser, P., James, K.D., Thomson, N.R., Wheeler, P.R., et al. (2001). The decaying genome of Mycobacterium leprae. Lepr Rev *72*, 387–398.

El-Gebali, S., Mistry, J., Bateman, A., Eddy, S.R., Luciani, A., Potter, S.C., Qureshi, M., Richardson, L.J., Salazar, G.A., Smart, A., et al. (2019). The Pfam protein families database in 2019. Nucleic Acids Research *47*, D427–D432.

Emsley, P., and Cowtan, K. (2004). Coot: model-building tools for molecular graphics. Acta Crystallogr. D Biol. Crystallogr. *60*, 2126–2132.

Fallahi-Sichani, M., Kirschner, D.E., and Linderman, J.J. (2012). NF-κB Signaling Dynamics Play a Key Role in Infection Control in Tuberculosis. Front Physiol *3*, 170.

Fay, A., Czudnochowski, N., Rock, J.M., Johnson, J.R., Krogan, N.J., Rosenberg, O., and Glickman, M.S. (2019). Two Accessory Proteins Govern

MmpL3 Mycolic Acid Transport in Mycobacteria. mBio *10*, 227–17.

Flynn, J.L., Chan, J., Triebold, K.J., Dalton, D.K., Stewart, T.A., and Bloom, B.R. (1993). An essential role for interferon gamma in resistance to Mycobacterium tuberculosis infection. Journal of Experimental Medicine *178*, 2249–2254.

Flynn, J.L. (2006). Lessons from experimental Mycobacterium tuberculosis infections. Microbes and Infection *8*, 1179–1188.

Flynn, J.L., Gideon, H.P., Mattila, J.T., and Lin, P.L. (2015). Immunology studies in non-human primate models of tuberculosis. Immunological Reviews *264*, 60–73.

Foley, H.N., Stewart, J.A., Kavunja, H.W., Rundell, S.R., and Swarts, B.M. (2016). Bioorthogonal Chemical Reporters for Selective In Situ Probing of Mycomembrane Components in Mycobacteria. Angewandte Chemie International Edition *55*, 2053–2057.

Foss, M.H., Pou, S., Davidson, P.M., Dunaj, J.L., Winter, R.W., Pou, S., Licon, M.H., Doh, J.K., Li, Y., Kelly, J.X., et al. (2016). Diphenylether-Modified 1,2-Diamines with Improved Drug Properties for Development against Mycobacterium tuberculosis. ACS Infect. Dis. *2*, 500–508.

Galagan, J.E., Minch, K., Peterson, M., Lyubetskaya, A., Azizi, E., Sweet, L., Gomes, A., Rustad, T., Dolganov, G., Glotova, I., et al. (2013). The Mycobacterium tuberculosis regulatory network and hypoxia. Nature *499*, 178–183.

Gaur, R.L., Ren, K., Blumenthal, A., Bhamidi, S., Gibbs, S., Jackson, M., Zare, R.N., Ehrt, S., Ernst, J.D., and Banaei, N. (2014). LprG-Mediated Surface Expression of Lipoarabinomannan Is Essential for Virulence of *Mycobacterium tuberculosis*. PLoS Pathog *10*, e1004376–14.

Gebhardt, H., Meniche, X., Tropis, M., Krämer, R., Daffe, M., and Morbach, S. (2007). The key role of the mycolic acid content in the functionality of the cell wall permeability barrier in Corynebacterineae. Microbiology (Reading, Engl.) *153*, 1424–1434.

Gibbons, H.S., Wolschendorf, F., Abshire, M., Niederweis, M., and Braunstein, M. (2007). Identification of Two Mycobacterium smegmatis Lipoproteins Exported by a SecA2-Dependent Pathway. Journal of Bacteriology *189*, 5090–5100.

Glickman, M.S., Cahill, S.M., and Jacobs, W.R. (2001). The Mycobacterium tuberculosis cmaA2 gene encodes a mycolic acid trans-cyclopropane synthetase. Journal of Biological Chemistry *276*, 2228–2233.

Glickman, M.S., Cox, J.S., and Jacobs, W.R. (2000). A novel mycolic acid cyclopropane synthetase is required for cording, persistence, and virulence of

Mycobacterium tuberculosis. Molecular Cell *5*, 717–727.

Glickman, M.S. (2003). The mmaA2 gene of Mycobacterium tuberculosis encodes the distal cyclopropane synthase of the alpha-mycolic acid. Journal of Biological Chemistry *278*, 7844–7849.

Gonzalez-Juarrero, M., Turner, O.C., Turner, J., Marietta, P., Brooks, J.V., and Orme, I.M. (2001). Temporal and Spatial Arrangement of Lymphocytes within Lung Granulomas Induced by Aerosol Infection with *Mycobacterium tuberculosis*. Infect. Immun. *69*, 1722–1728.

Good, M.C., Greenstein, A.E., Young, T.A., Ng, H.-L., and Alber, T. (2004). Sensor domain of the Mycobacterium tuberculosis receptor Ser/Thr protein kinase, PknD, forms a highly symmetric beta propeller. Journal of Molecular Biology *339*, 459–469.

Goren, M.B., Brokl, O., Roller, P., Fales, H.M., and Biochemistry, Das, B.C. (1976). Sulfatides of Mycobacterium tuberculosis: the structure of the principal sulfatide (SL-I). Biochemistry *15*, 2728–2735.

Grzegorzewicz, A.E., Pham, H., Gundi, V.A.K.B., Scherman, M.S., North, E.J., Hess, T., Jones, V., Gruppo, V., Born, S.E.M., Korduláková, J., et al. (2012). Inhibition of mycolic acid transport across the Mycobacterium tuberculosis plasma membrane. Nat Chem Biol *8*, 334–341.

Guan, L., and Nakae, T. (2001). Identification of Essential Charged Residues in Transmembrane Segments of the Multidrug Transporter MexB ofPseudomonas aeruginosa. Journal of Bacteriology *183*, 1734–1739.

Halloum, I., Viljoen, A., Khanna, V., Craig, D., Bouchier, C., Brosch, R., Coxon, G., and Kremer, L. (2017). Resistance to Thiacetazone Derivatives Active against Mycobacterium abscessus Involves Mutations in the MmpL5 Transcriptional Repressor MAB_4384. Antimicrobial Agents and Chemotherapy *61*, e02509–e02516.

Hamasaki, N., Isowa, K.-I., Kamada, K., Terano, Y., Matsumoto, T., Arakawa, T., Kobayashi, K., and Yano, I. (2000). In Vivo Administration of Mycobacterial Cord Factor (Trehalose 6,6′-Dimycolate) Can Induce Lung and Liver Granulomas and Thymic Atrophy in Rabbits. Infect. Immun. *68*, 3704–3709.

Hartkoorn, R.C., Uplekar, S., and Cole, S.T. (2014). Cross-Resistance between Clofazimine and Bedaquiline through Upregulation of MmpL5 in Mycobacterium tuberculosis. Antimicrobial Agents and Chemotherapy *58*, 2979–2981.

Hatzios, S.K., Schelle, M.W., Holsclaw, C.M., Behrens, C.R., Botyanszki, Z., Lin, F.L., Carlson, B.L., Kumar, P., Leary, J.A., and Bertozzi, C.R. (2009). PapA3 is an acyltransferase required for polyacyltrehalose biosynthesis in Mycobacterium tuberculosis. Journal of Biological Chemistry *284*, 12745–12751.

Hayashi, S., and Wu, H.C. (1985). Accumulation of prolipoprotein in Escherichia coli mutants defective in protein secretion. Journal of Bacteriology *161*, 949–954.

Hoffmann, C., Leis, A., Niederweis, M., Plitzko, J.M., and Engelhardt, H. (2008). Disclosure of the mycobacterial outer membrane: Cryo-electron tomography and vitreous sections reveal the lipid bilayer structure. Proc Natl Acad Sci USA *105*, 3963–3967.

Holm, L., and Rosenström, P. (2010). Dali server: conservation mapping in 3D. Nucleic Acids Research *38*, W545–W549.

Howard, N.C., Marin, N.D., Ahmed, M., Rosa, B.A., Martin, J., Bambouskova, M., Sergushichev, A., Loginicheva, E., Kurepina, N., Rangel-Moreno, J., et al. (2018). Mycobacterium tuberculosis carrying a rifampicin drug resistance mutation reprograms macrophage metabolism through cell wall lipid changes. Nature Microbiology *3*, 1099–1108.

Hunter, R.L., Olsen, M.R., Jagannath, C., and Actor, J.K. (2006a). Multiple roles of cord factor in the pathogenesis of primary, secondary, and cavitary tuberculosis, including a revised description of the pathology of secondary disease. Ann. Clin. Lab. Sci. *36*, 371–386.

Hunter, R.L., Olsen, M., Jagannath, C., and Actor, J.K. (2006b). Trehalose 6,6'-dimycolate and lipid in the pathogenesis of caseating granulomas of tuberculosis in mice. The American Journal of Pathology *168*, 1249–1261.

Indrigo, J. (2003). Cord factor trehalose 6,6'-dimycolate (TDM) mediates trafficking events during mycobacterial infection of murine macrophages. Microbiology *149*, 2049–2059.

Ishikawa, E., Ishikawa, T., Morita, Y.S., Toyonaga, K., Yamada, H., Takeuchi, O., Kinoshita, T., Akira, S., Yoshikai, Y., and Yamasaki, S. (2009). Direct recognition of the mycobacterial glycolipid, trehalose dimycolate, by C-type lectin Mincle. J. Exp. Med. *206*, 2879–2888.

Jackson, M. (2014). The mycobacterial cell envelope-lipids. Cold Spring Harb Perspect Med *4*, a021105–a021105.

Jain, M., and Cox, J.S. (2005). Interaction between Polyketide Synthase and Transporter Suggests Coupled Synthesis and Export of Virulence Lipid in *M. tuberculosis*. PLoS Pathog *1*, e2–e8.

Jain, M., Petzold, C.J., Schelle, M.W., Leavell, M.D., Mougous, J.D., Bertozzi, C.R., Leary, J.A., and Cox, J.S. (2007). Lipidomics reveals control of *Mycobacterium tuberculosis* virulence lipids via metabolic coupling. Proc Natl Acad Sci USA *104*, 5133–5138.

Jankute, M., Cox, J.A.G., Harrison, J., and Besra, G.S. (2015). Assembly of the

Mycobacterial Cell Wall. Annu. Rev. Microbiol. *69*, 405–423.

Jarlier, V., and Nikaido, H. (1990). Permeability barrier to hydrophilic solutes in Mycobacterium chelonei. Journal of Bacteriology *172*, 1418–1423.

Kalscheuer, R., Weinrick, B., Veeraraghavan, U., Besra, G.S., and Jacobs, W.R. (2010). Trehalose-recycling ABC transporter LpqY-SugA-SugB-SugC is essential for virulence of Mycobacterium tuberculosis. Proc Natl Acad Sci USA *107*, 21761–21766.

Kang, C.-M., Abbott, D.W., Park, S.T., Dascher, C.C., Cantley, L.C., and Husson, R.N. (2005a). The Mycobacterium tuberculosis serine/threonine kinases PknA and PknB: substrate identification and regulation of cell shape. Genes Dev. *19*, 1692–1704.

Kang, P.B., Azad, A.K., Torrelles, J.B., Kaufman, T.M., Beharka, A., Tibesar, E., DesJardin, L.E., and Schlesinger, L.S. (2005b). The human macrophage mannose receptor directs *Mycobacterium tuberculosis* lipoarabinomannan-mediated phagosome biogenesis. Journal of Experimental Medicine *202*, 987–999.

Kapopoulou, A., Lew, J.M., and Cole, S.T. (2011). The MycoBrowser portal: a comprehensive and manually annotated resource for mycobacterial genomes. Tuberculosis (Edinb) *91*, 8–13.

Kaur, P., Rausch, M., Malakar, B., Watson, U., Damle, N.P., Chawla, Y., Srinivasan, S., Sharma, K., Schneider, T., Jhingan, G.D., et al. (2019). LipidII interaction with specific residues of Mycobacterium tuberculosis PknB extracytoplasmic domain governs its optimal activation. Nature Communications *10*, 1231.

Keller, A., Nesvizhskii, A.I., Kolker, E., and Aebersold, R. (2002). Empirical statistical model to estimate the accuracy of peptide identifications made by MS/MS and database search. Anal. Chem. *74*, 5383–5392.

Kelley, L.A., Mezulis, S., Yates, C.M., Wass, M.N., and Sternberg, M.J.E. (2015). The Phyre2 web portal for protein modeling, prediction and analysis. Nature Protocols *10*, 845–858.

Kempe, S., Kestler, H., Lasar, A., and Wirth, T. (2005). NF-kappaB controls the global pro-inflammatory response in endothelial cells: evidence for the regulation of a pro-atherogenic program. Nucleic Acids Research *33*, 5308–5319.

Kremer, L., Maughan, W.N., Wilson, R.A., Dover, L.G., and Besra, G.S. (2002). The M. tuberculosis antigen 85 complex and mycolyltransferase activity. Letters in Applied Microbiology *34*, 233–237.

Krogh, A., Larsson, B., Heijne, von, G., and Sonnhammer, E.L. (2001). Predicting

transmembrane protein topology with a hidden Markov model: application to complete genomes. Journal of Molecular Biology *305*, 567–580.

Kudo, N., Kumagai, K., Tomishige, N., Yamaji, T., Wakatsuki, S., Nishijima, M., Hanada, K., and Kato, R. (2008). Structural basis for specific lipid recognition by CERT responsible for nonvesicular trafficking of ceramide. Proc. Natl. Acad. Sci. U.S.a. *105*, 488–493.

Kumar, N., Su, C.C., Chou, T.H., Radhakrishnan, A., Delmar, J.A., Rajashankar, K.R., and Yu, E.W. (2017). Crystal structures of the Burkholderia multivorans hopanoid transporter HpnN. Proc. Natl. Acad. Sci. U.S.a. *114*, 6557–6562.

Kumar, P., Schelle, M.W., Jain, M., Lin, F.L., Petzold, C.J., Leavell, M.D., Leary, J.A., Cox, J.S., and Bertozzi, C.R. (2007). PapA1 and PapA2 are acyltransferases essential for the biosynthesis of the Mycobacterium tuberculosis virulence factor sulfolipid-1. Proc Natl Acad Sci USA *104*, 11221–11226.

Kundu, P., Biswas, R., Mukherjee, S., Reinhard, L., Dutta, A., Mueller-Dieckmann, J., Weiss, M.S., Pal, N.K., and Das, A.K. (2016). Structure-based Epitope Mapping of Mycobacterium tuberculosis Secretary Antigen MTC28. J. Biol. Chem. *291*, 13943–13954.

Kurtz, S., McKinnon, K.P., Runge, M.S., Ting, J.P.Y., and Braunstein, M. (2006). The SecA2 Secretion Factor of Mycobacterium tuberculosis Promotes Growth in Macrophages and Inhibits the Host Immune Response. Infect. Immun. *74*, 6855–6864.

Lamichhane, G., Tyagi, S., and Bishai, W.R. (2005). Designer Arrays for Defined Mutant Analysis To Detect Genes Essential for Survival of Mycobacterium tuberculosis in Mouse Lungs. Infect. Immun. *73*, 2533–2540.

Lavollay, M., Arthur, M., Fourgeaud, M., Dubost, L., Marie, A., Veziris, N., Blanot, D., Gutmann, L., and Mainardi, J.-L. (2008). The Peptidoglycan of Stationary-Phase Mycobacterium tuberculosis Predominantly Contains Cross-Links Generated by l,d-Transpeptidation. Journal of Bacteriology *190*, 4360–4366.

Lee, K.-S., Dubey, V.S., Kolattukudy, P.E., Song, C.-H., Shin, A.-R., Jung, S.-B., Yang, C.-S., Kim, S.-Y., Jo, E.-K., Park, J.-K., et al. (2007). Diacyltrehalose of Mycobacterium tuberculosis inhibits lipopolysaccharide- and mycobacteria-induced proinflammatory cytokine production in human monocytic cells. FEMS Microbiology Letters *267*, 121–128.

Lee, W., VanderVen, B.C., Fahey, R.J., and Russell, D.G. (2013). Intracellular Mycobacterium tuberculosis exploits host-derived fatty acids to limit metabolic stress. J. Biol. Chem. *288*, 6788–6800.

Lerner, T.R., Queval, C.J., Fearns, A., Repnik, U., Griffiths, G., and Gutierrez, M.G. (2018). Phthiocerol dimycocerosates promote access to the cytosol and

intracellular burden of Mycobacterium tuberculosis in lymphatic endothelial cells. BMC Biol. *16*, 1.

Li, W., Obregón-Henao, A., Wallach, J.B., North, E.J., Lee, R.E., Gonzalez-Juarrero, M., Schnappinger, D., and Jackson, M. (2016). Therapeutic Potential of the Mycobacterium tuberculosis Mycolic Acid Transporter, MmpL3. Antimicrobial Agents and Chemotherapy *60*, 5198–5207.

Li, W., Upadhyay, A., Fontes, F.L., North, E.J., Wang, Y., Crans, D.C., Grzegorzewicz, A.E., Jones, V., Franzblau, S.G., Lee, R.E., et al. (2014). Novel Insights into the Mechanism of Inhibition of MmpL3, a Target of Multiple Pharmacophores in Mycobacterium tuberculosis. Antimicrobial Agents and Chemotherapy *58*, AAC.03229–14–6423.

Li, W., Yazidi, A., Pandya, A.N., Hegde, P., Tong, W., Calado Nogueira de Moura, V., North, E.J., Sygusch, J., and Jackson, M. (2018). MmpL3 as a Target for the Treatment of Drug-Resistant Nontuberculous Mycobacterial Infections. Front. Microbiol. *9*, 1547.

Lin, P.L., Ford, C.B., Coleman, M.T., Myers, A.J., Gawande, R., Ioerger, T., Sacchettini, J., Fortune, S.M., and Flynn, J.L. (2014). Sterilization of granulomas is common in active and latent tuberculosis despite within-host variability in bacterial killing. Nat. Med. *20*, 75–79.

Lönnroth, K., Jaramillo, E., Williams, B.G., Dye, C., and Raviglione, M. (2009). Drivers of tuberculosis epidemics: the role of risk factors and social determinants. Soc Sci Med *68*, 2240–2246.

Ma, D., Cook, D.N., Alberti, M., Pon, N.G., Nikaido, H., and Hearst, J.E. (1993). Molecular cloning and characterization of acrA and acrE genes of Escherichia coli. Journal of Bacteriology *175*, 6299–6313.

MacGurn, J.A., and Cox, J.S. (2007). A Genetic Screen for Mycobacterium tuberculosis Mutants Defective for Phagosome Maturation Arrest Identifies Components of the ESX-1 Secretion System. Infect. Immun. *75*, 2668–2678.

Mahapatra, S., Scherman, H., Brennan, P.J., and Crick, D.C. (2005). N Glycolylation of the Nucleotide Precursors of Peptidoglycan Biosynthesis of Mycobacterium spp. Is Altered by Drug Treatment. Journal of Bacteriology *187*, 2341–2347.

Manabe, Y.C., and Bishai, W.R. (2000). Latent Mycobacterium tuberculosis-persistence, patience, and winning by waiting. Nat. Med. *6*, 1327–1329.

Marks, S.M., Flood, J., Seaworth, B., Hirsch-Moverman, Y., Armstrong, L., Mase, S., Salcedo, K., Oh, P., Graviss, E.A., Colson, P.W., et al. (2014). Treatment practices, outcomes, and costs of multidrug-resistant and extensively drug-resistant tuberculosis, United States, 2005-2007. Emerging Infect. Dis. *20*, 812–

821.

Marrakchi, H., Lanéelle, M.-A., and Daffe, M. (2014). Mycolic Acids: Structures, Biosynthesis, and Beyond. Chemistry & Biology *21*, 67–85.

Martin, C.J., Cadena, A.M., Leung, V.W., Lin, P.L., Maiello, P., Hicks, N., Chase, M.R., Flynn, J.L., and Fortune, S.M. (2017). Digitally Barcoding Mycobacterium tuberculosis Reveals In Vivo Infection Dynamics in the Macaque Model of Tuberculosis. mBio *8*, e00312–e00317.

Martinot, A.J., Farrow, M., Bai, L., Layre, E., Cheng, T.-Y., Tsai, J.H., Iqbal, J., Annand, J.W., Sullivan, Z.A., Hussain, M.M., et al. (2016). Mycobacterial Metabolic Syndrome: LprG and Rv1410 Regulate Triacylglyceride Levels, Growth Rate and Virulence in Mycobacterium tuberculosis. PLoS Pathog *12*, e1005351–26.

McKinney, J.D., Bentrup, K.H.Z., Muñoz-Elías, E.J., Miczak, A., Chen, B., Chan, W.-T., Swenson, D., Sacchettini, J.C., Jacobs, W.R., Jr, and Russell, D.G. (2000). Persistence of Mycobacterium tuberculosis in macrophages and mice requires the glyoxylate shunt enzyme isocitrate lyase. Nature *406*, 735–738.

McNeil, M., Daffe, M., and Brennan, P.J. (1990). Evidence for the nature of the link between the arabinogalactan and peptidoglycan of mycobacterial cell walls. Journal of Biological Chemistry *265*, 18200–18206.

McNeil, M., Daffe, M., and Brennan, P.J. (1991). Location of the mycolyl ester substituents in the cell walls of mycobacteria. Journal of Biological Chemistry *266*, 13217–13223.

McNeil, M., Wallner, S.J., Hunter, S.W., and Brennan, P.J. (1987). Demonstration that the galactosyl and arabinosyl residues in the cell-wall arabinogalactan of Mycobacterium leprae and Mycobacterium tuberculosis are furanoid. Carbohydr. Res. *166*, 299–308.

Means, T.K., Wang, S., Lien, E., Yoshimura, A., Golenbock, D.T., and Fenton, M.J. (1999). Human toll-like receptors mediate cellular activation by Mycobacterium tuberculosis. The Journal of Immunology *163*, 3920–3927.

Mehaffy, C., Belisle, J.T., and Dobos, K.M. (2019). Mycobacteria and their sweet proteins: An overview of protein glycosylation and lipoglycosylation in M. tuberculosis. Tuberculosis *115*, 1–13.

Melly, G., and Purdy, G.E. (2019). MmpL Proteins in Physiology and Pathogenesis of M. tuberculosis. Microorganisms *7*, 70.

Melly, G.C., Stokas, H., Dunaj, J.L., Hsu, F.F., Rajavel, M., Su, C.C., Yu, E.W., and Purdy, G.E. (2019). Structural and functional evidence that lipoprotein LpqN

supports cell envelope biogenesis in M. tuberculosis. J. Biol. Chem. jbc.RA119.008781.

Mestre, O., Hurtado-Ortiz, R., Vultos, Dos, T., Namouchi, A., Cimino, M., Pimentel, M., Neyrolles, O., and Gicquel, B. (2013). High Throughput Phenotypic Selection of Mycobacterium tuberculosis Mutants with Impaired Resistance to Reactive Oxygen Species Identifies Genes Important for Intracellular Growth. PLoS ONE *8*, e53486.

Milano, A., Pasca, M.R., Provvedi, R., Lucarelli, A.P., Manina, G., Ribeiro, A.L. de J.L., Manganelli, R., and Riccardi, G. (2009). Azole resistance in Mycobacterium tuberculosis is mediated by the MmpS5-MmpL5 efflux system. Tuberculosis (Edinb) *89*, 84–90.

Minnikin, D.E. (1991). Chemical principles in the organization of lipid components in the mycobacterial cell envelope. Res. Microbiol. *142*, 423–427.

Mir, M., Asong, J., Li, X., Cardot, J., Boons, G.-J., and Husson, R.N. (2011). The extracytoplasmic domain of the Mycobacterium tuberculosis Ser/Thr kinase PknB binds specific muropeptides and is required for PknB localization. PLoS Pathog *7*, e1002182.

Molle, V., Gulten, G., Vilcheze, C., Veyron-Churlet, R., Zanella-Cléon, I., Sacchettini, J.C., Jacobs, W.R., and Kremer, L. (2010). Phosphorylation of InhA inhibits mycolic acid biosynthesis and growth of Mycobacterium tuberculosis. Molecular Microbiology *78*, 1591–1605.

Murakami, S., and Yamaguchi, A. (2003). Multidrug-exporting secondary transporters. Curr. Opin. Struct. Biol. *13*, 443–452.

Murakami, S., Nakashima, R., Yamashita, E., and Yamaguchi, A. (2002). Crystal structure of bacterial multidrug efflux transporter AcrB. Nature *419*, 587–593.

Murakami, S., Nakashima, R., Yamashita, E., Matsumoto, T., and Yamaguchi, A. (2006). Crystal structures of a multidrug transporter reveal a functionally rotating mechanism. Nature *443*, 173–179.

Niederweis, M., Ehrt, S., Heinz, C., Klöcker, U., Karosi, S., Swiderek, K.M., Riley, L.W., and Benz, R. (1999). Cloning of the mspA gene encoding a porin from Mycobacterium smegmatis. Molecular Microbiology *33*, 933–945.

NOLL, H., BLOCH, H., ASSELINEAU, J., and LEDERER, E. (1956). The chemical structure of the cord factor of Mycobacterium tuberculosis. Biochim. Biophys. Acta *20*, 299–309.

Ojha, A.K., Baughn, A.D., Sambandan, D., Hsu, T., Trivelli, X., Guerardel, Y., Alahari, A., Kremer, L., Jacobs, W.R., Jr, and Hatfull, G.F. (2008). Growth of *Mycobacterium tuberculosis* biofilms containing free mycolic acids and

harbouring drug-tolerant bacteria. Molecular Microbiology *69*, 164–174.

Okusu, H., Ma, D., and Nikaido, H. (1996). AcrAB efflux pump plays a major role in the antibiotic resistance phenotype of Escherichia coli multiple-antibiotic-resistance (Mar) mutants. Journal of Bacteriology *178*, 306–308.

Ortalo-Magne, A., Dupont, M.A., Lemassu, A., Andersen, A.B., Gounon, P., and Daffe, M. (1995). Molecular composition of the outermost capsular material of the tubercle bacillus. Microbiology (Reading, Engl.) *141 (Pt 7)*, 1609–1620.

Otwinowski, Z., and Minor, W. (1997). [20] Processing of X-ray diffraction data collected in oscillation mode. Meth. Enzymol. *276*, 307–326.

Owens, C.P., Chim, N., Graves, A.B., Harmston, C.A., Iniguez, A., Contreras, H., Liptak, M.D., and Goulding, C.W. (2013). The Mycobacterium tuberculosis secreted protein Rv0203 transfers heme to membrane proteins MmpL3 and MmpL11. J. Biol. Chem. *288*, 21714–21728.

Pacheco, S.A., Hsu, F.F., Powers, K.M., and Purdy, G.E. (2013). MmpL11 Protein Transports Mycolic Acid-containing Lipids to the Mycobacterial Cell Wall and Contributes to Biofilm Formation in *Mycobacterium smegmatis*. Journal of Biological Chemistry *288*, 24213–24222.

Pajuelo, D., Gonzalez-Juarbe, N., Tak, U., Sun, J., Orihuela, C.J., and Niederweis, M. (2018). NAD+ Depletion Triggers Macrophage Necroptosis, a Cell Death Pathway Exploited by Mycobacterium tuberculosis. Cell Reports *24*, 429–440.

Pak, J.E., Ekendé, E.N., Kifle, E.G., O'Connell, J.D., De Angelis, F., Tessema, M.B., Derfoufi, K.-M., Robles-Colmenares, Y., Robbins, R.A., Goormaghtigh, E., et al. (2013). Structures of intermediate transport states of ZneA, a Zn(II)/proton antiporter. Proc Natl Acad Sci USA *110*, 201318705–18489.

Pape, T., and Schneider, T.R. (2004). HKL2MAP: a graphical user interface for macromolecular phasing with SHELX programs. Journal of Applied Crystallography *37*, 843–844.

Pasca, M.R., Guglierame, P., De Rossi, E., Zara, F., and Riccardi, G. (2005). mmpL7 gene of Mycobacterium tuberculosis is responsible for isoniazid efflux in Mycobacterium smegmatis. Antimicrobial Agents and Chemotherapy *49*, 4775–4777.

Passemar, C., Arbues, A., Malaga, W., Mercier, I., Moreau, F., Lepourry, L., Neyrolles, O., Guilhot, C., and Dequeker, C.A. (2014). Multiple deletions in the polyketide synthase gene repertoire of Mycobacterium tuberculosis reveal functional overlap of cell envelope lipids in host–pathogen interactions. Cell Microbiol *16*, 195–213.

Patin, E.C., Geffken, A.C., Willcocks, S., Leschczyk, C., Haas, A., Nimmerjahn, F., Lang, R., Ward, T.H., and Schaible, U.E. (2017). Trehalose dimycolate interferes with FcγR-mediated phagosome maturation through Mincle, SHP-1 and FcγRIIB signalling. PLoS ONE *12*, e0174973.

Paulsen, I.T., Park, J.H., Choi, P.S., and Saier, M.H. (1997). A family of Gram-negative bacterial outer membrane factors that function in the export of proteins, carbohydrates, drugs and heavy metals from Gram-negative bacteria. FEMS Microbiology Letters *156*, 1–8.

Penn, B.H., Netter, Z., Johnson, J.R., Dollen, Von, J., Jang, G.M., Johnson, T., Ohol, Y.M., Maher, C., Bell, S.L., Geiger, K., et al. (2018). An Mtb-Human Protein-Protein Interaction Map Identifies a Switch between Host Antiviral and Antibacterial Responses. Molecular Cell *71*, 637–648.e5.

Petit, J.F., Adam, A., Wietzerbin-Falszpan, J., LEDERER, E., and Ghuysen, J.M. (1969). Chemical structure of the cell wall of Mycobacterium smegmatis. I. Isolation and partial characterization of the peptidoglycan. Biochemical and Biophysical Research Communications *35*, 478–485.

Peyron, P., Vaubourgeix, J., Poquet, Y., Levillain, F., Botanch, C., Bardou, F., Daffe, M., Emile, J.-F., Marchou, B., Cardona, P.-J., et al. (2008). Foamy macrophages from tuberculous patients' granulomas constitute a nutrient-rich reservoir for M. tuberculosis persistence. PLoS Pathog *4*, e1000204.

Pérez, J., Garcia, R., Bach, H., de Waard, J.H., Jacobs, W.R., Jr, Av-Gay, Y., Bubis, J., and Takiff, H.E. (2006). Mycobacterium tuberculosis transporter MmpL7 is a potential substrate for kinase PknD. Biochemical and Biophysical Research Communications *348*, 6–12.

Philips, J.A., and Ernst, J.D. (2012). Tuberculosis Pathogenesis and Immunity. Annu. Rev. Pathol. Mech. Dis. *7*, 353–384.

Poole, K., Krebes, K., McNally, C., and Neshat, S. (1993). Multiple antibiotic resistance in Pseudomonas aeruginosa: evidence for involvement of an efflux operon. Journal of Bacteriology *175*, 7363–7372.

Prisic, S., and Husson, R.N. (2014). Mycobacterium tuberculosis Serine/Threonine Protein Kinases. Microbiology Spectrum *2*, 1–26.

Prisic, S., Dankwa, S., Schwartz, D., Chou, M.F., Locasale, J.W., Kang, C.-M., Bemis, G., Church, G.M., Steen, H., and Husson, R.N. (2010). Extensive phosphorylation with overlapping specificity by Mycobacterium tuberculosis serine/threonine protein kinases. Proc. Natl. Acad. Sci. U.S.a. *107*, 7521–7526.

Quémard, A. (2016). New Insights into the Mycolate-Containing Compound Biosynthesis and Transport in Mycobacteria. Trends in Microbiology 1–14.

Quigley, J., Hughitt, V.K., Velikovsky, C.A., Mariuzza, R.A., El-Sayed, N.M., and Briken, V. (2017). The Cell Wall Lipid PDIM Contributes to Phagosomal Escape and Host Cell Exit of Mycobacterium tuberculosis. mBio *8*, e00148–17.

Radhakrishnan, A., Kumar, N., Wright, C.C., Chou, T.H., Tringides, M.L., Bolla, J.R., Lei, H.T., Rajashankar, K.R., Su, C.C., Purdy, G.E., et al. (2014). Crystal Structure of the Transcriptional Regulator Rv0678 of Mycobacterium tuberculosis. Journal of Biological Chemistry *289*, 16526–16540.

Raffetseder, J., Iakobachvili, N., Loitto, V., Peters, P.J., Lerm, M., and Ehrt, S. (2019). Retention of EsxA in the Capsule-Like Layer of Mycobacterium tuberculosis Is Associated with Cytotoxicity and Is Counteracted by Lung Surfactant. Infect. Immun. *87*, e00803–e00818.

Raymond, J.B., Mahapatra, S., Crick, D.C., and Pavelka, M.S. (2005). Identification of the namH gene, encoding the hydroxylase responsible for the N-glycolylation of the mycobacterial peptidoglycan. Journal of Biological Chemistry *280*, 326–333.

Rego, E.H., Audette, R.E., and Rubin, E.J. (2017). Deletion of a mycobacterial divisome factor collapses single-cell phenotypic heterogeneity. Nature *546*, 153–157.

Rezwan, M., Grau, T., Tschumi, A., and Sander, P. (2007). Lipoprotein synthesis in mycobacteria. Microbiology *153*, 652–658.

Richard, M., Gutiérrez, A.V., Viljoen, A., Rodriguez-Rincon, D., Roquet-Baneres, F., Blaise, M., Everall, I., Parkhill, J., Floto, R.A., and Kremer, L. (2019). Mutations in the MAB_2299c TetR Regulator Confer Cross-Resistance to Clofazimine and Bedaquiline in Mycobacterium abscessus. Antimicrobial Agents and Chemotherapy *63*, e01316–e01318.

Roach, D.R., Bean, A.G.D., Demangel, C., France, M.P., Briscoe, H., and Britton, W.J. (2002). TNF Regulates Chemokine Induction Essential for Cell Recruitment, Granuloma Formation, and Clearance of Mycobacterial Infection. The Journal of Immunology *168*, 4620–4627.

Rodrigues, L., Machado, D., Couto, I., Amaral, L., and Viveiros, M. (2012). Contribution of efflux activity to isoniazid resistance in the Mycobacterium tuberculosis complex. Infect. Genet. Evol. *12*, 695–700.

Rosales, C., and Uribe-Querol, E. (2017). Phagocytosis: A Fundamental Process in Immunity. BioMed Research International *2017*, 1–18.

Rousseau, C., Neyrolles, O., Bordat, Y., Giroux, S., Sirakova, T.D., Prevost, M.-C., Kolattukudy, P.E., Gicquel, B., and Jackson, M. (2003). Deficiency in mycolipenate- and mycosanoate-derived acyltrehaloses enhances early interactions of Mycobacterium tuberculosis with host cells. Cell Microbiol *5*, 405–

415.

Rousseau, C., Winter, N., Pivert, E., Bordat, Y., Neyrolles, O., Avé, P., Huerre, M., Gicquel, B., and Jackson, M. (2004). Production of phthiocerol dimycocerosates protects *Mycobacterium tuberculosis* from the cidal activity of reactive nitrogen intermediates produced by macrophages and modulates the early immune response to infection. Cell Microbiol *6*, 277–287.

Ruggerone, P., Murakami, S., Pos, K.M., and Vargiu, A.V. (2013). RND efflux pumps: structural information translated into function and inhibition mechanisms. Current Topics in Medicinal Chemistry *13*, 3079–3100.

Russell, D.G. (2007). Who puts the tubercle in tuberculosis? Nature Reviews Microbiology *5*, 39–47.

Sakai, H., Okafuji, I., Nishikomori, R., Abe, J., Izawa, K., Kambe, N., Yasumi, T., Nakahata, T., and Heike, T. (2012). The CD40-CD40L axis and IFN-γ play critical roles in Langhans giant cell formation. Int. Immunol. *24*, 5–15.

Sampson, S.L. (2011). Mycobacterial PE/PPE Proteins at the Host-Pathogen Interface. Clinical and Developmental Immunology *2011*, 1–11.

Sander, P., Rezwan, M., Walker, B., Rampini, S.K., Kroppenstedt, R.M., Ehlers, S., Keller, C., Keeble, J.R., Hagemeier, M., Colston, M.J., et al. (2004). Lipoprotein processing is required for virulence of Mycobacterium tuberculosis. Molecular Microbiology *52*, 1543–1552.

Sandhu, P., and Akhter, Y. (2015). The internal gene duplication and interrupted coding sequences in the MmpL genes of Mycobacterium tuberculosis: Towards understanding the multidrug transport in an evolutionary perspective. International Journal of Medical Microbiology *305*, 413–423.

Sandhu, P., and Akhter, Y. (2017). Siderophore transport by MmpL5-MmpS5 protein complex in Mycobacterium tuberculosis. Journal of Inorganic Biochemistry *170*, 75–84.

Sani, M., Houben, E.N.G., Geurtsen, J., Pierson, J., de Punder, K., van Zon, M., Wever, B., Piersma, S.R., Jiménez, C.R., Daffe, M., et al. (2010). Direct visualization by cryo-EM of the mycobacterial capsular layer: a labile structure containing ESX-1-secreted proteins. PLoS Pathog *6*, e1000794.

Saunders, B.M., and Britton, W.J. (2007). Life and death in the granuloma: immunopathology of tuberculosis. Immunology and Cell Biology *85*, 103–111.

Saunders, B.M., Frank, A.A., Orme, I.M., and Cooper, A.M. (2002). CD4 is required for the development of a protective granulomatous response to pulmonary tuberculosis. Cellular Immunology *216*, 65–72.

Schneewind, O., and Missiakas, D. (2014). Sec-secretion and sortase-mediated anchoring of proteins in Gram-positive bacteria. BBA - Molecular Cell Research *1843*, 1687–1697.

Schneider, T.R., and Sheldrick, G.M. (2002). Substructure solution with SHELXD. Acta Crystallogr. D Biol. Crystallogr. *58*, 1772–1779.

Seeger, M.A., Schiefner, A., Eicher, T., Verrey, F., Diederichs, K., and Pos, K.M. (2006). Structural asymmetry of AcrB trimer suggests a peristaltic pump mechanism. Science *313*, 1295–1298.

Seeliger, J.C., Holsclaw, C.M., Schelle, M.W., Botyanszki, Z., Gilmore, S.A., Tully, S.E., Niederweis, M., Cravatt, B.F., Leary, J.A., and Bertozzi, C.R. (2012). Elucidation and Chemical Modulation of Sulfolipid-1 Biosynthesis in Mycobacterium tuberculosis. Journal of Biological Chemistry *287*, 7990–8000.

Seiler, P., Aichele, P., Bandermann, S., Hauser, A.E., Lu, B., Gerard, N.P., Gerard, C., Ehlers, S., Mollenkopf, H.J., and Kaufmann, S.H.E. (2003). Early granuloma formation after aerosol Mycobacterium tuberculosis infection is regulated by neutrophils via CXCR3-signaling chemokines. European Journal of Immunology *33*, 2676–2686.

Sennhauser, G., Bukowska, M.A., Briand, C., and Grütter, M.G. (2009). Crystal Structure of the Multidrug Exporter MexB from Pseudomonas aeruginosa. Journal of Molecular Biology *389*, 134–145.

Singh, A., Mai, D., Kumar, A., and Steyn, A.J.C. (2006). Dissecting virulence pathways of *Mycobacterium tuberculosis* through protein-protein association. Proc Natl Acad Sci USA *103*, 11346–11351.

Singh, P., Rao, R.N., Reddy, J.R.C., Prasad, R., Kotturu, S.K., Ghosh, S., and Mukhopadhyay, S. (2016). PE11, a PE/PPE family protein of Mycobacterium tuberculosis is involved in cell wall remodeling and virulence. Nature Publishing Group *6*, 1–16.

Slayden, R.A., and Barry, C.E., 3rd (2002). The role of KasA and KasB in the biosynthesis of meromycolic acids and isoniazid resistance in Mycobacterium tuberculosis. Tuberculosis *82*, 149–160.

Song, H., Sandie, R., Wang, Y., Andrade-Navarro, M.A., and Niederweis, M. (2008). Identification of outer membrane proteins of Mycobacterium tuberculosis. Tuberculosis (Edinb) *88*, 526–544.

Sonnhammer, E.L., Heijne, von, G., and Krogh, A. (1998). A hidden Markov model for predicting transmembrane helices in protein sequences. Proc Int Conf Intell Syst Mol Biol *6*, 175–182.

Stahl, C., Kubetzko, S., Kaps, I., Seeber, S., Engelhardt, H., and Niederweis, M.

(2001). MspA provides the main hydrophilic pathway through the cell wall of Mycobacterium smegmatis. Molecular Microbiology *40*, 451–464.

Stover, C.K., la Cruz, de, V.F., Fuerst, T.R., Burlein, J.E., Benson, L.A., Bennett, L.T., Bansal, G.P., Young, J.F., Lee, M.H., and Hatfull, G.F. (1991). New use of BCG for recombinant vaccines. Nature *351*, 456–460.

Su, C.C., Klenotic, P.A., Bolla, J.R., Purdy, G.E., Robinson, C.V., and Yu, E.W. (2019). MmpL3 is a lipid transporter that binds trehalose monomycolate and phosphatidylethanolamine. Proc. Natl. Acad. Sci. U.S.a. *116*, 11241–11246.

Su, C.C., Li, M., Gu, R., Takatsuka, Y., McDermott, G., Nikaido, H., and Yu, E.W. (2006). Conformation of the AcrB Multidrug Efflux Pump in Mutants of the Putative Proton Relay Pathway. Journal of Bacteriology *188*, 7290–7296.

Sullivan, J.T., Young, E.F., McCann, J.R., Braunstein, M., and Flynn, J.L. (2012). The Mycobacterium tuberculosis SecA2 System Subverts Phagosome Maturation To Promote Growth in Macrophages. Infect. Immun. *80*, 996–1006.

Sulzenbacher, G., Canaan, S., Bordat, Y., Neyrolles, O., Stadthagen, G., Roig-Zamboni, V., Rauzier, J., Maurin, D., Laval, F., Daffe, M., et al. (2006). LppX is a lipoprotein required for the translocation of phthiocerol dimycocerosates to the surface of *Mycobacterium tuberculosis*. Embo J. *25*, 1436–1444.

Sutcliffe, I.C., and Harrington, D.J. (2004). Lipoproteins of Mycobacterium tuberculosis: an abundant and functionally diverse class of cell envelope components. FEMS Microbiol Rev *28*, 645–659.

Tahlan, K., Wilson, R., Kastrinsky, D.B., Arora, K., Nair, V., Fischer, E., Barnes, S.W., Walker, J.R., Alland, D., Barry, C.E., et al. (2012). SQ109 Targets MmpL3, a Membrane Transporter of Trehalose Monomycolate Involved in Mycolic Acid Donation to the Cell Wall Core of Mycobacterium tuberculosis. Antimicrobial Agents and Chemotherapy *56*, AAC.05708–11–1809.

Tapping, R.I., and Tobias, P.S. (2003). Mycobacterial lipoarabinomannan mediates physical interactions between TLR1 and TLR2 to induce signaling. J. Endotoxin Res. *9*, 264–268.

Tekaia, F., Gordon, S.V., Garnier, T., Brosch, R., Barrell, B.G., and Cole, S.T. (1999). Analysis of the proteome of Mycobacterium tuberculosis in silico. Tubercle and Lung Disease *79*, 329–342.

Terwilliger, T.C., Adams, P.D., Read, R.J., McCoy, A.J., Moriarty, N.W., Grosse-Kunstleve, R.W., Afonine, P.V., Zwart, P.H., and Hung, L.-W. (2009). Decision-making in structure solution using Bayesian estimates of map quality: the PHENIX AutoSol wizard. Acta Crystallogr. D Biol. Crystallogr. *65*, 582–601.

Thanassi, D.G., Cheng, L.W., and Nikaido, H. (1997). Active efflux of bile salts by

Escherichia coli. Journal of Bacteriology *179*, 2512–2518.

Thorsell, A.-G., Lee, W.H., Persson, C., Siponen, M.I., Nilsson, M., Busam, R.D., Kotenyova, T., Schüler, H., and Lehtiö, L. (2011). Comparative structural analysis of lipid binding START domains. PLoS ONE *6*, e19521.

Touchette, M.H., Van Vlack, E.R., Bai, L., Kim, J., Cognetta, A.B., Previti, M.L., Backus, K.M., Martin, D.W., Cravatt, B.F., and Seeliger, J.C. (2017). A Screen for Protein-Protein Interactions in Live Mycobacteria Reveals a Functional Link between the Virulence-Associated Lipid Transporter LprG and the Mycolyltransferase Antigen 85A. ACS Infect. Dis. *3*, acsinfecdis.6b00179–acsinfecdis.6b00348.

Trivedi, O.A., Arora, P., Vats, A., Ansari, M.Z., Tickoo, R., Sridharan, V., Mohanty, D., and Gokhale, R.S. (2005). Dissecting the Mechanism and Assembly of a Complex Virulence Mycobacterial Lipid. Molecular Cell *17*, 631–643.

Tschumi, A., Grau, T., Albrecht, D., Rezwan, M., Antelmann, H., and Sander, P. (2012). Functional analyses of mycobacterial lipoprotein diacylglyceryl transferase and comparative secretome analysis of a mycobacterial lgt mutant. Journal of Bacteriology *194*, 3938–3949.

Tschumi, A., Nai, C., Auchli, Y., Hunziker, P., Gehrig, P., Keller, P., Grau, T., and Sander, P. (2009). Identification of apolipoprotein N-acyltransferase (Lnt) in mycobacteria. J. Biol. Chem. *284*, 27146–27156.

Tseng, T.T., Gratwick, K.S., Kollman, J., Park, D., Nies, D.H., Goffeau, A., and Saier, M.H. (1999). The RND permease superfamily: An ancient, ubiquitous and diverse family that includes human disease and development proteins. J. Mol. Microbiol. Biotechnol. *1*, 107–125.

Tsirigotaki, A., De Geyter, J., Šoštaric, N., Economou, A., and Karamanou, S. (2017). Protein export through the bacterial Sec pathway. Nature Reviews Microbiology *15*, 21–36.

Turner, J., and Torrelles, J.B. (2018). Mannose-capped lipoarabinomannan in Mycobacterium tuberculosis pathogenesis. Pathog Dis *76*, S1130.

van Kessel, J.C., and Hatfull, G.F. (2007). Recombineering in Mycobacterium tuberculosis. Nature Methods *4*, 147–152.

VanderVen, B.C., Fahey, R.J., Lee, W., Liu, Y., Abramovitch, R.B., Memmott, C., Crowe, A.M., Eltis, L.D., Perola, E., Deininger, D.D., et al. (2015). Novel Inhibitors of Cholesterol Degradation in Mycobacterium tuberculosis Reveal How the Bacterium's Metabolism Is Constrained by the Intracellular Environment. PLoS Pathog *11*, e1004679–20.

Varela, C., Rittmann, D., Singh, A., Krumbach, K., Bhatt, K., Eggeling, L., Besra, G.S., and Bhatt, A. (2012). MmpL Genes Are Associated with Mycolic Acid Metabolism in Mycobacteria and Corynebacteria. Chemistry & Biology *19*, 498–506.

Velmurugan, K., Chen, B., Miller, J.L., Azogue, S., Gurses, S., Hsu, T., Glickman, M., Jacobs, W.R., Porcelli, S.A., and Briken, V. (2007). Mycobacterium tuberculosis nuoG Is a Virulence Gene That Inhibits Apoptosis of Infected Host Cells. PLoS Pathog *3*, e110–e119.

Vergne, I., Chua, J., Lee, H.-H., Lucas, M., Belisle, J., and Deretic, V. (2005). Mechanism of phagolysosome biogenesis block by viable Mycobacterium tuberculosis. Proc Natl Acad Sci USA *102*, 4033–4038.

Veyron-Churlet, R., Zanella-Cléon, I., Cohen-Gonsaud, M., Molle, V., and Kremer, L. (2010). Phosphorylation of the Mycobacterium tuberculosis beta-ketoacyl-acyl carrier protein reductase MabA regulates mycolic acid biosynthesis. J. Biol. Chem. *285*, 12714–12725.

Viljoen, A., Dubois, V., Girard-Misguich, F., Blaise, M., Herrmann, J.-L., and Kremer, L. (2017). The diverse family of MmpL transporters in mycobacteria: from regulation to antimicrobial developments. Molecular Microbiology *104*, 889–904.

Villeneuve, M., Kawai, M., Kanashima, H., Watanabe, M., Minnikin, D.E., and Nakahara, H. (2005). Temperature dependence of the Langmuir monolayer packing of mycolic acids from Mycobacterium tuberculosis. Biochim. Biophys. Acta *1715*, 71–80.

Wells, R.M., Jones, C.M., Xi, Z., Speer, A., Danilchanka, O., Doornbos, K.S., Sun, P., Wu, F., Tian, C., and Niederweis, M. (2013). Discovery of a Siderophore Export System Essential for Virulence of Mycobacterium tuberculosis. PLoS Pathog *9*, e1003120.

Welsh, K.J., Hunter, R.L., and Actor, J.K. (2013). Trehalose 6,6′-dimycolate – A coat to regulate tuberculosis immunopathogenesis. Tuberculosis *93*, S3–S9.

Williams, J.T., Haiderer, E.R., Coulson, G.B., Conner, K.N., Ellsworth, E., Chen, C., Alvarez-Cabrera, N., Li, W., Jackson, M., Dick, T., et al. (2019). Identification of new MmpL3 inhibitors by untargeted and targeted mutant screens defines MmpL3 domains with differential resistance. Antimicrobial Agents and Chemotherapy AAC.00547–19.

Wilmarth, P.A., Riviere, M.A., and David, L.L. (2009). Techniques for accurate protein identification in shotgun proteomic studies of human, mouse, bovine, and chicken lenses. J Ocul Biol Dis Inform *2*, 223–234.

Wolf, A.J., Desvignes, L., Linas, B., Banaiee, N., Tamura, T., Takatsu, K., and

Ernst, J.D. (2008). Initiation of the adaptive immune response to Mycobacterium tuberculosis depends on antigen production in the local lymph node, not the lungs. Journal of Experimental Medicine *205*, 105–115.

Wolf, A.J., Linas, B., Trevejo-Nuñez, G.J., Kincaid, E., Tamura, T., Takatsu, K., and Ernst, J.D. (2007). Mycobacterium tuberculosis Infects Dendritic Cells with High Frequency and Impairs Their Function In Vivo. The Journal of Immunology *179*, 2509–2519.

World Health Organization (2010). Treatment of Tuberculosis: Guidelines, Fourth Edition. 1–160.

World Health Organization (2018). Global tuberculosis report 2018.

Wright, C.C., Hsu, F.F., Arnett, E., Dunaj, J.L., Davidson, P.M., Pacheco, S.A., Harriff, M.J., Lewinsohn, D.M., Schlesinger, L.S., and Purdy, G.E. (2017). The Mycobacterium tuberculosis MmpL11 Cell Wall Lipid Transporter Is Important for Biofilm Formation, Intracellular Growth, and Nonreplicating Persistence. Infect. Immun. *85*, e00131–17.

Wu, H.C., Tokunaga, M., Tokunaga, H., Hayashi, S., and Giam, C.Z. (1983). Posttranslational modification and processing of membrane lipoproteins in bacteria. Journal of Cellular Biochemistry *22*, 161–171.

Xu, Z., Meshcheryakov, V.A., Poce, G., and Chng, S.S. (2017). MmpL3 is the flippase for mycolic acids in mycobacteria. Proc Natl Acad Sci USA *114*, 7993–7998.

Young, D.B., and Garbe, T.R. (1991). Lipoprotein antigens ofMycobacterium tuberculosis. Res. Microbiol. *142*, 55–65.

Yuan, Y., Lee, R.E., Besra, G.S., Belisle, J.T., and Barry, C.E. (1995). Identification of a gene involved in the biosynthesis of cyclopropanated mycolic acids in Mycobacterium tuberculosis. Proc Natl Acad Sci USA *92*, 6630–6634.

Yuan, Y., Zhu, Y., Crane, D.D., and Barry, C.E. (1998). The effect of oxygenated mycolic acid composition on cell wall function and macrophage growth in Mycobacterium tuberculosis. Molecular Microbiology *29*, 1449–1458.

Zgurskaya, H.I., and Nikaido, H. (1999). Bypassing the periplasm: Reconstitution of the AcrAB multidrug efflux pump of Escherichia coli. Proc Natl Acad Sci USA *96*, 7190–7195.

Zhang, B., Li, J., Yang, X., Wu, L., Zhang, J., Yang, Y., Zhao, Y., Zhang, L., Yang, X., Yang, X., et al. (2019). Crystal Structures of Membrane Transporter MmpL3, an Anti-TB Drug Target. Cell *176*, 636–648.e13.

Zimhony, O., Vilcheze, C., and Jacobs, W.R. (2004). Characterization of

Mycobacterium smegmatis expressing the Mycobacterium tuberculosis fatty acid synthase I (fas1) gene. Journal of Bacteriology *186*, 4051–4055.

Zuber, B., Chami, M., Houssin, C., Dubochet, J., Griffiths, G., and Daffe, M. (2008). Direct visualization of the outer membrane of mycobacteria and corynebacteria in their native state. Journal of Bacteriology *190*, 5672–5680.

Zulauf, K.E., Braunstein, M., and Miller, B.K. (2017). The Sec Pathways and Exportomes of Mycobacterium tuberculosis. Microbiology Spectrum *5*.